Nuclear Operating Company
South Texas Project Electric Generating Station P.O. Box 289 Wadsworth, Texas 77483

November 22, 2010
U7-C-STP-NRC-100241

U. S. Nuclear Regulatory Commission
Attention: Document Control Desk
One White Flint North
11555 Rockville Pike
Rockville, MD 20852-2738

South Texas Project
Units 3 and 4
Docket Nos. 52-012 and 52-013
Response to Request for Additional Information

Attached is the STP Nuclear Operating Company (STPNOC) response to Request for Additional Information (RAI) questions in RAI letter number 365 related to COLA Part 2, Tier 2, Sections 2.4S.4, "Potential Dam Failures," 2.4S.5, "Probable Maximum Surge and Seiche Flooding," and 2.4S.12, "Groundwater." This letter provides the complete response to RAI letter number 365. The attachment provides responses to the following RAI questions:

02.04.04-14 02.04.04-15 02.04.05-11 02.04.12-51

When a change to the COLA is required, it will be incorporated into the next routine revision of the COLA following NRC acceptance of the RAI response.

There are no commitments in this letter.

If you have any questions, please contact me at (361) 972-7136, or Bill Mookhoek at (361) 972-7274.

D091
NRO

STI 32772822

I declare under penalty of perjury that the foregoing is true and correct.

Executed on 11/22/10

Scott Head
Manager, Regulatory Affairs
South Texas Project Units 3 & 4

rhb

Attachments:
1. RAI 02.04.04-14
2. RAI 02.04.04-15
3. RAI 02.04.05-11
4. RAI 02.04.12-51

cc: w/o attachments and enclosure except*
(paper copy)

Director, Office of New Reactors
U. S. Nuclear Regulatory Commission
One White Flint North
11555 Rockville Pike
Rockville, MD 20852-2738

Regional Administrator, Region IV
U. S. Nuclear Regulatory Commission
611 Ryan Plaza Drive, Suite 400
Arlington, Texas 76011-8064

Kathy C. Perkins, RN, MBA
Assistant Commissioner
Division for Regulatory Services
Texas Department of State Health Services
P. O. Box 149347
Austin, Texas 78714-9347

Alice Hamilton Rogers, P.E.
Inspection Unit Manager
Texas Department of State Health Services
P. O. Box 149347
Austin, Texas 78714-9347

*Steven P. Frantz, Esquire
A. H. Gutterman, Esquire
Morgan, Lewis & Bockius LLP
1111 Pennsylvania Ave. NW
Washington D.C. 20004

*Tekia Govan
Two White Flint North
11545 Rockville Pike
Rockville, MD 20852

(electronic copy)

*George F. Wunder
*Tekia Govan
Loren R. Plisco
U. S. Nuclear Regulatory Commission

Steve Winn
Joseph Kiwak
Eli Smith
Nuclear Innovation North America

Peter G. Nemeth
Crain, Caton & James, P.C.

Richard Peña
Kevin Pollo
L. D. Blaylock
CPS Energy

02.04.04-14

QUESTION:

Describe the methods selected to estimate the MCR embankment breach parameters and will also describe the bases for the range of the selected breach parameters. The breach parameters shall account for the MCR storage volume and depth as well as the geometry and construction materials of the embankment.

Provide FSAR updates to include: (1) a description of various methods used for estimation of MCR breach parameters, (2) description of the identification process of the most conservative breach scenario among all plausible scenarios, (3) justification why a specific scenario is chosen or why certain scenario(s) were excluded as plausible, (4) a description of the sensitivity of flood characteristics to the chosen range of breach parameters, (5) flow depth maps for the simulated flood, (6) flow velocity maps for the simulated floods, (7) peak flood discharge at safety-related structures, systems, and components (SSC), (8) duration of inundation at the safety-related SSCs, and (9) maximum estimated hydrostatic and hydrodynamic forces on the safety-related SSCs.

Characteristics of the design-basis flood (e.g., flow velocities, scour, deposition) and post-construction cover (e.g., surface material map, associated properties) are to be consistent in RAIs 5101 and 5105. If the design-basis flood is revised, the revised characteristic shall be applied in FSAR Sections 2.4S.12 and 2.4S.13.

RESPONSE:

As explained in FSAR Subsection 2.4S.4.2.2.2.2, the MCR embankment breach parameters were estimated based on a report prepared by the Dam Safety Office of the US Bureau of Reclamation (FSAR Reference 2.4S.4-12d) and engineering judgment. The following empirical equations from Reference 2.4S.4-12d, which were developed from case studies of historical dam failures, were considered for this analysis as they provide conservative and reasonable estimates of the breach parameters. These equations estimate breach parameters based on the storage volume in the reservoir above the breach bottom elevation (V = 152,700 ac-ft) and the depth of water above the breach (h_w = 21.9 ft) or the height of the breach (h_b = 37 ft).

1. Froehlich, 1995

   Average Breach Width, $B_{ave} = 0.1803\ V^{0.32}\ h_b^{0.19}$ = 127 m (417 ft)

   Time to Failure, $t_f = 0.00254\ V^{0.53}\ h_w^{(-0.90)}$ = 11.1 hrs

   Peak Flow, $Q_p = 0.607\ V^{0.295}\ h_w^{1.24}$ = 1,772.8 m^3/s (62,600 cfs)

2. MacDonald & Langridge–Monopolis (MLM),1984

   Time to $_{Failure}$, $t_f = 0.0179(0.0261(V*h_w)^{0.769})^{0.364}$ = 1.7 hrs

An average breach width of 417 feet was conservatively estimated using Froelich's equation. Froelich's equation for the time to failure gives an estimated value of 11.1 hours. The MLM time to failure equation gives an estimated value of 1.7 hours. The shorter time to failure would produce higher peak outflow and hence is conservative; therefore, MLM time to failure equation is used. Froelich's equation for breach width predicts the largest breach width estimate of all methods presented in Reference 2.4S.4-12d and is considered conservative. MLM does not have an equation to estimate breach width, but gives an equation to estimate the total volume of the eroded material based on the storage volume and the hydraulic depth of the breach. However, this equation does not provide the volume of eroded material from the start to the time of peak outflow, so it is not possible to estimate the breach width at peak outflow with this information. The breach width and time to failure parameters estimated using the storage-based equations above were used as input to FLDWAV in the MCR Breach analysis.

The outflow hydrograph from the MCR embankment breach developed by FLDWAV using the selected breach parameters predicted a peak outflow of 130,000 cfs. The peak outflow predicted by FLDWAV is compared to peak outflow estimate using Froelich's equation, which is one of the better available methods for prediction of peak breach outflow according to Reference 2.4S.4-12d. The peak outflow from Froehlich's equation above gave a breach peak outflow of 62,600 cfs. Therefore, the peak flow predicted by FLDWAV is considered conservative. To further verify the conservatism of the breach parameters and FLDWAV results, an independent, confirmatory analysis of the MCR embankment breach was performed using the BREACH model, developed by the National Weather Service, to predict the breach development and outflow hydrograph. This analysis is presented in a new Subsection 2.4S.4.2.2.2.4 added in the FSAR markup included with this response. The following is a brief description of the BREACH model and the results.

BREACH is an erosion model for earthen dam failures and predicts breach characteristics, namely, breach width and time of formation of the breach, erosion rate and breach outflow hydrograph. The BREACH model accounts for the geometry and construction materials of the embankment. It considers piping type failure and uses the reservoir information, geometric properties of the dam, properties of the material of the dam namely, internal friction angle, cohesive strength, unit weight and average grain size diameter D_{50}.

The following table shows the comparison of the results from the BREACH program with the results provided in FSAR Subsections 2.4S.4.2.2.2.2 and 2.4S.4.2.2.2.3 based on empirical equations and the outflow hydrograph from FLDWAV program:

	BREACH	FLDWAV
Peak outflow through the beach (cfs)	83,200	130,000
Time to peak (hrs)	6.25	1.7
Breach bottom width at peak outflow (ft)	361	380
Breach bottom width at 30 hours* (ft)	448	-

*The BREACH model allows the breach width to continue to increase after the peak due to prolonged outflow from the breach, but at a slower rate due to the decreasing reservoir water level. Increase in breach width after the peak is not considered in the FLDWAV model.

The BREACH model allows for time-varying breach erosion rates and continued breach expansion after the peak outflow, whereas FLDWAV uses a linear expansion rate from 0 to a maximum breach bottom width of 380 feet in 1.7 hours, which is the time of peak outflow. From the BREACH analysis, the breach width increases initially at a faster rate to a breach width of 361 feet at the time the peak outflow occurs. However, considering the large volume of water remaining in the MCR, outflow from the breach continues at a lower discharge rate and a diminishing breach width erosion rate due to the decrease in reservoir water level. The breach width predicted by BREACH at 30 hours is less than 20 percent greater than the breach width at the time of peak outflow used for FLDWAV. A comparison of breach outflow hydrographs from FLDWAV output and the BREACH program output is presented in the FSAR markup included in this response.

The BREACH model provides an independent assessment of the postulated breach of the MCR embankment at the STP 3 and 4 site. The BREACH model estimates a longer time to peak and a narrower breach width at the time of peak than the parameters selected for use in the FLDWAV model. Breach also predicted a lower peak outflow than the peak outflow predicted using the FLDWAV model. Therefore, the parameters selected for FLDWAV and predicted breach hydrograph are considered conservative and acceptable. The existing MCR embankment breach analysis is not changed as a result of this RAI; therefore, the maximum flood level resulting from the MCR embankment breach at STP 3 and 4 will not change.

The following address the FSAR update items (1) through (9) requested in this RAI:

(1) An expanded discussion of the methods used for breach parameter estimation is added to Subsection 2.4S.4.2.2.2.2. See FSAR markup.

(2) The Subsection 2.4S.4.2.2 is revised to address the identification process of the most conservative breach scenario among all plausible scenarios. See FSAR markup.

(3) The Subsection 2.4S.4.2.2 is revised to discuss why a specific scenario was chosen or why certain scenario(s) were excluded as plausible. See FSAR markup.

(4) A new Subsection 2.4S.4.2.2.2.4 is added to the FSAR to include a presentation of the sensitivity of the outflow hydrograph to different breach parameters. The BREACH model simulation, described in this response, is presented to further confirm that the originally selected breach characteristics and flood hydrograph were conservative. See FSAR markup.

(5) FSAR Figures 2.4S.4-20 and 2.4S.4-21 provide water surface elevations for each simulated breach scenario at various locations around the power block. FSAR Figures 2.4S.4-21(a) and 2.4S.4-21(b), provide peak water surface elevations over the site area. Flow depths can be obtained by subtracting the grade elevation from the water surface elevations. A nominal grade elevation of 34.0 feet may be used for the power block. Subsection 2.4S.4.2.2.4.1 is updated to include a brief discussion of this process. See FSAR markup.

(6) FSAR Figures 2.4S.4-21(c) and 2.4S.4-21(d) provide peak velocities over the entire site area. Figures 2.4S.4-21(e) and 2.4S.4-21(f) provide peak velocities for each simulated breach scenario at various locations around the power block. No FSAR revision is required for this item.

(7) Peak water surface elevations and flow velocities are provided in FSAR figures described in items 5 and 6. Peak discharge per unit width at any point is obtained by multiplying the velocity with the flow depth. A paragraph has been added to Subsection 2.4S.4.2.2.4.1 to describe this process and the flow rates per unit width at locations near the power block buildings are provided in Table 2.4S.4-7a. See FSAR markup.

(8) The duration of inundation at the power block is considered to be the duration during which the flood elevations are greater than the grade elevation of 34 feet. Subsection 2.4S.4.2.2.4.5 and Figure 2.4S.4-21(j) are added to address the duration of inundation. See FSAR markup.

(9) FSAR Subsection 2.4S.4.2.2.4.3 was updated in response to RAI 03.04.02-11 (Letter U7-C-STP-NRC-100208, dated September 15, 2010) to provide an expanded discussion of hydrodynamic forces.

Subsection 2.4S.4.2.2 will be updated as shown in gray shaded text as follows:

2.4S.4.2.2 MCR Embankment Breach Analysis

FLDWAV, a computer program developed by the National Weather Service (Reference 2.4S.4-12), was used to generate the outflow flood hydrograph from the MCR embankment breach, based on breach parameters discussed in Subsection 2.4S.4.2.2.2.2. This flood hydrograph was used as input to the two-dimensional flow model downstream of the breach.

RMA2 is a two-dimensional (2-D), depth-averaged finite-element hydrodynamic numerical model developed by the United States Army Corps of Engineers (USACE) (Reference 2.4S.4-12a). RMA2 was used to determine the flood elevations and velocities at the safety-related facilities of STP Units 3 and 4. The computer program can simulate dynamic water surface elevations and horizontal velocity components for subcritical, free-surface flow in a 2-dimensional flow field. The governing equations of RMA2 are the depth-integrated equations of fluid mass and momentum conservation in two horizontal directions. The governing equations are solved by finite-element method using the Galerkin Method of weighted residuals, and the integration in space is performed by Gaussian integration. Derivatives in time are replaced by a nonlinear finite difference approximation. The solution is fully implicit and the set of simultaneous equations is solved by the Newton-Raphson nonlinear iteration scheme. The computer code executes the solution by means of a front-type solver, which assembles a portion of the matrix and solves it before assembling the next portion of the matrix.
A 2-D model grid was developed based on topographic information and assigned parameters, such as Manning's roughness coefficient. Breach characteristics and a breach outflow hydrograph were incorporated into the 2-D grid, based on the breach

analysis and FLDWAV results. A sensitivity analysis was conducted to evaluate the RMA2 results.

RMA2 does not have sediment transport modeling capability, and therefore, SED2D computer model (Reference 2.4S.4-12b) was used to conduct sediment transport simulation using RMA2 results as the driving hydrodynamics. The SED2D model, developed by the USACE, included a dynamic inflow load of sediments that was developed based on the breach erosion and sediment load analysis. The SED2D results were then evaluated for sediment concentrations and deposition depths at any given location. The Surface Water Modeling System (SMS) (Reference 2.4S.4-12c) was used as the pre- and post-processor for RMA2 and SED2D models.

The following paragraphs discuss the failure scenarios considered for the initiation of the postulated MCR breach. An overtopping failure of the MCR embankment is not considered because the freeboard above the normal maximum operating level is greater than 15 feet.

The MCR embankment contains an internal drainage system that provides control of through-reservoir seepage and underseepage potential within the embankment. This prevents the phreatic surface (where the hydraulic pressure head is zero) from increasing within the embankment to such a level as to lead to a potential catastrophic exiting of water at the downstream face of the embankment. Since the upstream (reservoir side) of the embankment has a soil-cement facing, seepage potential through the embankment is greatly reduced. However, the failure scenario adopted for this study conservatively assumes that the internal drainage system within the embankment substantially fails to provide its intended seepage relief function. This failure could occur through:

- Disruption of the horizontal drainage blanket through either a seismic event or activity of a growth fault that causes a break in this drain system.
- Blockage of relief wells by debris, rodents, siltation from embankment toe drainage backwater, or other means.

Disruption of the horizontal blanket drains could occur through shifting of the horizontal material layer during a seismic event or through activity of a growth fault. According to Subsection 2.5S.3.8.1, the potential for deformation due to seismic activity at the STP site is negligible, and there are no capable tectonic faults within the site vicinity. The potential for non-tectonic deformation and growth faults at the STP site are discussed in Subsections 2.5S.3.2.2 and 2.5S3.8.2. It was concluded that the potential for permanent ground deformation from activity on the growth fault structure at the site is negligible. Additionally, the potential for non-tectonic deformation at the site and the potential for non-tectonic deformation from movement on growth faults are considered negligible. Therefore, it is very unlikely that a failure of the drainage blanket would occur due to a postulated seismic event or activity due to growth faults.

The blockage of relief wells could conceivably occur if the existing surface drainage system at the toe of the embankment drains slowly or becomes plugged, creating a backwater effect. This backwater situation would allow silt within the standing water to settle, thus filling the drainage outlets. The internal seepage would then build-up within the embankment. This pressure build-up would eventually exit at the downstream toe of

embankment. The saturation of the embankment could induce sloughing of the downstream toe section, providing a larger release area and a shorter flow path of seepage. Any free exiting of the seepage flow could allow movement of embankment material with subsequent generation of a piping failure.

The potential for an embankment failure due to piping caused by an uncontrolled water level build-up within the MCR embankment is considered very improbable for the following reasons: the engineered design of the MCR embankment; established operation and maintenance requirements that include embankment inspections and piezometer monitoring; the low probability of outlet drain plugging due to rodent activity; and the low probability of sediment deposition plugging the outlet drains. Therefore, the postulation of MCR embankment failure by piping is very conservative.

Subsection 2.4S.4.2.2.2 will be updated as shown in gray shaded text as follows:

2.4S.4.2.2.2 FLDWAV Flow Model Simulation

FLDWAV is a parametric, numerical model used to generate the breach outflow hydrograph based on user-input breach parameters. The breach parameters are estimated using empirical equations developed from case studies of historical dam failures.

2.4S.4.2.2.2.1 Initial (Starting) Water Level in the MCR

The starting water level in the MCR considered for the breach analysis was 50.9 feet. This level corresponds to the response of the MCR to one-half PMP on the normal maximum operating level plus the effect of wind set-up produced by the 2-year wind speed (50 mph) from the south (Reference 2.4S.4-7).

2.4S.4.2.2.2.2 Selection of the MCR Embankment Breach Parameters

Reference 2.4S.4-12d by the Dam Safety Office of the U.S. Bureau of Reclamation describes several dam failure case studies that support empirical breach parameter relationships, and is considered the most complete and knowledgeable source for estimation of dam breach parameters. The breach parameters for the MCR embankment breach analysis were established based on discussions within this reference.

The portion of the northern embankment in line with and due south of Units 3 and 4 is the closest to the units, and therefore is considered the most critical location for a breach of the MCR embankment, with respect to flooding at STP 3 & 4. The top elevation of the embankment in this area is approximately El. 65.75 ft. A service road runs along the toe of the exterior slope of the MCR northern embankment. Due to an anticipated large scour hole that would occur at the breach location, it was assumed that the road would be eroded. The terrain immediately downstream of the road is considered to be the control for the breach bottom elevation. Therefore, the breach bottom elevation was taken to be at El. 29 ft. Breach side slopes were taken to be 1 horizontal to 1 vertical, a ratio consistent with observations for earth-filled structures described in Reference 2.4S.4-12d.

Reference 2.4S.4-12d by the Dam Safety Office of the U.S. Bureau of Reclamation describes several dam failure case studies that support empirical breach parameter relationships. This reference describes several methods for estimating breach parameters. These methods include:

- Physically Based Methods: predicting the development of a breach and resulting outflow through use of an erosion model based on principles of hydraulics, sediment transport and soil mechanics.
- Parametric Models: using case studies of known dam failures to estimate time to failure and final breach geometry, then using these estimates within a computer model using principles of hydraulics.
- Predictor Equations: estimating peak discharge from empirical equations based on case studies of known dam failures.
- Comparative Analysis: using the breach shape and peak outflow of a dam that was of similar size and construction that had failed.

Physically based methods incorporate sediment transport and soil mechanics. In general, most of the available numerical dam breach models rely on bed-load type erosion formulas that utilize assumptions of gradually varied flow and relatively large flow depth in comparison to the size of roughness elements. These formulations are not consistent with the mechanics of the breaching process as observed in the field and in the laboratory. The other three methods listed above rely on case study data for selection of appropriate equations or parameters. In general, the database of well-documented dam failure case studies is small and contains few examples of very large storage volumes such as the Main Cooling Reservoir.

Of the various methods, the parametric model method is the most generally utilized method, the method having the greatest research, and the method fully described within Reference 2.4S.4-12d. Table 2 of Reference 2.4S.4-12d describes nine dam failure case studies that lead to empirical breach parameter relationships. The breach parameters consisting of breach bottom width, time to fail, and breach side slopes were established based on discussions within Reference 2.4S.4-12d, engineering judgment, and the comparison to the Teton Dam failure. Of all the dam failures presented in Reference 2.4S.4-12d, the Teton Dam failure was chosen for comparison because the failure mode was piping and the Teton Dam reservoir had one of the largest storage volumes presented, similar to the MCR. The storage volume in the Teton Dam reservoir was approximately 1.5 times the storage volume in the MCR, and the Teton Dam had a significantly larger breach height of 254 feet versus 21.9 feet in the MCR. Each parameter is estimated independently and conservatively for use in FLDWAV.

The breach bottom width was based on Froehlich (1995b), presented in Reference 2.4S.4-12d. Froehlich's equation, shown in Table 2.4S.4-5, predicts the largest breach width estimate of all methods presented in Reference 2.4S.4-12d. Froehlich's equation provides conservative breach width results in comparison with breach widths from observed dam failures. For example, Froehlich's equation predicts an average breach width of 220 m (722 ft) for the Teton Dam. However, the actual average breach width of Teton Dam at failure was only 151 m (495 ft). Therefore, the breach width determined for the MCR embankment using Froehlich's equation is considered conservative. Froehlich's equation predicts an average breach width of 417 feet. Given the trapezoidal geometry of the breach, the average breach width of 127 m (417 ft) yields a bottom

breach width of 116 m (380 ft = 417 - 2(65.75 -29) / 2)), which was used for FLDWAV embankment breach modeling.

Time to fail was based on the equation given by MacDonald and Langridge-Monopolis (1984) presented in Reference 2.4S.4-12d. This equation, shown in Table 2.4S.4-5, predicts a time to fail that came closest to describing a breach expansion rate meeting that of Teton Dam. Breach expansion rate is determined using the predicted breach width and the time to fail. Typical rates of expansion vary from 60 feet lateral per hour to 120 feet lateral per hour. Teton Dam displayed a fairly rapid rate of breach expansion. Based on information presented in Reference 2.4S.4-12d, the time from beginning of rapid growth of breach to significant lateral erosion process stopping at Teton Dam was estimated at 1.25 hours and the final breach width was 496 feet, resulting in an expansion rate of 198 feet per hour. This rapid rate of erosion was due to the higher hydraulic depth to drive the outflow and associated erosion. The MacDonald and Langridge-Monopolis equation predicts a time to fail of 1.7 hours for the MCR. This gives a breach expansion rate for the MCR of approximately 112 feet lateral per hour, which is smaller than the Teton Dam and considered acceptable.

Finally, the breach side slopes were assumed to be 1 vertical to 1 horizontal. This ratio is consistent with all researchers' observations for earth-filled structures, as discussed in Reference 2.4S.4-12d.

Table 2.4S.4-5 presents empirical equations from Reference 2.4S.4-12d and the resulting breach parameters.

~~Empirical relationships presented in Reference 2.4S.4-12d were used to determine the breach parameters consisting of (1) breach width, (2) time to failure, and (3) estimated peak flow from the breach, which was compared later to the peak flow from the breach resulting from FLDWAV modeling. Table 2.4S.4-5 presents empirical equations from Reference 2.4S.4-12d and the resulting breach parameters.~~

~~From Table 2.4S.4-5, it can be seen that Froehlich's equation yields the largest breach width estimate of all methods presented in Reference 2.4S.4-12d. Therefore, the Froehlich equation was used to estimate the breach width because it provides a conservative result in comparison with observed dam failures. Given the trapezoidal geometry of the breach, the average breach width of 417 feet yields a bottom breach width of 380 feet (417 - 2(65.75 -29)/2), which was used for FLDWAV embankment breach modeling.~~

~~The breach parameters estimated for the MCR embankment were also compared with the Teton Dam breach parameters, obtained from Reference 2.4S.4-12d. Teton Dam had more volume (310,000,000 m3) and a greater breach height, hb (86.9 m), which would allow significantly greater erosion to take place in creating the breach width. Froehlich's equation predicts an average breach width of 220 m (722 ft) for the Teton Dam. However, the actual average breach width of Teton Dam at failure was only 151 m (495 ft). Thus, Froehlich's equation over predicts the breach width; therefore, the breach width determined for the MCR embankment using Froehlich's equation is considered conservative.~~

~~Time to failure, presented in Table 2.4S.4-5, was based on the equation given by MacDonald and Langridge-Monopolis (Reference 2.4S.4-12d). The breach width erosion rate (380/2 = 190 ft in 1.7 hours) is 112 feet per hour, assuming erosion opens equally to right and left of centerline. In comparison, the Teton Dam displayed a fairly rapid embankment erosion rate (496/2 = 248 ft in 1.25 hours) of about 200 feet per hour (Reference 2.4S.4-12d). This rapid rate was due to the higher hydraulic depth at the time of failure, which provides more energy to drive breach propagation. The water depth in Teton Dam was more than 200 ft, whereas the water depth in the MCR is less than 30 ft. Therefore, the estimated time to failure and breach width for the MCR embankment breach are considered reasonable.~~

~~Reference 2.4S.4-12d states that the Froehlich equation as shown in Table 2.4S.4-5 is one of the better available methods for prediction of peak breach discharge, because it correlates well with observed dam failure peak flow rates. The peak discharge estimated from that equation is 62,600 cfs.~~

2.4S.4.2.2.2.3 MCR Embankment Breach Outflow Hydrograph

The outflow hydrograph from the MCR embankment breach, generated by FLDWAV based on the aforementioned initial conditions and breach parameters is presented in Table 2.4S.4-6. The peak breach outflow predicted by FLDWAV is 130,000 cfs.

The peak discharge predicted by FLDWAV is compared to peak discharge estimates from other methods. Reference 2.4S.4-12d states that the Froehlich equation as shown in Table 2.4S.4-5 is one of the better available methods for prediction of peak breach discharge, because it correlates well with observed dam failure peak flow rates. The peak discharge estimated using ~~, whereas~~ Froehlich's equation ~~estimates~~ is 62,600 cfs. The relationship of estimated peak discharges associated with the respective hydraulic head at time of failure from Reference 2.4S.4-12e is given in Figure 2.4S.4-13. From this figure, the peak flow for the MCR embankment breach is only 20,000 cfs, compared to 130,000 cfs as determined by the FLDWAV program. Therefore, the outflow hydrograph with a peak outflow of 130,000 cfs used in the breach analysis is conservative. To further verify the conservatism of the breach parameters and FLDWAV results, an independent analysis of the MCR embankment breach was performed using the BREACH model (Reference 2.4S.4-12e(1)) to predict the breach development and outflow hydrograph. This analysis is presented in Subsection 2.4S.4.2.2.2.4.

2.4S.4.2.2.2.3.1 Sensitivity Analysis of FLDWAV Parameters

A sensitivity analysis was performed on the breach parameters selected for use in the FLDWAV model. The time to fail and the breach bottom width were tested separately to determine the effect of these parameters on the peak discharge predicted using FLDWAV. The results of the sensitivity analysis are shown in Table 2.4S.4-6a.

The data shown in Table 2.4S.4-6a indicates that the breach width has a significant effect on peak discharge. This is reasonable since the large storage to height ratio of this structure would allow little change to the hydraulic head due to volume loss of the breach hydrograph for any of the breach widths analyzed. Therefore, the change in breach width would produce a directly proportional change in breach area, which would in turn produce a directly proportional change in peak discharge.

Timing does not appear to be a significant factor. Lengthening the time to fail reduces the peak discharge, however, this reduction is slight. The results of the sensitivity of these parameters indicate that the peak breach outflow is more sensitive to changes in breach width than to the time to fail, or the breach formation time.

2.4S.4.2.2.2.4 Confirmatory Analysis Using the BREACH Model

To verify the conservatism of the selected breach parameters and the FLDWAV results, an independent, confirmatory analysis of the MCR embankment breach was performed using the BREACH model. BREACH is a physically based mathematical model used to predict the breach development (breach size and time of formation) and the outflow hydrograph from the predicted breach of an earthen dam embankment (Reference 2.4S.4-12e(1)). Input data used by BREACH include embankment geometry and material properties, reservoir surface area-elevation relationship, and hydraulic characteristics of the channel formed directly downstream of the breach. BREACH couples the conservation of mass and momentum of the reservoir storage and breach outflow with the sediment transport capacity of the unsteady uniform flow along the breached channel. The growth of the breach is dependent on the dam embankment material properties (unit weight, friction angle, cohesive strength and particle size D_{50}, for which 50 percent of the soil particles in the embankment material are smaller). The model simulates the development of the breach through the mechanism of one or more sudden structural collapses that occur when the hydrostatic force exceeds the resisting shear and cohesive forces; enlargement of the breach width by slope stability theory; and initiation of the breach via piping with subsequent progression to a free surface breach flow. For the BREACH model analysis, piping is considered as the breaching mechanism.

2.4S.4.2.2.2.4.1 Assumptions used in the BREACH Model Analysis

The following assumptions were used for the BREACH model analysis of the MCR embankment:

1. It is assumed that the lateral expansion of the breach will not be limited geologically or structurally to either the right or left of centerline.

2. It is assumed that the piping starts at elevation 34.0 feet, which is the approximate centroid of the initial saturated zone in the failure scenario.

3. The downstream control location was assumed to be the ditch along a service road. Due to an anticipated large scour hole that would occur downstream of the breach location, the slightly perched road was assumed to be removed by erosion and the natural terrain immediately downstream of the road considered to be the control for the breach bottom elevation of 29 feet. A Manning's roughness coefficient of 0.06 was conservatively selected for the downstream channel routing reach. This reach has service roads, ditches, and small buildings that provide a roughness condition that would support the selected roughness coefficient. The downstream bottom slope was assumed to be 8 feet per mile.

4. The cross section of the embankment has a berm on the downstream slope at approximately elevation 35 feet. This berm extends outward approximately 45 feet

with a 6H:1V down slope. It was assumed that a potential breach mechanism would be an embankment slope failure that would, effectively, remove the berm altogether. Therefore, no effort was made in describing this berm cross section within the BREACH model. This is a conservative assumption.

5. The soil cement protective layer on the upstream slope of the embankment was not considered in the BREACH model. The assumed piping failure would generate a head-cut progressing from downstream to upstream. The head-cutting action would remove the material from behind the soil cement protection layer, undermining the slope protection. Since soil cement has little tensile strength, the soil cement would not be able to maintain its integrity when unsupported. However, it would be reasonable to expect that the soil cement would not crumble immediately but would require some time after a piping failure has progressed. In addition, the effect of the soil cement liner is to decrease the breach erosion rate and hence increase the time to peak, resulting in a decreased peak breach outflow rate. Therefore, it is conservative to exclude consideration of the soil cement liner.

2.4S.4.2.2.2.4.2 Sensitivity Analysis of BREACH Model Inputs

A sensitivity analysis was performed on selected embankment material parameters. The unit weight, internal friction angle and cohesive strength are based on field measurements or laboratory testing, and therefore sensitivity analyses were not performed for these three parameters.

It was found that varying both the critical shear stress coefficient and the critical stress coefficient (C_a and C_b) within their respective ranges recommended in Reference 2.4S.4-12e(1) had no effect on the predicted peak breach discharge. Also, varying the plasticity index (PI) from 0 to 40 had no effect on the predicted peak discharge. Decreasing the value of D_{50} to that of a fine clay material (0.0001 mm) increased the peak discharge by less than a percent. Therefore, the peak breach discharge is not considered sensitive to these four parameters.

Changing the ratio of D_{90} (the soil particle size for which 90 percent of the embankment material is smaller) to D_{30} (the soil particle size for which 30 percent of the embankment material is smaller) by a factor of two either way changed the peak discharge by about 3 percent and hence was considered non-sensitive. Using a D_{90} to D_{30} ratio of 16 produced a higher discharge, but this ratio would indicate a well-graded material, which is not the case for the embankment material. The porosity ratio also was found to have a fairly insignificant effect on the breach outflow results. The 0.35 porosity ratio used is considered to be an upper end value. A compacted soil porosity value of 0.20 would be reasonable to assume for the embankment. Using a porosity ratio of 0.20 reduced the peak discharge by about three percent. Therefore, the higher porosity value of 0.35 was considered to be conservative.

Of all the parameters, the Manning's n-value has the greatest effect on the predicted peak discharge. The Manning's n-value within the BREACH model is computed using the Strickler relation of roughness to the average grain size (D_{50}). The formula is defined as follows (Reference 2.4S.4-12e(1)):

$$n = 0.013 * (D_{50})^{0.67}$$

This formula produced an n-value of 0.001 for the MCR embankment. This value is unrealistically low. While using the BREACH model for Teton Dam breach analysis, Fread (Reference 2.4S.4-12e(1)) commented that the Strickler equation was judged not to be applicable for the fine breach material and used a relatively higher n-value of 0.013 for the analysis. For the present analysis a range of n-values were tested.

N-values similar to those for a natural channel with clay material on all sides of the flow path were estimated based on engineering judgment and methods developed by others such as Ven te Chow (Reference 2.4S.4-12e(2)). Using Table 5-5 within Reference 2.4S.4-12e(2), the n-value based on an earthen channel would be 0.02. Applying an additional 0.005 for irregularity of the flow channel, a combined total n-value of 0.025 was considered. The degree of irregularity and variation in cross section may be such that the overall n-value could be doubled, for an upper end value of 0.05. Therefore, an n-value within the range from approximately 0.025 to 0.05 was considered reasonable.

The BREACH algorithms are such that the lowest n-value considered, 0.025, produced a lower peak discharge than the highest n-value considered, 0.05. Therefore, consideration was given to a higher n-value of 0.08 that was still considered within the range of feasibility. Table 2.4S.4-6b presents the predicted peak discharge, breach width at time of peak discharge, time to peak discharge and reservoir level at time of peak discharge for each of the three n-values modeled. Figure 2.4S.4-13(a) presents the breach width development over time for all three n-values tested. The results of the sensitivity analysis indicate that higher roughness coefficients produce higher peak discharge values, which is counterintuitive. One explanation for this may be attributed to the model predicting a sudden collapse of the pipe section of the dam sooner with the lower n-values, thus lowering the peak discharge at a critical time. It is noted that the peak discharge and breach opening rate is based on several modeling algorithms that are balancing discharge forces, sediment transport rates and structural features with predicted storage depth and tailwater depth. An n-value of 0.05 is used in the FLDWAV analysis.

2.4S.4.2.2.4.3 BREACH Model Results and Comparison with FLDWAV

The BREACH model results showing breach width development with respect to time of breach formation are presented in Figure 2.4S.4-13(b). The breach width increases initially at a fairly constant rate for the first five hours, after which the rate of breach expansion decreases. The peak discharge of approximately 83,200 occurs when the breach bottom width is 361 feet. The reservoir water level continues to drop as water flows out of the reservoir through the breach and the downstream channel erodes as it carries the large outflow from the breach. It is noted that the rate of erosion would decrease substantially after the first five hours of the breach process. However, considering the large volume of water remaining in the MCR, the breach continues to expand with diminishing outflow and a decreasing breach width erosion rate. The final breach width reached after 30 hours is 448 feet.

Table 2.4S.4-6c and Figure 2.4S.4-13(c) provide a comparison of the results from BREACH and FLDWAV. The breach width and time to peak used as input to the FLDWAV program were conservatively estimated based on case studies of historical dam failures presented in Reference 2.4S.4-12d. FLDWAV assumed a linear increase

of the breach bottom width from 0 to a maximum width of 380 feet in 1.7 hours, which is the time the peak outflow occurs. The BREACH model produced the peak discharge 6.25 hours after the start of the breach development and allowed the breach width to continue to expand after the peak discharge. The BREACH model estimates a lower peak discharge as compared to the peak discharge predicted using the FLDWAV model. Even using an unrealistically high n-value of 0.08, the BREACH peak flow results are lower than the peak flow obtained with the FLDWAV model.

The BREACH model provides an independent assessment of the postulated breach of the MCR embankment at the STP 3 and 4 site. The BREACH model estimates a longer time to peak and a narrower breach width at the time of peak compared to the parameters selected for use in the FLDWAV model. BREACH also predicted a lower peak discharge than the peak discharge predicted using the FLDWAV model. Therefore, the parameters selected for FLDWAV and predicted breach hydrograph are considered conservative and acceptable.

Subsection 2.4S.4.2.2.4 will be updated as shown in gray shaded text as follows:

2.4S.4.2.2.4.1 Water Levels and Velocities

Critical STP 3 and 4 site locations for RMA2 model results are shown on Figure 2.4S.4-19. The variation in water surface elevation at these locations from 1.2 hours to 2.5 hours of the model simulation are presented in Figures 2.4S.4-20 and 2.4S.4-21 for the east breach and west breach, respectively. This selected period includes the peak water level and peak velocity near the plant buildings. The peak water level of 38.8 feet occurred at the Unit 4 Ultimate Heat Sink structure for the west breach scenario. Peak water surface elevations for the east breach and west breach are shown on the plan grid in Figures 2.4S.4-21(a) and 2.4S.4-21(b), respectively. Peak velocities associated with the east breach and west breach are shown in Figures 2.4S.4-21(c) and 2.4S.4-21(d), respectively. The maximum velocity of the flood flow was found to be 4.72 feet per second and occurred between Units 3 and 4 (point 8 on Figure 2.4S.4-19). The variation in velocity at locations 1 through 8 for the period containing peak velocities for the east and west breach scenarios is shown in Figures 2.4S.4-21(e) and 2.4S.4-21(f), respectively.

As discussed above, the flood simulation provides peak water depth and peak velocity values at critical STP 3 and 4 site locations. Peak flood discharges per unit width near the power block buildings may be estimated using these values. Table 2.4S.4-7a provides examples of peak discharge per unit width estimated for locations near the Unit 4 UHS, the power block on the south side of Unit 4, and at a location between Units 3 and 4. These estimates are based on the west breach simulation results for peak water surface elevation and peak velocity, as shown in Figures 2.4S.4-21 and 2.4S.4-21(f), respectively. The water depths are obtained by subtracting the nominal site grade elevation in the power block of 34 feet from the peak flood water surface elevations.

A sensitivity analysis was conducted to determine the effect of boundary condition on the resulting water levels. The analysis indicated that changing the water surface elevation at the downstream boundary from 32.5 feet to 34 feet does not affect the peak flood levels for the site.

Subsection 2.4S.4.2.2.4 will be updated as shown in gray shaded text as follows:

2.4S.4.2.2.4.5 Duration of Inundation at Safety-Related SSCs

The duration of inundation at the power block is considered to be the duration during which the flood elevations are greater than the grade elevation of 34 feet. Since the primary purpose of the breach flood modeling was to determine the maximum flood elevation at safety-related facilities, the simulation was terminated after the maximum flood elevation was reached, well before all the water had drained from the site. As a result, a full RMA2 simulation for the duration of the flood water above elevation 34 feet was not performed. However, a reasonable estimate of this duration of inundation can be obtained by relating the resulting flood elevations generated from the RMA2 run to the corresponding flow rates from the breach outflow hydrograph, occurring at the same time. The flood elevations and outflows are plotted on the same graph with time as the common base, as shown in Figure 2.4S.4-21(j). Extrapolated flood elevations were estimated by fitting a non-linear polynomial regression curve. The time elapsed between the two points corresponding to a flood elevation of 34 feet at the power block is estimated at 20.5 hours. Therefore, the estimated duration of inundation (above 34 feet) at safety-related SSCs is 20.5 hours.

The following references will be added:

2.4S.4-12e(1) Fread, D. L., BREACH, "An Erosion Model for Earthen Dam Failures", Hydrologic Research Laboratory, Office of Hydrology, National Weather Service, U.S. National Oceanic and Atmospheric Agency, Silver Spring, Maryland, July, 1988.

2.4S.4-12e(2) Chow, Ven te, Open Channel Hydraulics, McGraw-Hill Book Company, 1959.

The following table will be revised as shown in gray shaded text:

Table 2.4S.4-5 MCR Embankment Breach Parameters and Peak Discharge Based on Empirical Equations from Reference 2.4S.4-12d

Parameter	Equation	Results
(1) Time to Failure (hrs)	$t_f = 0.0179(0.0261(V^*h_w)^{0.769})^{0.364}$	1.7 hours
(2) Average Breach Width (m)	$B_{ave} = 0.1803\ V^{0.32}\ h_b^{0.19}$	127 m (417 ft)
(3) Peak Flow Q (m^3/s)	$Q_p = 0.607\ V^{0.295}\ h_w^{1.24}$	1172.8 m^3/s (62,600 cfs)

B_{ave} = average breach width

h_w = depth of water above breach in m = 50.9' – 29' = 21.9' = 6.7 m

h_b = the height of breach from the top of embankment in m = 66' – 29' = 37' = 11.3 m

V = volume of water in the MCR between El. 29' and El. 50.9' in m^3 = 188,400,000 m^3 (152,700 ac-ft)

(1) MacDonald and Langridge-Monopolis Time to Failure

(2) Froelich's Average Breach Width

(3) Froelich's Peak Flow

The following table will be added to the FSAR:

Table 2.4S.4-6a Results of Sensitivity Analysis for Breach Parameters Selected for use with FLDWAV

Parameter	Time to Fail t_f (hours)	Percent Difference	Breach Width B (ft)	Percent Difference	Peak Flow Qp (cfs)	Percent Difference
Adopted	1.7		380		130,000	
Increased t_f	1.4	18			132,000	+1.5
Decreased t_f	2.0	18			128,200	-1.1
Increased B			446	18	157,700	+21
Decreased B			310	18	104,400	-20

The following table will be added to the FSAR:

Table 2.4S.4-6b Comparison of Manning's n-value to BREACH Analysis Results

Manning's Roughness Coefficient (n-value)	Peak Discharge (cfs)	Time to Peak (hrs)	Breach Bottom Width at Peak Flowrate (ft)	Final Breach Bottom Width (ft)	Reservoir Water Level at Time of Peak Flowrate (ft)
0.025	30,760	15.9	132	179	46.4
0.05	83,200	6.25	361	448	46.8
0.08	122,800	2.4	465	619	48.9

The following table will be added to the FSAR:

Table 2.4S.4-6c Comparison of Results from BREACH and FLDWAV Models

Model	Peak Discharge (cfs)	Time to Peak (hrs)	Breach Bottom Width at Time of Peak Flowrate (ft)
FLDWAV	130,100	1.7	380
BREACH	83,200	6.25	361

The following table will be added to the FSAR:

Table 2.4S.4-7a Peak Flood Discharge per Unit Width at Safety-Related SSCs

Location	Water Surface Elevation (ft)	Water Depth (ft)	Peak Velocity (ft/s)	Peak Discharge per Unit Width (cfs/ft)
Unit 4 UHS	38.8	4.8	0.4	1.9
Unit 4 Power Block, South	38.2	3.8	3.8	14.4
Between Unit 3 and Unit 4	37.6	4.25	4.4	18.7

NOTE: The examples above are based on the West Breach simulation.

The following figure will be added to the FSAR:

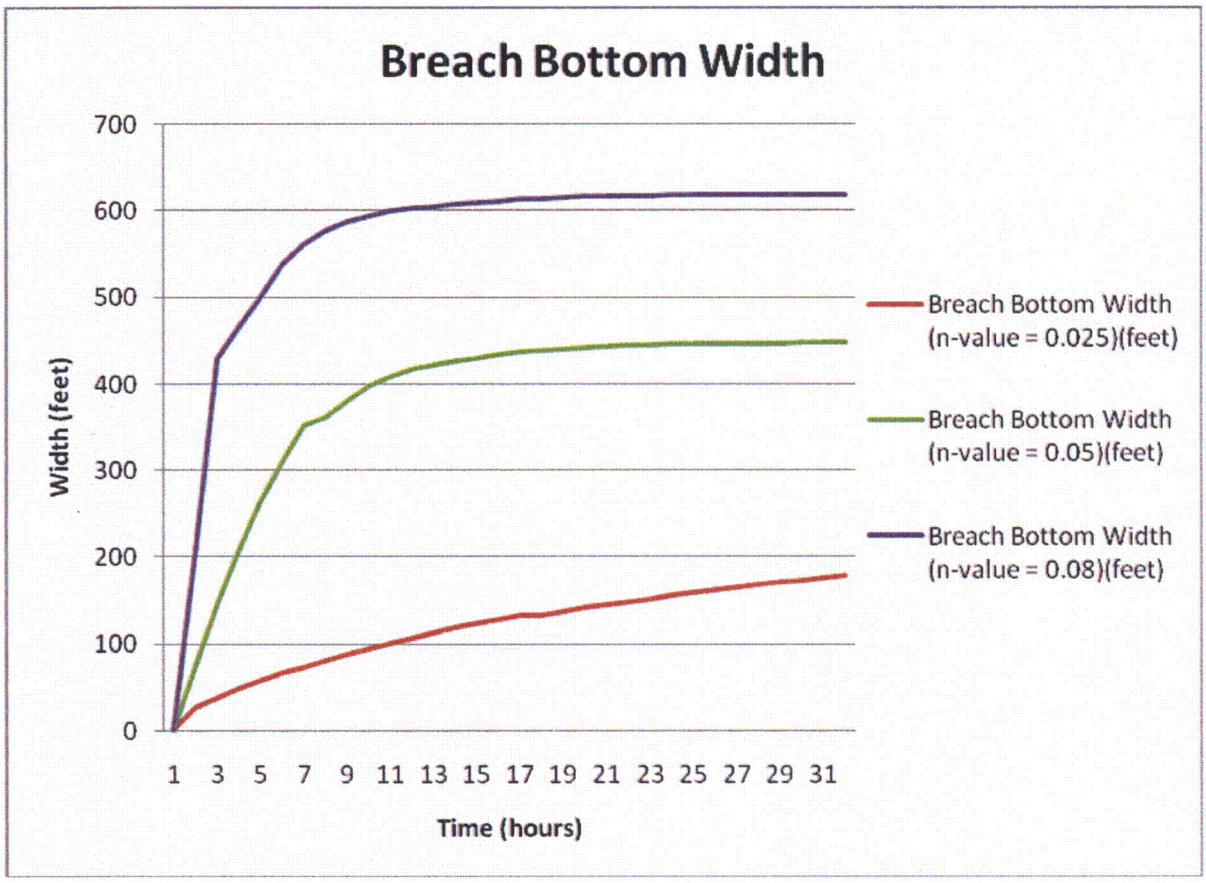

Figure 2.4S.4-13a Breach Width Development for Different n-values

The following figure will be added to the FSAR:

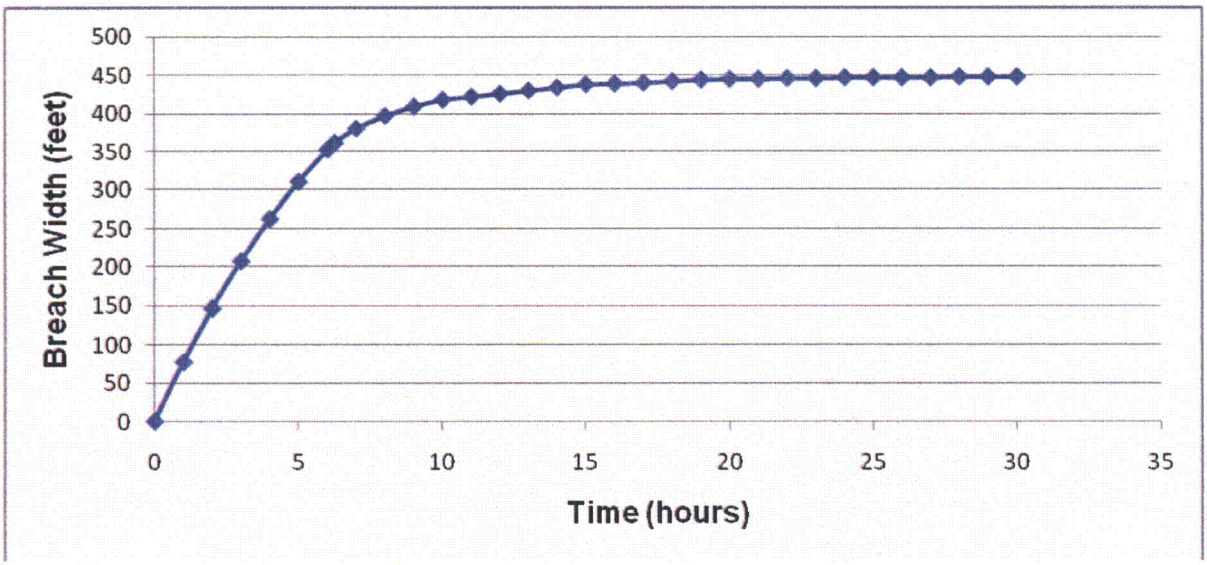

Figure 2.4S.4-13b Breach Bottom Width Development from BREACH analysis

The following figure will be added to the FSAR:

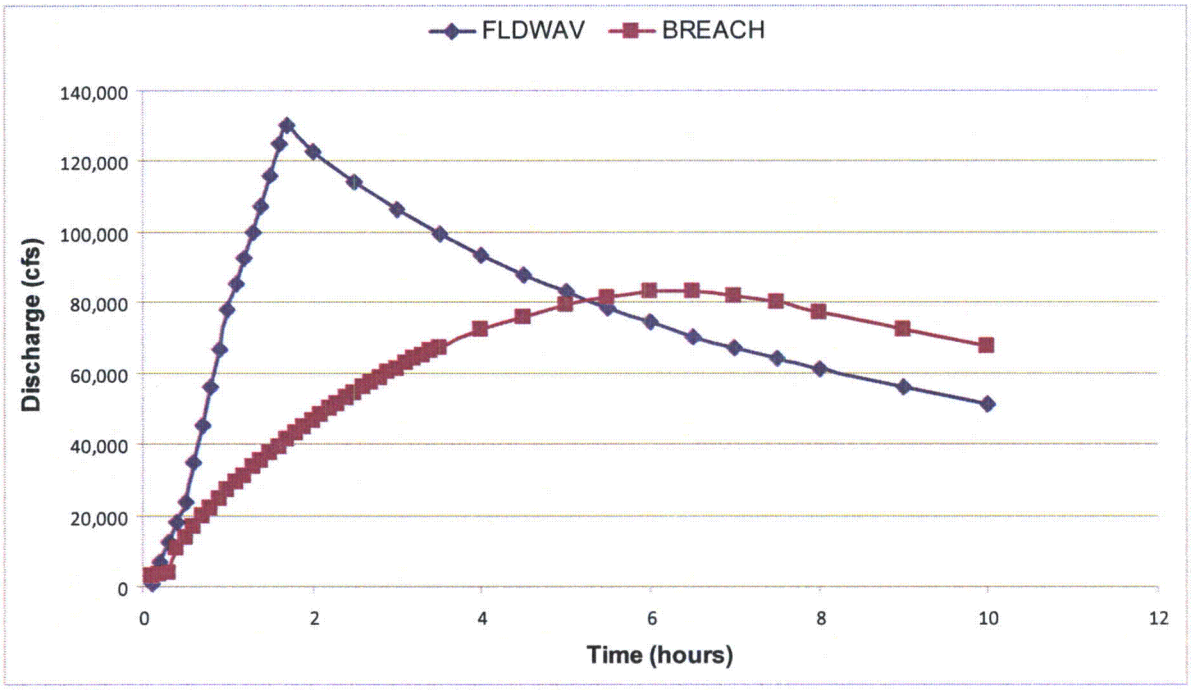

Figure 2.4S.4-13c Comparison of BREACH and FLDWAV Outflow Hydrographs

The following figure will be added to the FSAR:

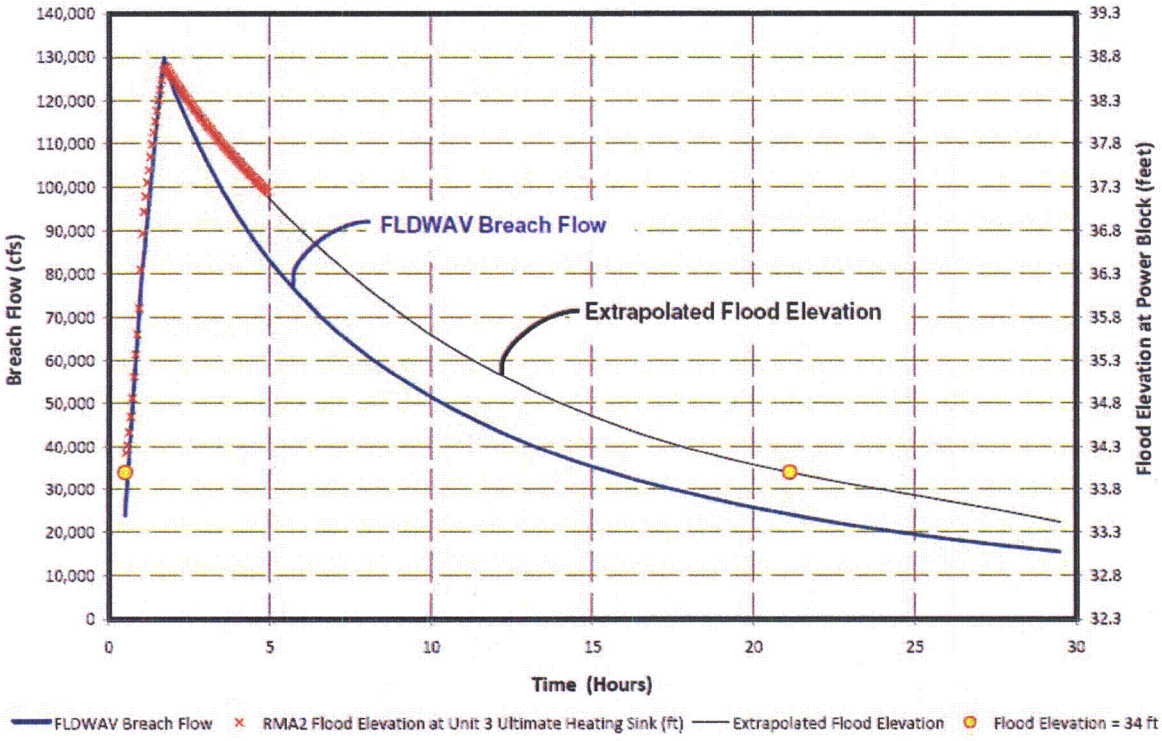

Figure 2.4S.4-21j Breach Outflow and Flood Elevation to Determine Duration of Inundation at Safety-Related SSCs

02.04.04-15

QUESTION:

Provide FSAR updates that address the issues raised above: (1) justification for reliability and accuracy of RMA2 predictions at the STP site, (2) selection and justification of a reasonable value for the DEPLIMIT parameter, (3) a description of results of the SED2D simulation(s) that use the selected value of the DEPLIMIT parameter, (4) a qualitative and quantitative description of sediment deposition and scouring in the powerblock area, (5) a description of the physical and hydraulic integrity of the powerblock surface following the flood event, (6) a description of sediment mass balance for the SED2D simulations, (7) sediment deposition height and scouring depth maps within the powerblock area, (8) citations for precedents for the use of artificial sumps in applications of RMA2/SED2D.

Characteristics of the design-basis flood (e.g., flow velocities, scour, deposition) and post-construction cover (e.g., surface material map, associated properties) are to be consistent in RAIs 5101 and 5105. If the design-basis flood is revised, the revised characteristic shall be applied in FSAR Sections 2.4S.12 and 2.4S.13.

RESPONSE:

(1) A discussion of the reliability and accuracy of the RMA2 model is added to Subsection 2.4S.4.2.2.3. Refer to FSAR markup.

(2) Subsection 2.4S.4.2.2.4.2 is updated to describe the selection and justification of the value for the DEPLIMIT parameter used in the SED2D analysis. Refer to FSAR markup.

(3) Subsection 2.4S.4.2.2.4.2 is updated to describe how the DEPLIMIT parameter affects the SED2D results. Refer to FSAR markup.

(4) Subsection 2.4S.4.2.2.4.2 is updated to describe sediment deposition and scouring observed during the model simulation. Refer to FSAR markup.

(5) A description of the integrity of the powerblock surface following the flood event is included in Subsection 2.4S.4.2.2.4.2. Refer to FSAR markup.

(6) Subsection 2.4S.4.2.2.4.2 is updated to include a description of sediment mass balance for the SED2D simulations. Refer to FSAR markup.

(7) Figures 2.4S.4-21f1 and 2.4S.4-21f2 provide sediment deposition height maps. As discussed in Subsection 2.4S.4.2.2.4.2 the anticipated erosion/scouring within the powerblock area is not significant.

(8) Citations for precedents for the use of artificial sumps in applications of RMA2/SED2D have been added to Subsection 2.4S.4.2.2.3.1.

The FSAR will be revised as follows as a result of this response:

Subsection 2.4S.4.2.2.3 will be updated as follows:

2.4S.4.2.2.3 RMA2 and SED2D Two-Dimensional Model Simulations

After developing the maximum credible breach scenario, resulting hydrograph and resulting embankment erosion rates, the next step is to route the breach hydrograph to the safety-related facilities. Because of the complex topography of the site, a 2-dimensional (2D) simulation was considered appropriate. The RMA2 and SED2D models were selected to conduct the 2D hydrodynamic and sediment transport simulations. These models have been widely used and are part of the model package supported by US Army Corps of Engineers (Reference 2.4S.4-12a). RMA2 and SED2D have been used widely to conduct dynamic simulations of water level, velocity distribution and sediments in rivers, reservoirs, and estuaries, and are considered an acceptable tool to model the flood flow from the MCR embankment breach. The Surfacewater Modeling System (SMS) was used as the pre- and post-processor for RMA2 and SED2D.

2.4S.4.2.2.3.1 Bathymetry Elevations and Two-Dimensional Grid Development

The topography of the STP site was used to determine model bathymetry for routing the flood flow resulting from the MCR embankment breach. The 2-D grid was developed using: (1) STP Site Topography; (2) STP Units 3 and 4 Site Grading Plan; and (3) STP Units 3 and 4 Plot Plan. The grading plan around Units 3 and 4 power block site is shown in Figure 2.4S.4-14. The grade elevation at the center of the power block is EL. 36.6 ft and slopes to El. 32 ft at the four corners. Facilities included in the model grid are the Reactor, Turbine, Control, Radwaste, Service and Hot Machine Shop buildings for Units 1 through 4. The Ultimate Heat Sinks for Units 3 and 4 and Essential Cooling Pond (ECP) for Units 1 and 2 were also included in the model grid.

The datums of the 2-D grid are in NAD 27 State Plane Texas South Central for the horizontal datum and NGVD 29 for the vertical datum. The northern embankment of the MCR was selected as the southern boundary of the 2-D grid, and road FM 521 was chosen as the northern boundary of the grid. The western and eastern boundaries of the grid were selected to be sufficiently far from Units 3 and 4 so the target area is not impacted by the model boundaries (Figure 2.4S.4-15).

To assist the 2-D model stability associated with the wetting and drying of model elements and to further ensure that the target area is not impacted by model boundaries, a hypothetical sump was modeled along the east, north, and west boundaries of the developed 2-D grid outside of FM-521. The use of the sump to help with model stability is a common practice in the 2-D modeling field. Reference 2.4S.4-12e3 and Reference 2.4S.4-12e4 describe the use of sumps in physical models to control (and vary) the boundary conditions for calibration and the concept of "hybrid modeling" where results from a physical model of a complex region are used as input or boundary conditions for a comprehensive numerical model. References 2.4S.4-12e5 through 2.4S.4-12e8 show precedents for the use of artificial sump in RMA2/SED2D applications ~~and t~~ The

sensitivity analysis described below indicates that the hypothetical sump has no impact on model results in and around Units 3 and 4. As a result, the developed 2-D grid (excluding the artificial sump area) covers an area of 1,477 acres: 5,873 ft in the north-south direction, and 12,455 ft in the east-west direction. Figures 2.4S.4-16 and 2.4S.4-17 show the 2-D grid with elevations for the east breach and west breach, respectively. The sump is the deeper area on the outside of the model grid. The 2-D grid includes 2,348 nodes and 1,088 elements. The size and location of these elements were selected to best represent physical features, particularly around Units 3 and 4. The areas of the 2-D elements range from about 2,500 square feet near the reactor buildings to about 144,000 square feet away from the units.

Subsection 2.4S.4.2.2.4.1 will be updated as follows:

2.4S.4.2.2.4.1 Water Levels and Velocities

Critical STP 3 and 4 site locations for RMA2 and SED2D model results are shown on Figure 2.4S.4-19. To determine the maximum effect on each of the units 3 and 4, separate east and west breach locations were simulated. The variation in water surface elevation at these locations from 1.2 hours to 2.5 hours of the model simulation are presented in Figures 2.4S.4-20 and 2.4S.4-21 for the east breach and west breach, respectively. This selected period includes the peak water level and peak velocity near the plant buildings. The peak water level of 38.8 feet occurred at the Unit 4 Ultimate Heat Sink structure for the west breach scenario. Peak water surface elevations for the east breach and west breach are shown on the plan grid in Figures 2.4S.4-21(a) and 2.4S.4-21(b), respectively. Peak velocities associated with the east breach and west breach are shown in Figures 2.4S.4-21(c) and 2.4S.4-21(d), respectively. The maximum velocity of the flood flow was found to be 4.72 feet per second and occurred between Units 3 and 4 (point 8 on Figure 2.4S.4-19). The variation in velocity at locations 1 through 8 for the period containing peak velocities for the east and west breach scenarios is shown in Figures 2.4S.4-21(e) and 2.4S.4-21(f), respectively.

Subsection 2.4S.4.2.2.4.2 will be updated as follows:

2.4S.4.2.2.4.2 Effects of Sedimentation and Erosion

The MCR embankment breach analysis also considered the material eroded during the breach. The embankment material eroded is comprised mostly of clay, with a small percentage of sand from the internal drainage system and soil cement from the interior embankment slope lining. The erosion process will also produce a scour hole downstream of the breach that extends below the breach bottom elevation. The dimensions of this scour hole, based on lab results from Reference 2.4S.4-12i, are estimated to be 20 feet deep, 203 feet long and 380 feet wide. The scour hole contributes 1,543,000 cubic feet of clay to the flood flow. The material eroded from the MCR embankment contributes an additional 1,697,314 cubic feet of clay; 75,644 cubic feet of sand; and 117,562 cubic feet of soil cement. The total volume of sediment eroded under the breach scenario is 3,433,517 cubic feet. The flood flow from the MCR embankment breach would not cause erosion ~~aterode~~ the STP 3 and 4 plant site area because surfacing in this area is mostly concrete or asphalt pavement or compacted stone surfacing~~gravel and grass~~. The maximum velocity of 4.72 ft/s would not cause

severe erosion of these surfaces, and any minor erosion around corners of the buildings would not impact the safety-related facilities of Units 3 and 4. Therefore, the integrity of the power block surfacing would remain intact following the MCR embankment breach flood.

SED2D sediment modeling indicated some deposition on the outer edge of the model domain and relatively little deposition within the STP site. Figures 2.4S.4-21(f1) and 2.4S.4-21(f2) show the sediment accumulation pattern with accumulation at points where current velocities are relatively low for the east and west breaches, respectively. Table 2.4S.4-7b shows the amount of sediment accumulation at locations defined in Figures 2.4S.4-21(f3) and 2.4S.4-21(f4). These sediment deposition locations only involve a single 2D grid node, i.e. the node with sediment accumulation depth is surrounded by nodes with no sediment accumulation at all. This single-node result indicates isolated settling location due to very localized small velocity at the node. These results are consistent with the sediment concentration results in that the majority of the clay and sand loads would be suspended in the flood flow and washed downstream, beyond the STP site. SED2D modeling provides point elevation results that are not easy to integrate into a volume over a large area, but the small accumulation within the study area (Figures 2.4S.4-21f1 and f2) and the large accumulations noted in the sump outside of FM 521 indicated that the great majority of the sediment eroded settled in the model sump outside of FM 521. The localized single-node sediment accumulation predicted by SED2D also makes it impractical to apply the underlying 2D element area for sediment accumulation volume calculations because it will greatly over-estimate the amount of accumulated sediment volume if an artificial "pyramid" were assumed to be the sediment accumulation volume. While the user's manual of SED2D does not provide specific information about sediment mass balance in a model simulation, it states that the derivation of the SED2D model formulation is based on the basic convection - diffusion equation (Reference 2.4S.4-12j). This basic convection - diffusion equation is a mass balance equation based on the conservation of mass (Reference 2.4S.4-12k). Therefore, mass balance is embedded in the fundamental equations of SED2D and sediment mass balance is maintained by the program during the simulation.

The soil cement lining on the interior wall of the embankment was not simulated. This material would likely enter the water as chunks or blocks as the embankment collapses, and these large concrete blocks would be carried only a short distance from the breach before settling to the bottom. The sediment loading would cease when the breach opening expansion ends; however, low-sediment ~~free-high~~ flows would continue for a number of hours~~long-period~~ afterwards until the water in MCR is totally emptied. This continued~~high~~ flow period would prevent any remaining clay or sand particles from settling ~~and would wash away any small depositions in the study area~~.

The RMA2 and SED2D models are designed to function together. If sedimentation from SED2D results in a significant change in depth, the simulation can be stopped and the depth grid for the RMA2 model adjusted to reflect the changes in topography. This can be important for long-term simulations where a change in depth and resulting current velocities can interact with the settling process and affect the results of the simulations. The SED2D model employs a parameter termed DEPLIMIT that is used to test whether bottom elevation changes due to sediment deposition or scouring might produce a significant effect on current velocities. A DEPLIMIT value of 0.25 is a default value in SED2D that is designed to terminate SED2D execution wherever and whenever a

sediment scour or deposition depth is higher than 25 percent of the water depth at the location and time of the exceedance.

During the breach scenario, water velocities in most parts of the project area are too high to allow settling of the predominantly clay material. Most of this material would be carried to the north of FM 521 and ultimately flow to the Colorado River. However, because the artificial sump area is a large and relatively quiescent zone outside of FM 521, it is the location in the model where most of the sediment deposition takes place. With a 0.25 value of DEPLIMIT, the SED2D simulation would be terminated prematurely and extensive iterations between RMA2 and SED2D would be required. The solution was to select a large DEPLIMIT parameter (50,000,000) so that it did not produce inappropriate model terminations. By having DEPLIMIT set to a big number we were able to complete the run and then check the SED2D results to ensure that no significant sediment accumulation occurred within the real project domain. This was determined to be the only reasonable approach for handling the DEPLIMIT parameter.

To test if selecting a large DEPLIMIT parameter was a potential issue, a sensitivity analysis was performed using the ultimate sediment accumulations within the STP site to create a revised RMA2 grid. The results of these sensitivity simulations for both the east and west breach scenarios are shown on Figures 2.4S.4-21(f5) and 2.4S.4-21(f6). The maximum velocity differences (up to 1 ft/s) occurred near the sediment deposition locations, which are a few local areas of low velocity. These figures show that velocity differences are very small over the rest of the power block area. No significant difference in the maximum current velocities between the two elevation grids, except at localized grid points, indicates that the sediment accumulation effect is not significant in this very short term simulation. From this it was concluded that the selected large DEPLIMIT parameter set to avoid model terminations was appropriate to the particular simulations, and it does not impact the simulated water surface elevation or sediment deposition in the vicinity of safety-related SSCs. The areas around the SSCs are high velocity areas where little or no sediment accumulation was predicted by the model.

Subsection 2.4S.4.2.2.4.4 will be updated as follows:

2.4S.4.2.2.4.4 Spatial Extent of Flooding Due To MCR Embankment Breach

For both the east and west MCR embankment breach scenarios flood water from the breach opening will flow through the area encompassing Units 1 and 2 and Units 3 and 4, and will spread into the area bounded by FM 521. The model simulations end at the boundary cells immediately outside of FM 521. This road has a top of road elevation of approximately 28 feet to 30 feet, as seen from the USGS topographic map of the area (Figure 2.4S.4-21(i)). North of FM 521 and west of the west MCR embankment there are levees with approximate top elevations of 29 feet to 30 feet. South of the MCR along its south embankment is an east - west canal with levees on both sides. The area around the STP plant has an approximate grade elevation varying from 25 feet to 30 feet.

The area around the STP plant slopes east towards the Colorado River. Therefore, most of the flood water from the breach would flow to the Colorado River. A portion of the breach flow will also reach the Little Robins Slough to the west, which flows south along the west MCR embankment. From there, the water will either flow east to the Colorado

River or will flow under the east-west canal through existing siphons and may flow through several swampy areas to the intracoastal waterway.

~~It is unlikely that the breach flood water will overflow over FM 521 and west levees. If this happens, a~~A small portion of the breach flood flow may reach the Tres Palacios River to the west of the STP site.

The following references will be added:

2.4S.4-12e3 Ettema, R. Hydraulic modeling: concepts and practice. Environmental and Water Resources Institute (U.S.). ASCE Publications. 390 pages. 2000.

2.4S.4-12e4 Hughes, S.A. 1993. Physical Models and laboratory techniques in coastal engineering. USACE. ERDC.

2.4S.4-12e5 Su, Y.C., E. Lehotsky, and D. Fuller. 2009. "The Sabine Pass LNG Terminal, Challenges for a new LNG Terminal in Louisiana", Caring for the Coast. Texas Coastal Conference 2009, Galveston, Texas, June 4-5, 2009.

2.4S.4-12e6 Su, Y.C. and J. Mahmoud. 2007. Beneficial use of dredged materials at Louisiana shoreline near Sabine Pass. International Erosion Control Association Conference, Reno NV.

2.4S.4-12e7 Su, Y.C., J. Koutny, J. Benoliel, J. Mahmoud, M. Heaney, and D. Granger. 2005. "Sediment Transport Modeling of Dredged Disposal Materials Near Sabine Pass." Coastal Texas 2020 Technical Erosion Conference 2005, Houston, Texas, September 14-16, 2005.

2.4S.4-12e8 Su, Y.C., C. Woodward, J. Koutny, and J. Benoliel, and W. Crull. 2004. "Modeling of Flood Control Channels Using SMS/RMA2." TFMA 17th Annual Texas Flood Conference, Fort Worth, Texas, 2004.

2.4S.4-12j Ariathurai, M. R., MacArthur, R. C., and Krone, R. B. "Mathematical Model of Estuarial Sediment Transport," Technical Report D-77-12, US Army Engineer Waterways Experiment Station, Vicksburg, Mississippi, 1977.

2.4S.4-12k Clark, Mark M., Transport Modeling for Environmental Engineers and Scientists. Department of Civil and Environmental Engineering, University of Illinois at Urbana-Champaign, Urbana, Illinois. Pub. John Wiley & Sons. 559 pp. 1996.

The following table will be added to the FSAR:

Table 2.4S.4-7b Ultimate Sediment Accumulation Depths at Selected High-Deposition Locations for Both East znd West Breach Scenarios

East Breach Scenario		West Breach Scenario	
Location	Sediment Deposition Depth (ft)	Location	Sediment Deposition Depth (ft)
Point 1	8.2	Point 1	7.5
Point 2	9.4	Point 2	10.2
Point 3	8.6	Point 3	5.1
Point 4	5.5	Point 4	7.4
Point 5	3.9	Point 5	3.5
Point 6	1.2	Point 6	1.9
Point 7	1.7	Point 7	1.5
Point 8	2.4	Point 8	1.8
Point 9	1.8	Point 9	2.1
Point 10	1.3	Point 10	1.4
-	-	Point 11	1.4

Note: The listed Sediment Deposition Depths are SED2D output at corresponding reference point locations only. (See Figures 2.4S.4-21(f3) and 2.4S.4-21(f4)) The SED2D outputs show zero sediment deposition at 2D grid nodes surrounding these reference locations.

The following figure will be added to the FSAR:

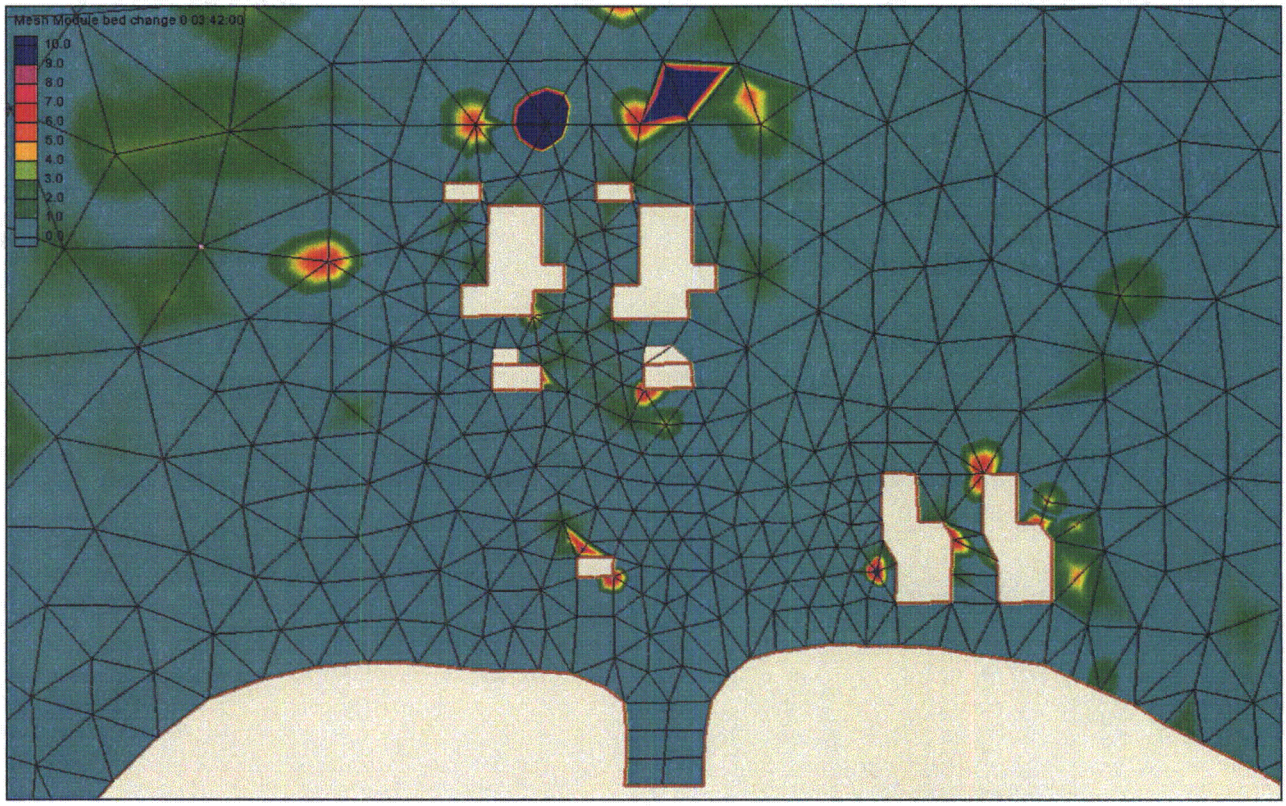

Figure 2.4S.4-21f1 Sediment Accumulation (in feet) from East Breach Scenario

The following figure will be added to the FSAR:

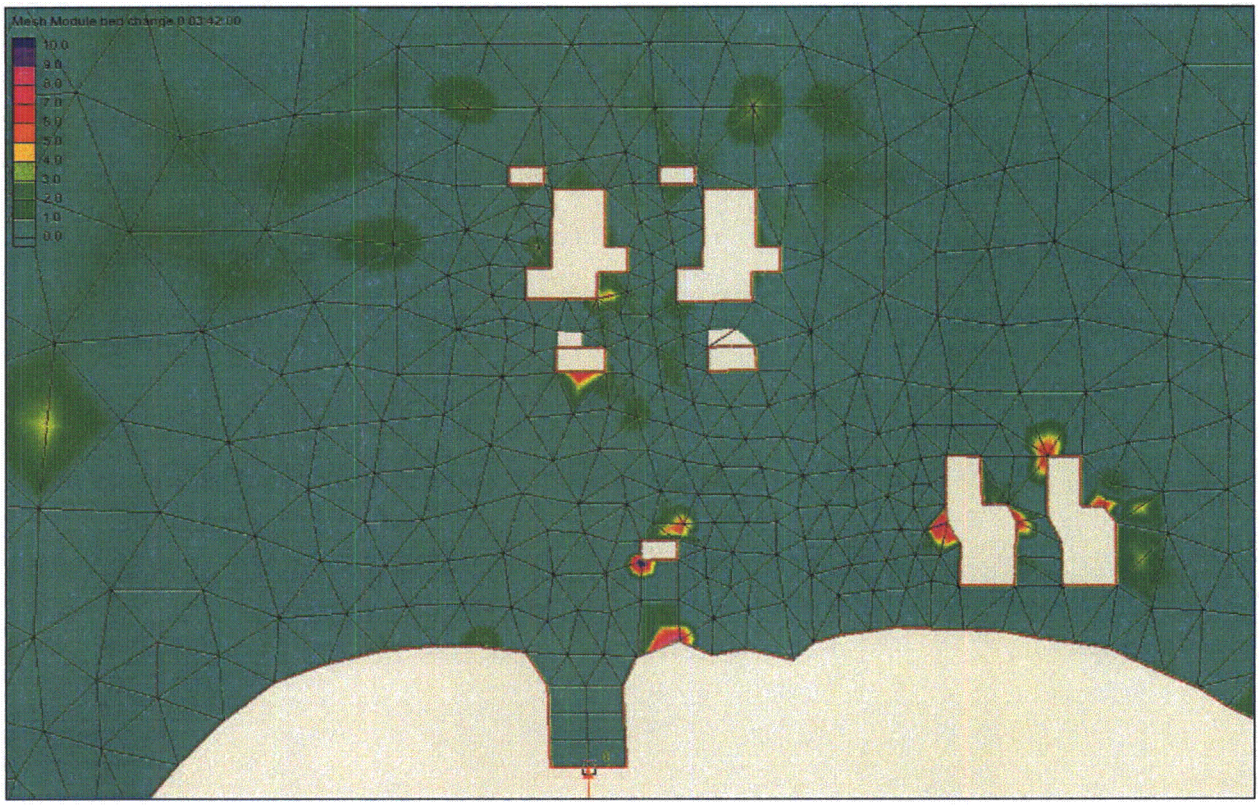

Figure 2.4S.4-21f2 Sediment Accumulation (in feet) from West Breach Scenario

The following figure will be added to the FSAR:

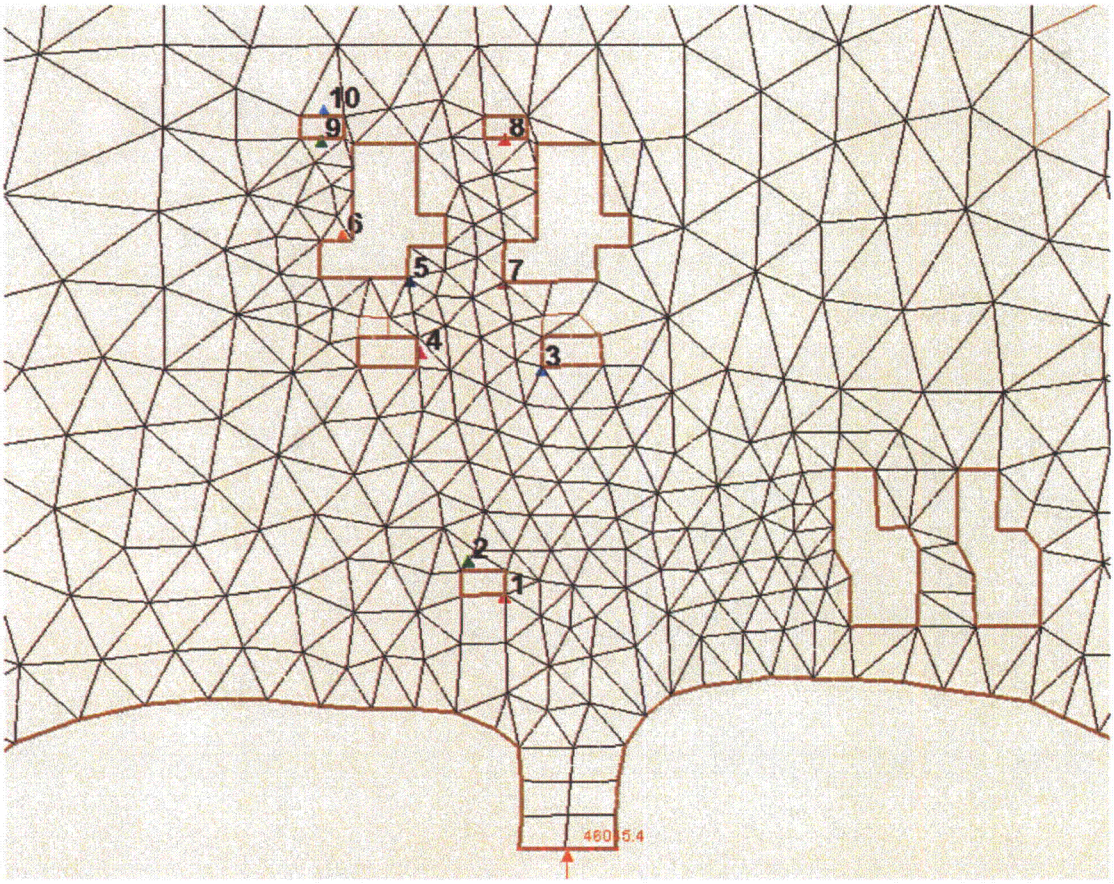

Figure 2.4S.4-21f3 Locations for Sediment Accumulation for East Breach Scenario

The following figure will be added to the FSAR:

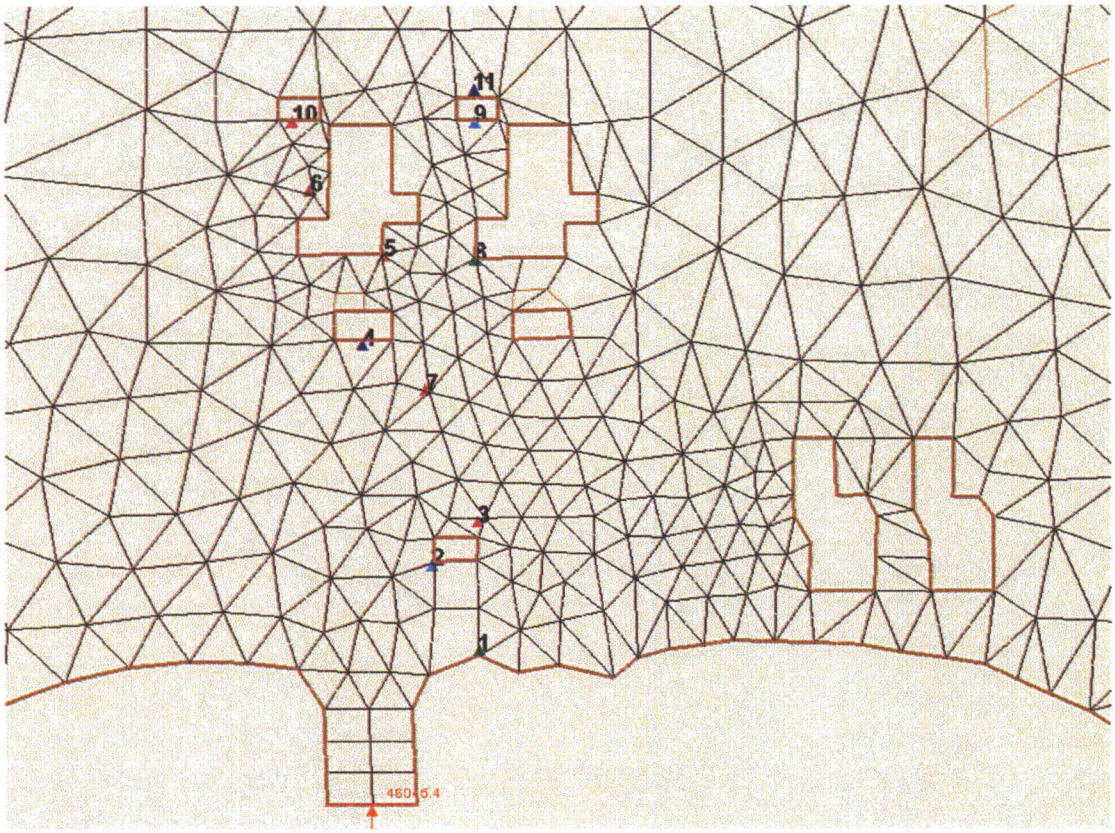

Figure 2.4S.4-21f4 Locations for Sediment Accumulation for West Breach Scenario

The following figure will be added to the FSAR:

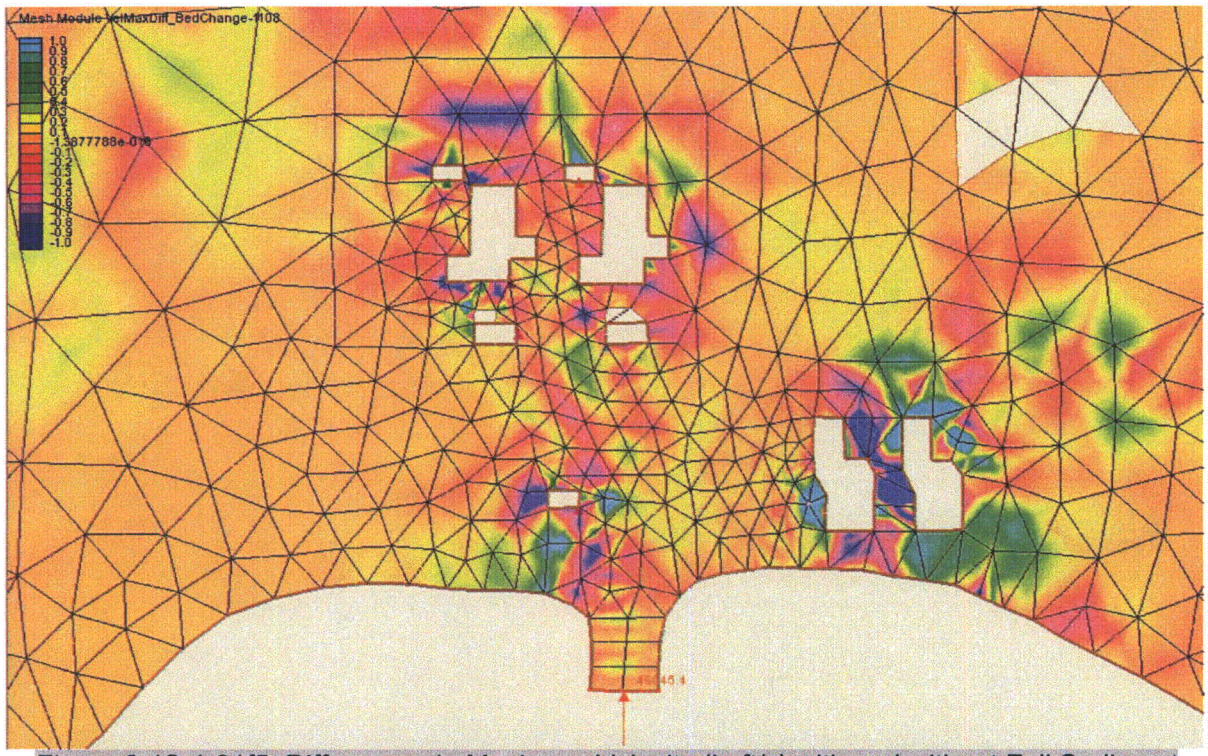

Figure 2.4S.4-21f5 Differences in Maximum Velocity (in ft/s) with and without Full Sediment Accumulation for East Breach Scenario

The following figure will be added to the FSAR:

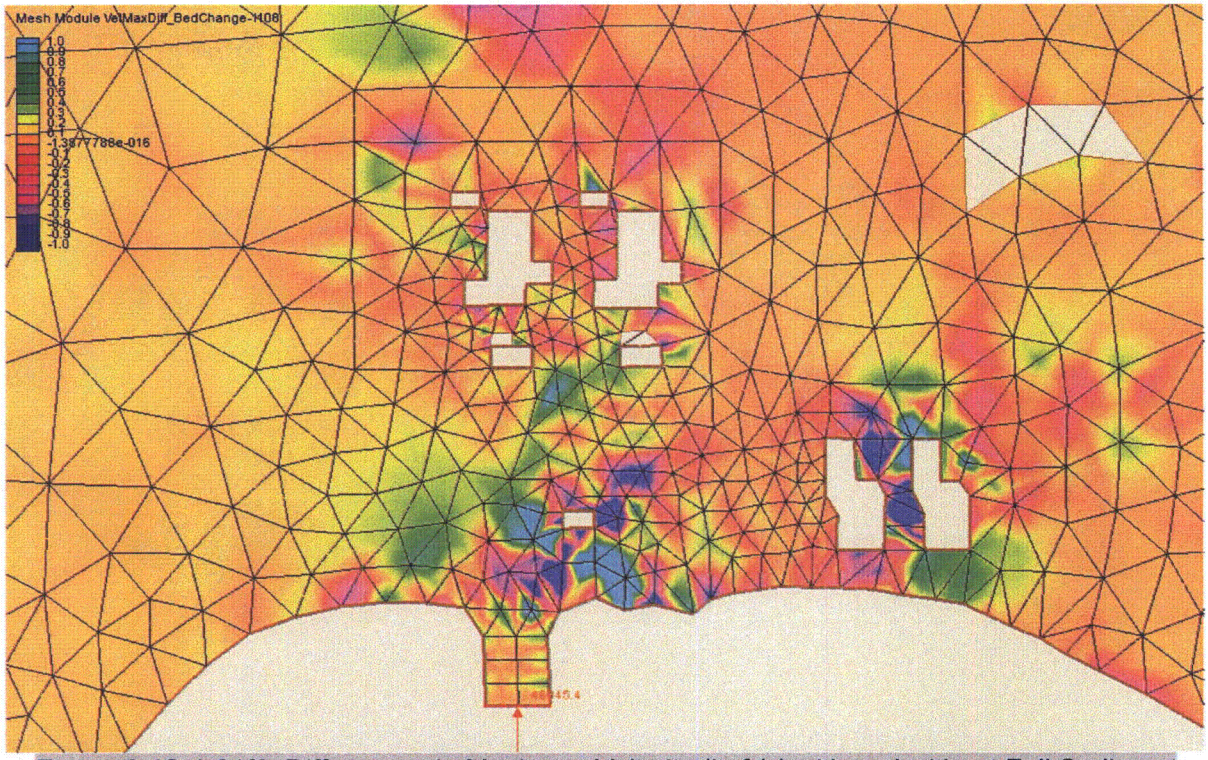

Figure 2.4S.4-21f6 Differences in Maximum Velocity (in ft/s) with and without Full Sediment Accumulation for West Breach Scenario

02.04.05-11

QUESTION:

In RAI 2.4.5-10, the staff asked the applicant to (a) an analysis of the PMSS event using a conservative approach such as that by a storm surge model (e.g., SLOSH) with input from appropriate PMH models and (b) reasons why exposure of the outer face of the MCR embankment to the PMSS event would not lead to a breach. The applicant responded to RAI 2.4.5-10 in a letter dated July 27, 2010. The applicant further described its analyses in support of response to RAI 2.4.5-10 during a site audit conducted by the staff on August 31-September 1, 2010.

Provide the following information with applicable FSAR updates on: (1) a detailed description of the ADCIRC model including the wind-wave submodel, (2) a detailed description of supporting data sets including the topographic and bathymetric grid, (3) a list of conservatively selected plausible PMH scenarios, consistent with NWS 23 ranges of PMH parameters, used as input to ADCIRC, (4) a description and justification of why other plausible PMH scenarios were not selected as conservative, (5) a description of the sensitivity of the ADCIRC-simulated PMSS to PMH parameters, including radius to maximum winds, forward speed, track direction, and location of landfall, (6) a description of nonlinearity in estimated PMSS corresponding to various combinations of PMH parameters, and (7) the selected PMSS near the STP site including windwave runup.

Also provide information on: (8) a detailed description of various methods used to estimate current velocities during a PMSS event, (9) a detailed description and justification of simplifying assumptions made, (10) conservatively selected current velocities and durations for which these currents will affect the MCR embankment, and (11) justification, including relevant citations, for the ability of the grass-lined outer face of the northern MCR embankment to withstand the current velocities without erosion severe enough to cause an embankment breach.

RESPONSE:

In the response to RAI 02.04.05-10 (Letter U7-C-STP-NRC-100170, Mark McBurnett to Document Control Desk, "Response to Request for Additional Information," dated July 27, 2010 (ML102100047)), STPNOC provided predictions of the Probable Maximum Storm Surge (PMSS) for a Probable Maximum Hurricane (PMH) at the STP site. These predictions were based on four different computer models: 1) the combined SURGE and HEC-RAS hydraulic model described in FSAR 2.4S.5.2; 2) the 2007 Display CDI Version of the Sea, Lake, and Overland Surges from Hurricanes (SLOSH) model described in FSAR 2.4S.5.2.4; 3) the April 2010 Version of SLOSH; and, 4) Version 49 of the Advanced Circulation (ADCIRC) Model. The PMSS predictions based on these computer models varied between 24.3 feet Main Sea Level (MSL) and 38.5 feet MSL before inclusion of wave runup. Wave runup potentially adds approximately 2 to 3.3 feet to the predicted surge levels. A detailed description of assumptions used with each of the four computer models and the corresponding PMSS predictions, including wave runup, is provided in the response to RAI 02.04.05-10.

The response to RAI 02.04.05-10 and presentations by STPNOC during a site audit conducted by the NRC staff on August 31-September 1, 2010, provided detailed justification for the conclusion that the ADCIRC model provided the most reliable PMSS predictions for the STP site. ADCIRC predicted the PMSS for the STP site, including wave runup, is 26.5 feet MSL, which is significantly lower than the 34-foot MSL nominal plant grade at STP 3 & 4. In response to this RAI question, STPNOC performed additional ADCIRC modeling using "conservatively selected plausible PMH scenarios, consistent with NWS 23 ranges of PMH parameters." Using these very conservative assumptions which are detailed in this response, ADCIRC predicts the PMSS for the STP site, including wave runup, is 29.3 feet MSL, which is still significantly lower than the 34 foot MSL nominal plant grade at STP 3 & 4.

FSAR 2.4S.2.2 documents that all STP 3 & 4 power block safety-related structures have flood protection measures, such as watertight doors and components that will prevent any flooding of the safety-related structures with water levels below an elevation of 40.0 feet MSL. The Ultimate Heat Sink and Reactor Service Water pump house are water tight below elevation 50 feet MSL. As documented in the response to RAI 02.04.05-10, all four of the computer models (and the NRC confirmatory analysis) predict PMSS is less than 38.5 feet MSL before inclusion of wave runup. When wave runup is included, only one model, based on the implausible assumption that hurricane intensity will not decay even after the hurricane makes landfall, predicts that wave runup could exceed 40 feet MSL. RAI 02.04.05-10 concluded that, collectively, the PMSS predictions from all four computer models (and the NRC confirmatory analysis) provide a very high degree of assurance that 10 CFR Part 50, Appendix A, GDC 2, is met for the probable maximum storm surge because STP 3 & 4 structures, systems and components important to safety are designed for a design basis flood level of 40.0 feet MSL.

Items 1 through 7 in this response provide the detailed description of the ADCIRC computer model and the assumptions used in the model that ensure that the results are based on "conservatively selected plausible PMH scenarios, consistent with NWS 23 ranges of PMH parameters." Using these assumptions, ADCIRC predicts the PMSS for the STP site is 29.3 feet MSL, including wave runup, which is significantly lower than the 34-foot MSL nominal plant grade at STP 3 & 4.

RAI 02.04.05-10 and this RAI both required that STP postulate that the PMSS induces a failure of the north face main cooling reservoir (MCR) embankment because of the sloshing and erosive action of floodwaters surrounding the main cooling reservoir. The response to RAI 02.04.05-10 and presentations by STPNOC during a site audit conducted by the NRC staff on August 31-September 1, 2010, provided a qualitative evaluation that concluded a PMSS could not cause a breach of the north face of the MCR embankment. Items 8 through 11 in this response provide the specific details requested in this RAI about MCR embankment breach due to PMSS. Additionally, the response provides the basis for the conclusion that a PMH induced failure of the north face of the MCR embankment due to sloshing and erosive action of floodwaters surrounding the main cooling reservoir is not a credible event.

Part 1: Additional Information about Advanced Circulation Model (ADCIRC)

Item 1: Detailed Description of the ADCIRC Model Including the Wind-Wave Sub-Model

ADCIRC Overview

The Advanced Circulation Model (ADCIRC) is a hydrodynamic circulation model that simulates water level and current over an unstructured gridded domain. Run as a two-dimensional or three-dimensional (2-D or 3-D) model, ADCIRC is used for the following: modeling tide driven and wind and wave driven circulation in coastal waters; forecasting hurricane storm surge and flooding; inlet sediment transport/morphology change studies; and, dredging/material disposal studies.

The numerical computer program was developed over the past 20 years to solve the equations of motion for a moving fluid on a rotating earth. These equations were formulated using traditional hydrostatic pressure and Boussinesq approximations. The equations are discretized in space using the finite element method (FEM), and in time using the finite difference method (FDM). The water elevation is obtained from the solution of a depth-integrated continuity equation in Generalized Wave-Continuity Equation (GWCE) form. Velocity is obtained from the solution of either the 2D or 3D momentum equations. All nonlinear terms have been retained in these equations. ADCIRC is run using either a Cartesian or a spherical coordinate system. The GWCE can be solved using either a consistent or a lumped mass matrix, and an implicit or explicit time stepping scheme.

ADCIRC boundary conditions include:

- specified elevation (harmonic tidal constituents or time series),
- specified normal flow (harmonic tidal constituents or time series),
- zero normal flow,
- slip or no slip conditions for velocity,
- external barrier overflow out of the domain,
- internal barrier overflow between sections of the domain,
- surface stress (wind and/or wave radiation stress),
- atmospheric pressure, and
- outward radiation of waves (Sommerfield condition).

ADCIRC can be forced with the following:

- elevation boundary conditions,
- normal flow boundary conditions,
- surface stress boundary conditions,
- tidal potential, and
- earth load/self-attraction tide.

ADCIRC includes a least squares analysis routine that computes harmonic constituents for elevation and depth averaged velocity during the course of the run, thus avoiding the need to

output long time series for post processing. ADCIRC has been optimized for enhanced performance on multiple computer architectures, and is able to operate at high efficiency on parallel (i.e. multi-processor) computing systems.

The Federal Emergency Management Agency (FEMA) certified ADCIRC for use in performing storm surge analyses as part of their program for developing Flood Insurance Rate Maps (FIRMs) along coastal areas of the United States. This model has been, and remains, the standard coastal model used by the Unites States Army Corps of Engineers (USACE). In addition to USACE projects, it is used the National Oceanic and Atmospheric Administration (NOAA) and the Naval Research Laboratory (NRL). ADCIRC is now being applied under the Interagency Performance Evaluation Task Force (IPET) study to evaluate the wave and water level impacts on the levees and floodwalls in southeastern Louisiana and Lake Pontchartrain. This study requires efficient, high-resolution surge modeling of complex geometries and bathymetries over large areas. Based on the above, ADCIRC was selected by the South Texas Project (STP) as a method for validating storm surge levels selected as the design basis for STP Units 3 & 4.

ADCIRC Description (Reference 1)

STP selected ADCIRC-2DDI, the two-dimensional, depth-integrated implementation of the ADCIRC coastal ocean model, to perform the hydrodynamic computations used to estimate storm surge levels at the site. The model uses depth-integrated equations of mass and momentum conservation subject to incompressibility, Boussinesq, and hydrostatic pressure approximations. The primitive, non-conservative continuity and momentum equations can be found in Reference 1.

Developers of ADCIRC have spent over 20 years creating numerical solutions to shallow water equations on unstructured grids using finite element methods. Unstructured finite element-based methods permit solutions of shallow water equations with localized resolution that lead to more accurate solutions globally and locally. Four finite element-based unstructured shallow water equation algorithms were developed. The algorithms are sufficiently robust to be applied to the wide range of scales of motion, and wide range of hydrodynamic balances, that exist when computing flows in the deep ocean to computing flows in inlets, floodplains, and rivers. These algorithms include the Generalized Wave Continuity Equation (GWCE) formulation, considered the most mature of the four algorithms. The GWCE solution was ultimately selected as the current base algorithm in ADCIRC.

ADCIRC accounts for the fact that friction varies with depth. A higher friction term is required in shallow, near shore regions (generally less than 30 feet deep), while a smaller value is more appropriate in deep basins. However, the friction term is also proportional to the flow velocity. Therefore, a larger friction term value is applied in high-flow regions that can be deep, such as rivers and inlets. Operationally, the GWCE solution was implemented to accommodate spatially variable friction term for quiescent waters deeper than 30 feet offshore; in waters shallower than 30 feet outside of the Texas Study Area; in rivers and inlets where higher velocities lead to higher frictional resistance; and within the remainder of Texas Study Area. In addition, the

friction term is increased within the Texas Study Area based on the total water column height and local currents. This automated current-dependent value within ADCIRC optimizes both accuracy and robustness, particularly for the very high current speeds encountered during hurricanes.

The GWCE and the momentum equations are solved sequentially. The FE solution is implemented using Lagrange linear finite elements in space; and three- and two-level schemes in time for the GWCE and momentum equations, respectively. The present simulations were done using an implicit discretization for all linear and some nonlinear terms in the equations, and an explicit discretization for most nonlinear terms.

Modeling storm surge inundation requires that the model accurately represent wetting and drying processes at the mesh scale. ADCIRC applies a wet/dry algorithm that is based on a combination of nodal and elemental criteria. The algorithm requires all nodes within an element to be wet in order for that element to be included in the hydrodynamic computations. Two parameters are used to define the wetting/drying criteria. The first parameter defines the nominal water depth for a node to be considered wet, H_0. The second parameter, a minimum velocity, U_{min}, is specified that must be exceeded for water to propagate from a wet node to a dry node. Nodes are defined as initially dry if they lie above the defined starting water level, or if they are below the starting water level, but are within protected regions, such as within ring levees.

The algorithm proceeds through the following steps to update the wet and dry elements for the next time level. Wetting is accomplished by examining each dry element with at least two wet nodes with depth greater than 1.2 H_0 (ensuring sufficient water depth to sustain flow to the adjacent node). The velocity of the flow from the wet nodes toward the dry node along each element edge is computed based on a simple force balance between the free surface gradient and the bottom friction. If this velocity exceeds U_{min}, then the third node and the element are wetted. Finally, a check is made for elements that are surrounded by wet elements to ensure sufficient water column height (greater than 1.2 H_0 at all flow originating nodes) to allow flow to occur through these elements. While a purely nodal wetting scheme will allow these elements to wet, the elemental check may prevent this wetting scheme from occurring. For hurricane storm surge inundation, wet/dry parameters that are relatively unrestrictive have been found to be most effective are $H_0 = 0.10$ m and $U_{min} = 0.01$ m/s.

The wind model used in ADCIRC is an asymmetric model based on Holland (1980), with the following input parameters:

- maximum hurricane wind speed (at 10 meters),
- central pressure,
- peripheral or background pressure,
- radius to maximum winds,
- distance from the storm center, and
- pressure profile parameter (calculated).

The Holland wind model requires calculation of the maximum gradient wind, which is based on the maximum hurricane wind speed and surface roughness. Once calculated, the maximum gradient wind is then used to calculate the pressure profile parameter (referred to as the Holland

B parameter). The wind field is subsequently adjusted to account for asymmetry associated with the forward movement and surface roughness.

Land roughness in overland regions is characterized by land-use conditions such as urban, forested, agricultural, or marsh as described by the Unites States Geological Service (USGS) National Land Cover Data Classification raster map based upon Landsat imagery and on USGS Gap Analysis Program data. This information is then combined with land roughness lengths defined by the FEMA HAZUS software program. Directional roughness values are computed for each node in the ADCIRC computational grid for 12 upwind directions as a weighted average of the roughness lengths for all pixels in the USGS land classification raster image that are within 30 km upwind of the computational node. The weighted pixel land roughness values upwind of the computational node are finally added together to get the weighted upwind land roughness coefficient for 12 different directions.

The directional changes in surface roughness from open marine conditions do not fully characterize the changes in surface stress on the water column during storm surge inundation. As inundation takes place, the land roughness elements (e.g., marsh grass, crops, and bushes) are slowly submerged and the drag is reduced. The overland roughness length is therefore reduced in the model depending on the local water column height. The reduced roughness length is limited to the marine roughness value, which is reached as the water depth increases.

The wind reduction factor is calculated for each of the 12 directions as a ratio between the surface roughness for open marine conditions and the weighted upwind land roughness adjusted for local inundation. The approximation of the wind speed reduction is based on applying a power law approximation to logarithmic boundary layer theory. Actual wind reduction factors used at each node during the simulation are determined from the pre-computed directional roughness values closest to the wind direction at that time and place.

The ADCIRC model was developed to ensure an efficient solution, and large computational platforms have been used to solve these problems. First, the sparse matrix that results from the GWCE formulation is solved via an efficient conjugate gradient solver that enables the solution of problems with a large number of degrees of freedom with cost linearly related to the number of nodes. Second, parallel processing techniques are used to run the ADCIRC model on distributed memory processors. Domain decomposition is employed to divide the computational mesh into portions that can be solved on individual processors. A number of dedicated (up to three) output processors eliminate any slowdowns when writing the large files to disk. When a relatively low ratio of interface-to-interior nodes is maintained to minimize inter-processor communications, linear or even super-linear speedups are achieved due to the on-chip memory on RISC based chips. Wall clock times are therefore reduced by a factor at least equal to the number of processors.

The ADCIRC model as applied to the STP analysis underwent an extensive flood level evaluation process to validate it over a range of conditions to ensure that the flow physics of the system were accurately characterized. The set of validation storms specific to the Texas coastal areas included Hurricanes Carla (1961), Celia (1970), Allen (1980), Alicia (1983), Bret (1999), Rita (2005), and Ike (2008). Hurricanes Rita and Ike were particularly useful storms for

validation because of the large degree of surge they produced, and the accurate measurements of wind, atmospheric pressure, waves, and surge levels that exist for these two storms.

Wind-Wave Sub-Model Description

ADCIRC is linked to a computer program called SWAN to calculate wave-induced setup, in addition to the wind-induced setup. SWAN is a third-generation wave model developed by Delft University of Technology. SWAN computes random, short-crested wind-generated waves in coastal regions and inland waters. SWAN computations can be made on a regular grid, a curvilinear grid, and a triangular mesh in a Cartesian or spherical co-ordinate system. SWAN accounts for the following physics:

- wave propagation in time and space, shoaling, refraction due to current and depth, frequency shifting due to currents and non-stationary depth,
- wave generation by wind,
- three- and four-wave interactions,
- white capping, bottom friction, and depth-induced breaking,
- dissipation due to vegetation,
- wave-induced set-up,
- propagation from laboratory up to global scales, and
- transmission through and reflection against obstacles.

SWAN Description (Reference 2)

SWAN predicts the evolution in geographical space and time of the wave action density spectrum with the relative frequency and the wave direction. The unstructured-mesh version of SWAN implements an analog to the four-direction Gauss-Seidel iteration technique employed in the structured version, and it maintains the unconditional stability in SWAN. SWAN computes the wave action density spectrum at the vertices of an unstructured triangular mesh. It orders the mesh vertices so it can sweep through them and update the action density using information from neighboring vertices. It then sweeps through the mesh in opposite directions until the wave energy has propagated sufficiently through geographical space in all directions. As a spectral model, SWAN does not attempt to represent physical processes at scales less than a wave length even in regions with very fine-scale mesh resolution. Phase-resolving wave models should be employed at these scales if sub-wave length scale flow features need to be resolved. However, this fine-scale mesh resolution may be necessary for other reasons, such as representing the complex bathymetry and topography of the region, or to improve the numerical properties of the computed solution.

SWAN is driven by wind speeds, water levels and currents computed at the vertices by ADCIRC. Marine winds can be input to ADCIRC in a variety of formats, and these winds are adjusted directionally to account for surface roughness. ADCIRC interpolates spatially and temporally to project these winds to the computational vertices, and then it passes them to SWAN. The water levels and ambient currents are computed in ADCIRC before being passed to

SWAN, where they are used to recalculate the water depth and all related wave processes such as wave propagation and depth-induced breaking.

ADCIRC and SWAN run in series on the same local mesh and core. The two models step through time, each being forced with information from the other model. Because of the sweeping method used by SWAN to update the wave information at the computational vertices, it can take much larger time steps than ADCIRC, which is diffusion and Courant-time-step limited due to its semi-explicit formulation and its wetting-and-drying algorithm. For that reason, the coupling interval is taken to be the same as the SWAN time step. On each coupling interval, ADCIRC is run first, because it is assumed that, in the near shore and the coastal floodplain, wave properties are more dependent on circulation.

At the beginning of a coupling interval, ADCIRC can access the radiation stress gradients computed by SWAN at times corresponding to the beginning and end of the previous interval. ADCIRC uses that information to extrapolate the gradients at all of its time steps in the current interval. These extrapolated gradients are used to force the ADCIRC solution as described above. Once the ADCIRC stage is finished, SWAN is run for one time step, to bring it to the same moment in time as ADCIRC. SWAN can access the wind speeds, water levels, and currents computed at the mesh vertices by ADCIRC, at times corresponding to the beginning and end of the current interval. SWAN applies the mean of those values to force its solution on its time step. In this way, the radiation stress gradients used by ADCIRC are always extrapolated forward in time, while the wind speeds, water levels, and currents used by SWAN are always averaged over each of its time steps.

The unstructured-mesh SWAN spectral wave model and the ADCIRC shallow-water circulation model have thus been integrated into a tightly coupled SWAN + ADCIRC model. The model components are applied to an identical, unstructured mesh; share parallel computing infrastructure; and run sequentially in time. Wind speeds, water levels, currents, and radiation stress gradients are vertex-based, and therefore can be passed through memory or cache to each model component. The integrated SWAN + ADCIRC system is highly scalable and allows for localized increases in resolution without the complexity or cost of nested meshes or global interpolation between heterogeneous meshes. Hurricane waves and storm surge as estimated by the coupled SWAN + ADCIRC model have been validated for Hurricane Katrina and Hurricane Rita, demonstrating the importance of inclusion of the wave-circulation interactions.

Item 2: Detailed Description of Supporting Data Sets Including the Topographic and Bathymetric Grid

Topographic Grid (Reference 3)

Accurate mapping of the topography surrounding the STP site is essential to simulate correctly inland flood propagation. Topography influences the speed and direction of wind-wave and surge propagation, and frictional dissipation. Topography can also regionally amplify or

attenuate storm surge. For these reasons, the topography in Coastal Texas was mapped in the ADCIRC hydrodynamic model using the most accurate and current topographic survey data. Topographic values were applied from a variety of data sources. The most recent and most trusted topographic values came from LIDAR (Reference 4) data sets from the Texas Water Development Board (TWDB), Harris County Flood Control District (HCFCD), FEMA, and LSU/Louisiana Oil Spill Contingency Office Atlas. The nodal elevations in the ADCIRC mesh were carefully reviewed at the interface between data sources and adjusted to smooth out any discontinuities. All data sets were converted to North American Datum of 1983 (NAD83) and elevations adjusted to NAVD88.

Topographic data for the majority of the terrain in Texas were obtained from the TWDB (2007), HCFCD (2002), FEMA (2006), and LSU LIDAR. These data were available in Digital Elevation Model (DEM) form on a 10-meter-by-10-meter basis, and some later became available on a 1-meter by 1-meter basis. Small-scale hydro-dynamically relevant features, like levees, riverbanks, and roadbeds, are represented in the data. The ADCIRC mesh was primarily built using the 10-meter LIDAR because its nominal resolution best matched the intended resolution of most areas of the mesh. Some refinements of highly resolved, hydraulically relevant features were later made using the 1-meter LIDAR DEM.

Aerial photography was not utilized as a source of bathymetric or topographic definition when creating the TX2008 Grid. However, once topography and bathymetry were defined using the most accurate data available, the horizontal alignment of major features like roadways, shorelines, and river banks was checked against aerial photographs using both satellite images and Google Earth images (Google, 2007).

TX2008 Domain/Grid Definition

Version 13 of the Texas topographic grid, herein referred to as TX2008 model, is an extension of the earlier EC2001 U.S. East Coast and Gulf of Mexico tide model and the TX04 Coastal Texas storm surge model. These models all incorporate the western North Atlantic Ocean, the Gulf of Mexico, and the Caribbean Sea to allow for full dynamic coupling between oceans, continental shelves, and the coastal floodplain without requiring definition of these complicated couplings in the boundary conditions. The TX2008 model extends the geographic coverage of these earlier models to include all the floodplains of Coastal Texas. In addition, improved feature definitions, surface roughness definition, wave radiation stress definition, and grid resolution were all incorporated into the TX2008 model. Figure 1 shows the topographic data sources used to create the TX2008 Grid.

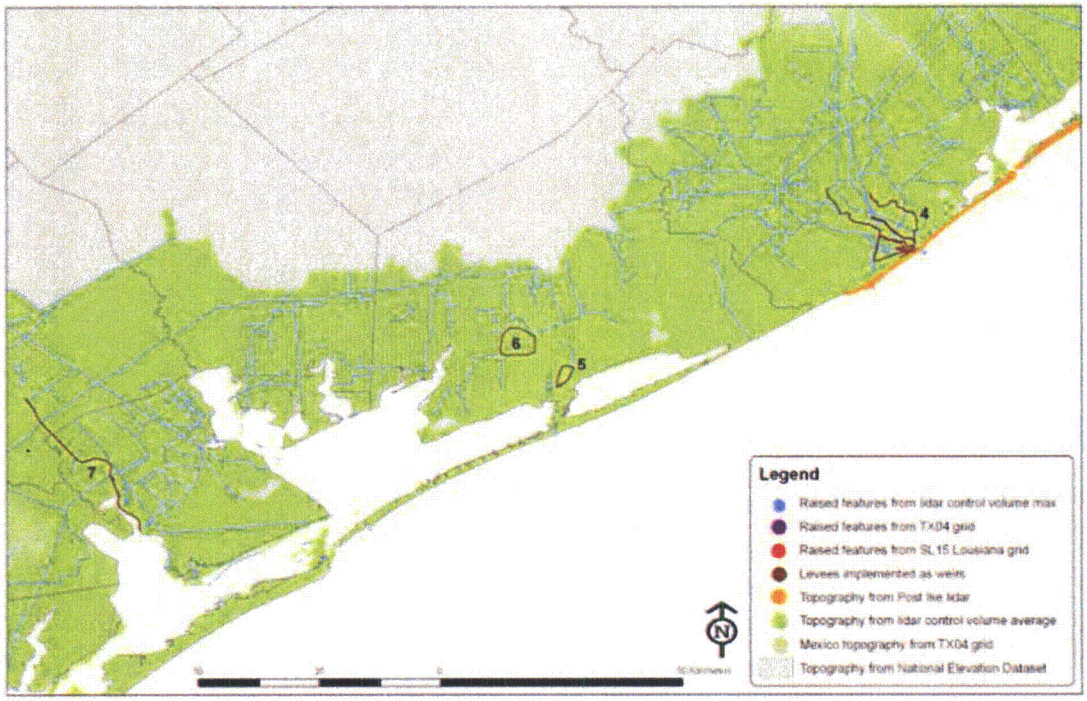

Figure 1 Topographic Data Sources for the TX2008 Grid

The development of an accurate unstructured grid storm surge model of Coastal Texas requires appropriate selection of the model domain and optimal resolution of features controlling surge propagation. The TX2008 model domain has an eastern open ocean boundary that lies along the 60-degree west meridian, extending south from the vicinity of Glace Bay in Nova Scotia, Canada, to the vicinity of Coracora Island in eastern Venezuela. This domain has a superior open ocean boundary that is primarily located in the deep ocean and lies outside of any resonant basin. This boundary has nominal geometric complexity. Tidal response is dominated by the astronomical constituents. Nonlinear energy is limited due to the depth. The boundary is not located near tidal amphidromes. Hurricane storm surge response along this boundary is essentially an inverted barometric pressure effect directly correlated to the atmospheric pressure deficit in the meteorological forcing. It can therefore be easily specified. This boundary allows the model to accurately capture basin-to-basin and shelf-to-basin physics.

Much of the domain is bordered by a land boundary made up of the eastern coastlines of North, Central, and South America. The highly detailed/resolved region extends along the coast from Brownsville to Port Arthur, Texas. The coastal regions adjacent to Texas, northern Mexico, and western Louisiana were also included at high resolution in order to allow storm surge to realistically attenuate and laterally spread into the adjacent regions. In the Texas model, the domain includes a large overland region that is at risk for storm surge induced flooding. Details of the domain with bathymetry and topography as well as levees and raised roadways across Coastal Texas near the STP site can be seen on Figure 2. The inland extent of the Texas model follows high topography or major hydraulic controls. The land boundary runs along the 30 to 75 foot land contour. The boundary was positioned such that lower-lying valleys and the adjacent

highlands were included. It is critical that boundary location and boundary condition specification do not hinder physically realistic model response.

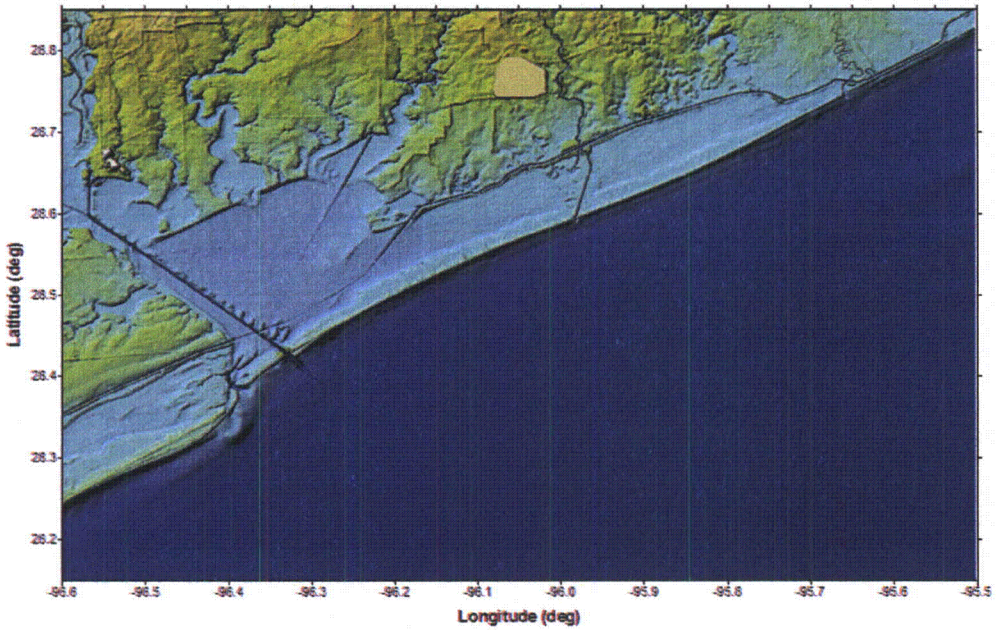

Figure 2 Topographic Features of the TX2008 Grid

Critical hydraulic features and controls are included in the TX2008 grid that both enhance and attenuate storm surge. Rivers and channels can be conduits for storm surge propagation far inland. Topographical features such as levee systems stop flow and can focus storm surge energy into local areas, resulting in the amplification of storm surge. Floodplains and wetlands cause attenuation of flood wave propagation. Many interconnected features are in Texas, including deep naturally scoured channels, wetlands, and an extensive and intricate system of river banks, levees, and raised roadways. Rivers, such as the Brazos River, Nueces River and Rio Grande, and numerous major dredged navigation canals including the Gulf Intracoastal Waterway (GIWW) are incorporated into the grid. All significant levee systems, elevated roads, and railways have been specifically included in the domain as barrier boundaries. These raised features are represented as a continuous row of elevated nodes, as internal barrier boundaries, or as external barrier boundaries when they are at the edge of the domain.

The computational mesh shown in Figure 2 was constructed to provide sufficient resolution for the tidal, wind, atmospheric pressure, and riverine flow forcing functions from the ocean basins to the coastal floodplain. Efficient and effective resolution of tidal response within the basins and on the shelf is determined by tidal wavelength and topographic length scale criteria. Based on propagation of the predominant tidal wavelength, a minimum wavelength-to-grid spacing ratio of at least 50 is required, and more satisfactory is closer to 100. The mesh also has increased resolution at the shelf break guided by a topographic length scale criteria in order to capture the higher localized wave number content.

The mesh design provides localized refinement of the Texan coastal floodplains and of the important hydraulic features. The level of detail in Coastal Texas is very high, with nodal spacing reaching as low as 100 feet in the most highly refined areas. Unstructured meshes can resolve the critical features and the associated local flow processes with orders of magnitude of fewer computational nodes than a structured grid because the latter is limited in its ability to provide resolution on a localized basis, and fine resolution generally extends far outside the necessary area. The TX2008 mesh is refined locally to resolve features such as inlets, rivers, navigation channels, levee systems, and local topography/bathymetry.

Previous mesh-resolution sensitivity studies applying the ADCIRC model to the rivers and the Lake Pontchartrain-Lake Borgne inlet system indicate that under-resolution severely dampens tidal and surge propagation into rivers and inlets. Regardless of channel dimensions, a small number of meshing stipulations were adhered to while mapping inland waterway bathymetry in the model. The most stringent constraint was to set a maximum resolution of 100 feet throughout the mesh in order to control computational cost. A finer level of resolution creates additional nodes, elements, and thus calculations per time step. In addition, a smaller time step is needed within the ADCIRC model in order to accommodate for the high spatial resolution. A second important attribute of channel meshes is the placement of a minimum number of nodes across a channel. When possible, at least five nodes were placed across a channel for two reasons. First and foremost, channels require high resolution in order to adequately capture bathymetric characteristics. Second, multiple nodes are placed within the channel to prevent the ADCIRC wetting and drying algorithm from artificially reducing the conveyance of the channel.

The TX2008 computational mesh contains more than 2.8 million nodes and nodal spacing varies significantly throughout the mesh. Grid resolution varies from approximately 12 to 15 miles in the deep Atlantic Ocean to about 100 feet in Texas. The high grid resolution required for the study region leads to a final grid with more than 90 percent of the computational nodes placed within or upon the shelf adjacent to Texas, enabling sufficient resolution while minimizing the cost of including such an extensive domain. Use of a large-scale domain therefore only adds 10 percent to the computational cost of the simulations. The result, however, is the application of highly accurate boundary conditions and full dynamic coupling between all scales from basins to inlets.

Bathymetric Grid

Accurate model bathymetry is crucial to accurately represent the flow physics of a region. Bathymetry controls physical processes including long wave and short wind-wave propagation speed and direction, structure, and dissipation. Bathymetry in the regions in the western North Atlantic, Gulf of Mexico, and Caribbean Sea that are included in the models was drawn from a number of sources including the raw bathymetric sounding database from NOS, the Digital Nautical Charts (DNC) bathymetric database, and ETOPO5 data from NOAA. The NOS raw sounding database provides the most comprehensive coverage over U.S. continental shelf waters, which include more than 13 million sounding values and is the basis of NOS/NOAA bathymetric charts. Although the surveys are not as comprehensive as the NOS raw soundings, DNC values are available within the Gulf of Mexico and much of the western North Atlantic and Caribbean

Sea, while ETOPO5 coverage is worldwide. Data accuracy and preferences are in the order NOS, DNC, and finally ETOPO5. Bathymetry for inland waterways in Coastal Texas is provided by regional bathymetric surveys and dredging surveys from the USACE SWG, NOAA, TWDB, or nautical charts. Figure 3 shows the source for ADCIRC mesh bathymetric data for Matagorda Bay and the surrounding water bodies.

Bathymetric/Topographic Definition

Geometry, topography, and bathymetry in the TX2008 model were all defined to replicate the prevailing conditions, post-Hurricane Ike 2008. To simplify specification of accurate tide and hurricane storm surge boundaries, the Gulf of Mexico and a portion of the Atlantic Ocean were included in the computational mesh. Open ocean bathymetric depths were first interpolated from a 5-degree-by-5-degree regular grid based on the ETOPO5 values. The DNC bathymetric values were then applied over much of the Atlantic, Gulf of Mexico, and Caribbean. Bathymetric values were subsequently applied using the NOAA depth-sounding database. Thus, bathymetric values were applied with a priority/availability system with preference being given to the NOAA sounding database, then the DNC database, and then the ETOPO5 database. This preference is related to the accuracy of each database.

Bathymetric values were then evaluated at computational nodes using an element-based gathering/averaging procedure instead of a direct interpolation procedure. The gathering/averaging procedure searches for all available sounding/bathymetric survey values within the cluster of elements connected to one specific node. It then averages these values and assigns the average value as the depth/bathymetric elevation to that node. This gathering/averaging procedure essentially implements grid scale filtering to the bathymetric data and ensures that bathymetry is consistent with the scale of the grid. Bathymetry was locally checked with available NOAA navigational charts. In regions with missing or incorrect data, supplemental data from the USACE SWG, USGS, or NOS bathymetric charts were applied. Bathymetry was typically specified to various tidal datum and then adjusted to NAVD88 by adding the difference so the correct datum was defined. Inland bathymetry for the TX2008 grid was taken primarily from regional bathymetric surveys from the USACE SWG and other sources. Particular care was taken to define bathymetry for the channels. Due to the scale, averaging methods were not appropriate. Background base grids were therefore prepared directly from the sounding tracks that were then used to interpolate channel values.

Quality checks were also performed on the bathymetry prior to putting the model into production. First, the connectivity of the flow channels and conveyances were inspected to ensure the data were representative of the flow features. Second, transitions between features were smoothed so flow was not cut off or re-routed in a physically inaccurate manner due to discontinuities between the datasets. Third, the channels as implemented in the mesh were quality checked for smoothness at the resolved mesh scale. In sections of some channels, especially at channel intersections, survey data were not available or not adequate to capture correctly the intersection bathymetry. The presence of steep, fluctuating gradients is not physically realistic. Thus, ridges artificially interpolated into the channels were removed in order to represent the channel conveyance in a manner more representative of the channel's

natural state. Finally, grid quality checks were done within the mesh editing software in order to ensure that the mesh would yield accurate numerical performance.

Topography in Texas was obtained predominantly using 10-meter LIDAR data supplied by FEMA. All topographic and bathymetric data were spatially averaged to the local mesh scale. The topographic data were applied to the grid by searching for all LIDAR points within a rectangle defined by the average distance from the node for which we are assigning a topographic value to the connected nodes. This rectangular averaging paradigm was applied because the search algorithms to find all the topographic values work significantly faster than the unstructured grid element cluster gather/averaging schemes used for the bathymetric data. Given the number of on land nodes and the tremendous size of the LIDAR databases, speed is critical. Finally, the rectangular averaging scheme also effectively implements grid scale averaging to the topographic values assigned to the nodes in the grid.

Vertical Features with Small Horizontal Scales

In addition to describing bathymetry and topography, the TX2008 grid model must account for pronounced vertical features with small horizontal scales relative to the grid scale. While features such as barrier islands and riverbanks are generally well resolved in grids with resolutions down to about 100 feet, features like levees, floodwalls, railroads, and raised highways will not be sufficiently well resolved with 100-foot grid resolution. Frequently, these small-scale features can be significant horizontal obstructions to flow causing water to rise or be diverted elsewhere. These obstructions must therefore be carefully incorporated into the model as sub-grid scale weirs or lines of nodes specified as feature crown elevations. Their horizontal and vertical position must be well defined (see Figure 2). Sub-grid scale weirs were included with sub- and super-critical weir coefficients for features that were notably higher (i.e., 10 feet) than prevailing ground.

Federal, state, and local roads, and railroads and other continuous raised features, were positioned horizontally using LIDAR data or satellite images. Vertical positions were typically defined from the Texas 10-meter-by-10-meter LIDAR data set. However, the elevations were also confirmed or adjusted with 1-meter-by-1-meter LIDAR where available. The crown height was obtained automatically by searching a defined region around the raised feature's point of interest. Features were only included if the crown height was more than three feet above the adjacent topography and the feature was long enough to substantially impede flow.

Feature Definition

Levee and road crown heights are important because they define the overtopping water surface elevation, thus controlling the local flow of water during a surge event. Even after overtopping, raised features can lead to localized storm surge buildup. Levee and road systems that are barriers to flood propagation are features that generally fall below the defined grid scale and represent a non-hydrostatic flow scenario. In the TX2008 grid, raised features lying three meters or less above prevailing ground were defined using a continuous line of nodes to impede the

flow. This definition allows the ADCIRC model to predict flow over relatively low-lying raised features dynamically using the shallow water equations. For these roads, railroads, and ridges, a line of ADCIRC nodes were carefully placed along the centerline of the feature. The finite element edges were aligned to follow the feature, thereby accurately implementing the topographic feature into the mesh.

However, in instances that raised features are substantially higher than prevailing ground, it is most effective to treat these structures as sub-grid scale parameterized weirs within the domain. ADCIRC defines weirs as barrier boundaries by a pair of computational nodes with a specified crown height that accommodate both super- and sub-critical overflows. Once the water level reaches a height exceeding the crown height, the flow across the structure is computed according to basic weir formulae. This is accomplished by examining each node in the defined pair for their respective water surface heights and computing flow according to the difference in water elevation. The resulting flux is specified as a normal flow from the node with the higher water level to the node with the lower water level for each node pair. Weir boundary conditions also are implemented for external barrier boundaries, which permit surge that overtops levee structures at the edge of the domain to transmit flow out of the computational area.

All raised feature heights are defined using the most recent surveys available from the various sources, including LIDAR sources, USACE SWG surveys, and surveys from local jurisdictions. In the case of surveys, crown heights were mapped to the mesh using the nearest relevant survey point. Low-lying road and railroad crown heights in Texas were defined using LIDAR-applied elevations in a similar paradigm as the grid scale averaging topographic definition. The exception being that a crown height was defined as the maximum within a nodal control volume, rather than as a mesh scale averaged value.

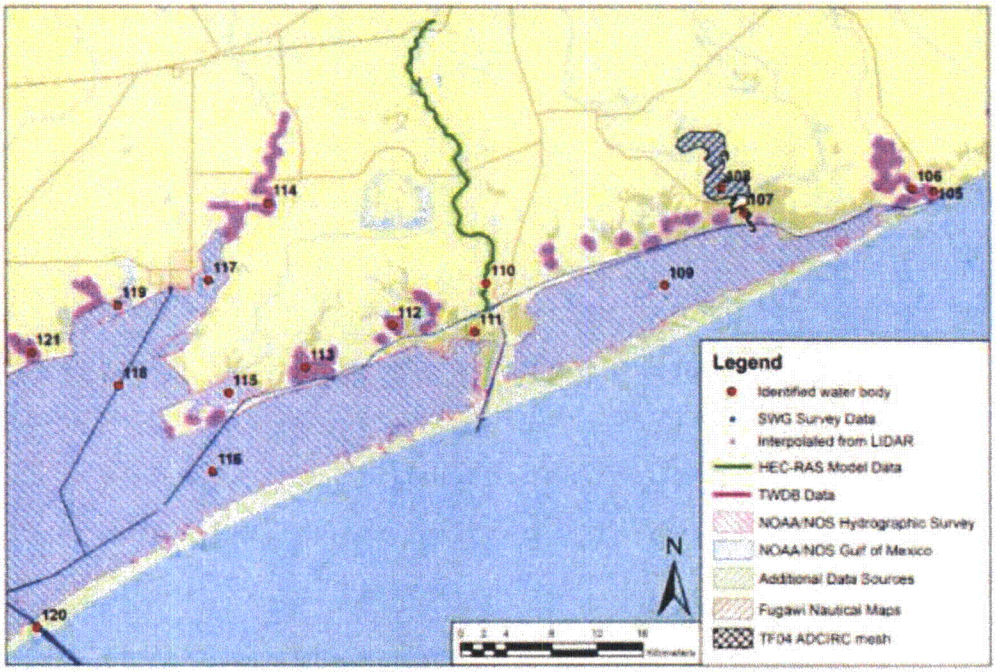

Figure 3 Bathymetric Data Sources for the TX2008 Grid

Item 3: A List of Conservatively Selected Plausible PMH Scenarios, Consistent with NWS 23 Ranges of PMH Parameters, Used as Input to ADCIRC

As indicated in response to RAI 02.04.05-10 (Letter U7-C-STP-NRC-100170, Mark McBurnett to Document Control Desk, "Response to Request for Additional Information," dated July 27, 2010 (ML102100047)), NWS 23 specifies ranges of PMH parameters for the STP site. These ranges include a radius to maximum winds of 6.0 to 20.8 miles; an approach direction of 97.5° to 190° clockwise from the north; and, a forward speed of 6.9 to 21.8 mph. STP used combinations of these three parameters, in addition to three different landfall points, to specify several PMH scenarios that may occur at the STP site. Three individual values were selected for each of these scenarios, resulting in 81 PMH storm tracks. The radius to maximum winds was set to 6, 12.9, and 20.8 miles; the approach angle to 97.5°, 143.8°, and 190° clockwise from the north; and the forward speeds to 6.9, 14.4, and 21.8 mph for each run. Three landfall points were selected, with the first landfall point located at a distance equal to the radius of maximum winds, west of the mouth of the Colorado River Navigation Channel at the barrier islands. The second point was centered on the mouth of the Colorado River Navigation Channel at the barrier islands. The third point was located a distance equal to the radius of the maximum winds east of the mouth of the Colorado River Navigation Channel, at the barrier islands. All storm tracks were straight. A total of 81 combinations resulted from the selection of these parameters.

The results of storm surge simulations using SLOSH indicated that the maximum water surface elevation near STP Units 3 and 4 sites would be produced by a large (in terms of radius to maximum winds), fast-moving (in terms of forward speed) storm that would produce prevailing winds blowing from the east toward STP Units 3 and 4. Because hurricanes rotate counter clockwise in the northern hemisphere, the highest surges are expected on the east side of the hurricane eye due to the fastest onshore wind being toward the right of the eye. Storms with larger forward speeds generate faster responses in surge, leaving less time for the surge to dissipate over and around the surrounding terrain. Considering these factors, the site would be most vulnerable to flooding when the eye of the hurricane passes quickly to the west of the site on the leading edge of the storm. Based on the above outcomes and observations, STP concluded that the PMH estimated from the NWS 23 method would result from a storm with a radius to maximum winds of 20.8 miles, an approach angle of 143.8° clockwise from the north, and a forward speed of 21.8 mph.

Based on these results, a series of hurricane scenarios were simulated using ADCIRC to determine the maximum water surface elevation near STP Units 3 and 4 resulting from storm surge. The PMH parameters selected for the ADCIRC runs were based on the storm scenario that produced the maximum surge at the site during the prior analysis with SLOSH. Specifically, the PMH parameters selected for the ADCIRC runs based on NWS 23 are a radius to maximum winds of 24 miles (21 nm); an approach direction of 135° clockwise from the north (i.e. a northwesterly direction); a forward speed of 23 mph (20 knots); a central pressure of 26.19 in Hg; and a peripheral pressure of 30.12 in Hg. The only variables were the distance of the storm track from the site and the track direction. Table 1 shows the resulting features of each of the seven simulated hurricanes. Scenarios 1 through 7 show the actual storm tracks and related inputs used for each of the seven ADCIRC runs.

As discussed during the on-site audit by the NRC audit team on August 31 through September 1, 2010, when using similar storm features ADCIRC will produce smaller values for surge heights at the site of STP Units 3 and 4 when compared to values produced by SLOSH. The reasons for these differences are as follows:

- Grid Resolution
- Terrain Features (e.g., City of Matagorda Levee)
- Wind Model
- Friction Coefficients (Bottom and Surface)
- Pressure Differential (SLOSH: 133 Mb; ADCIRC: 123 Mb to 126 Mb)

When executing the ADCIRC runs, the program uses the Holland wind profile as the basis for calculating surface wind speeds as a function of distance from the storm center. SLOSH uses a different wind profile based on NWS 48. When comparing the two models, for the same gradient wind speed and distance from the storm center, the SLOSH wind profile based on NWS 48 will generate a greater value for wind speed than the Holland wind profile. The ADCIRC code was therefore changed, with the NWS 48 wind profile equation inserted in place of the Holland wind profile equation. The pressure differential was also increased during the ADCIRC runs to 133 Mb. These steps were taken to mitigate differences between the program outputs that might otherwise be attributable to the wind model and to the pressure differential. The only remaining differences between the two models are gird resolution, terrain features, and friction coefficients.

TABLE 1. ADCIRC Hurricane Scenarios

Scenario	1	2	3	4	5	6	7
Central Pressure	887 Mb (26.19 Hg)	887 Mb (26.19 Hg)	887 Mb (26.19 Hg)	887 Mb (26.19 Hg)	887 Mb (26.19 Hg)	887 Mb (26.19 Hg)	887 Mb (26.19 Hg)
Peripheral Pressure	1020 Mb (30.12 Hg)	1020 Mb (30.12 Hg)	1020 Mb (30.12 Hg)	1020 Mb (30.12 Hg)	1020 Mb (30.12 Hg)	1020 Mb (30.12 Hg)	1020 Mb (30.12 Hg)
Pressure Differential	133 Mb (3.93 Hg)	133 Mb (3.93 Hg)	133 Mb (3.93 Hg)	133 Mb (3.93 Hg)	133 Mb (3.93 Hg)	133 Mb (3.93 Hg)	133 Mb (3.93 Hg)
Radius to Maximum Winds	24 miles (21 nm)	24 miles (21 nm)	24 miles (21 nm)	24 miles (21 nm)	24 miles (21 nm)	24 miles (21 nm)	24 miles (21 nm)
Forward Speed	23 mph (20 knots)	23 mph (20 knots)	23 mph (20 knots)	23 mph (20 knots)	23 mph (20 knots)	23 mph (20 knots)	23 mph (20 knots)
Maximum Sustained Wind	184 mph (180 knots)	184 mph (180 knots)	184 mph (180 knots)	184 mph (180 knots)	184 mph (180 knots)	184 mph (180 knots)	184 mph (180 knots)
Shortest Distance from site	12 miles (10.4 nm)	24 miles (20.9 nm)	36 miles (31.3 nm)	24 miles (21 nm)	24 miles (21 nm)	24 miles (21 nm)	24 miles (21 nm)
Track Direction	NW	NW	NW	N	N-NW	W-NW	W

SCENARIO 1 (12 NW)

Center of Eye	Time to Landfall (hrs)	Coordinates Latitude (°N)	Coordinates Longitude (°W)	Storm Features Category (SSI)	Storm Features Central Pressure (Mb)	Storm Features Radius to Max. Winds (miles)	Distance Between Points (nm)	Distance Between Points (miles)	Forward Speed (mph)	Forward Speed (knots)
D	-12	30.32	96.72	1	984	30	24	30	10	8.7
C	-9	30.07	97.86	2	975	31	34	39	13	11.3
B	-6	29.66	97.39	3	964	34	44	51	17	14.9
A	-3	29.14	98.80	4	944	38	52	60	20	17.3
Landfall	0	28.54	96.11	5	887	24	60	69	23	20
1	3	27.84	95.31	5	887	24	60	69	23	20
2	6	27.11	94.53	5	887	24	60	69	23	20
3	9	26.39	93.75	5	887	24	60	69	23	20
4	12	25.66	92.98	5	887	24	60	69	23	20
5	15	24.93	92.22	5	887	24	60	69	23	20
6	18	24.21	91.46	5	887	24	60	69	23	20
7	21	23.49	90.70	4	944	28	60	69	23	20
8	24	22.80	89.91	3	964	28	60	69	23	20
9	27	22.10	89.13	2	979	18				

NORTHWEST

PMH Storm Features		
Central Pressure:	887 Mb	(26.19 in. Hg)
Peripheral Pressure:	1020 Mb	(30.12 in. Hg)
Radius to Maximum Winds:	21 nm	(24 miles)
Forward Speed:	20 knots	(23 mph)
Maximum Sustained Wind:	160 knots	(184 mph)
Shortest Distance from site:	10.4 nm	(12 miles)

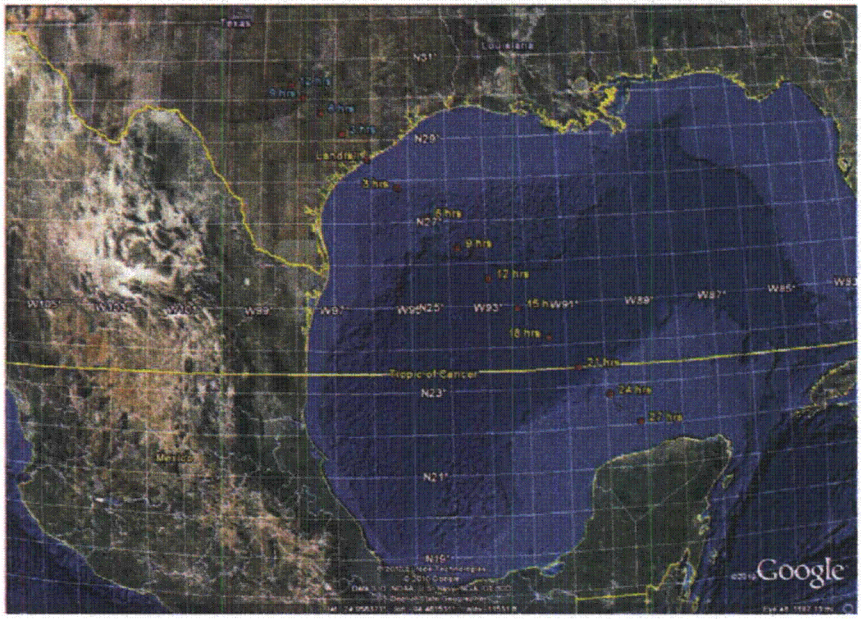

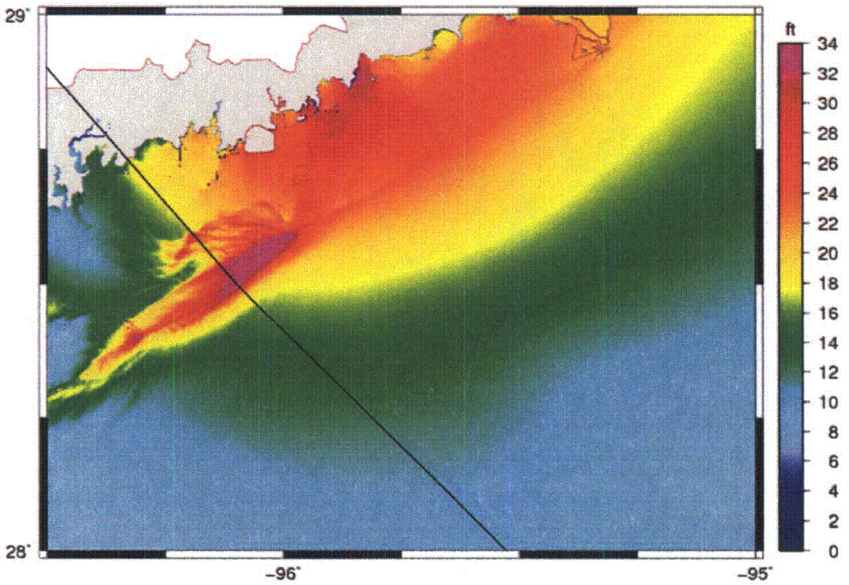

SCENARIO 2 (24 NW)

Center of Eye	Time to Landfall (hrs)	Coordinates Latitude (°N)	Coordinates Longitude (°W)	Storm Features Category (SSI)	Storm Features Central Pressure (Mb)	Storm Features Radius to Max. Winds (miles)	Distance Between Points (nm)	Distance Between Points (miles)	Forward Speed (mph)	Forward Speed (knots)
D	-12	30.26	98.43	1	980	28	26	30	30	26.1
C	-9	29.90	98.06	2	975	23	34	39	33	28.8
B	-6	29.56	97.69	3	964	18	43	51	37	32.2
A	-3	29.04	97.01	4	944	20	52	60	26	17.3
Landfall	0	28.42	96.32	5	887	24	60	69	23	20
1	3	27.72	95.52	5	887	24	60	69	23	20
2	6	26.99	94.73	5	887	24	60	69	23	20
3	9	26.27	93.96	5	887	24	60	69	23	20
4	12	25.54	93.19	5	887	24	60	69	23	20
5	15	24.82	92.42	5	887	24	60	69	23	20
6	18	24.09	91.67	5	887	24	60	69	23	20
7	21	23.37	90.91	4	944	20	60	69	23	20
8	24	22.68	90.12	3	964	16	60	69	23	20
9	27	21.98	89.34	2	979	13				

NORTHWEST

PMH Storm Features		
Central Pressure:	887 Mb	(26.25 in. Hg)
Peripheral Pressure:	1020 Mb	(30.12 in. Hg)
Radius to Maximum Winds:	21 nm	(24 miles)
Forward Speed:	20 knots	(23 mph)
Maximum Sustained Wind:	160 knots	(184 mph)
Shortest Distance from site:	20.9 nm	(24 miles)

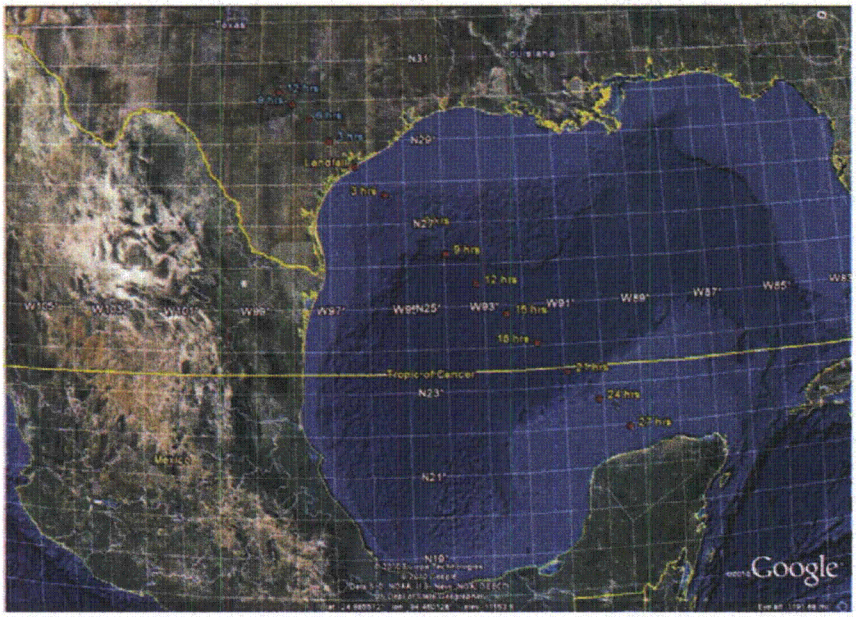

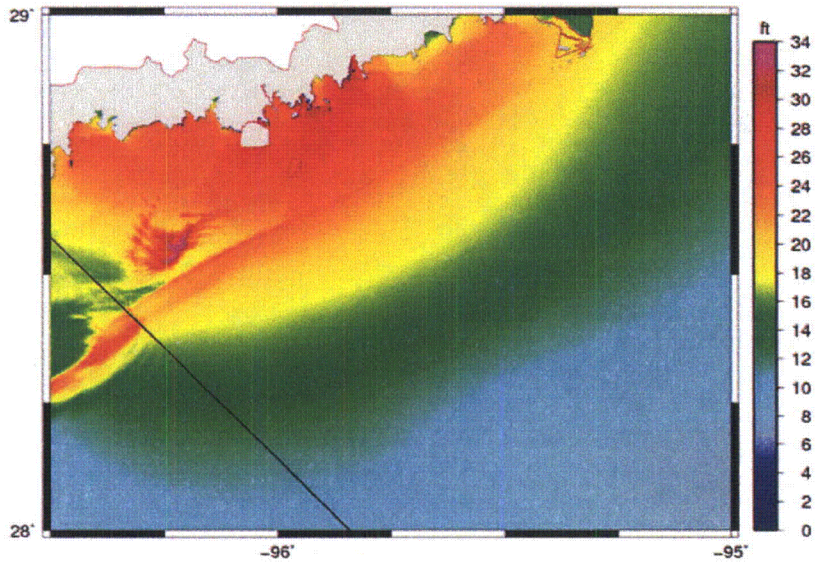

SCENARIO 3 (36 NW)

Center of Eye	Time to Landfall (hrs)	Coordinates Latitude (°N)	Coordinates Longitude (°W)	Storm Features Category (SSI)	Storm Features Central Pressure (Mb)	Storm Features Radius to Max. Winds (miles)	Distance Between Points (nm)	Distance Between Points (miles)	Forward Speed (mph)	Forward Speed (knots)
D	12	30.50	98.50	1	994	30	26	30	30	26.0
C	9	29.85	98.10	2	975	18	34	39	31	31.5
B	6	28.46	97.22	3	964	16	44	50	17	14.7
A	3	28.94	97.31	4	944	20	32	40	20	17.3
Landfall	0	28.32	96.66	5	887	24	60	69	25	20
1	1	27.62	95.64	5	887	24	60	69	23	20
2	6	26.89	94.86	5	887	24	60	69	23	20
3	9	26.17	94.08	5	887	24	60	69	23	20
4	12	25.44	93.31	5	887	24	60	69	23	20
5	15	24.71	92.53	5	887	24	60	69	23	20
6	18	23.99	91.79	5	887	24	60	69	23	20
7	21	23.27	91.03	4	944	20	60	69	25	20
8	24	22.56	90.24	3	964	16	60	69	23	20
9	27	21.88	89.46	2	979	11				

NORTHWEST

PMH Storm Features		
Central Pressure:	887 Mb	(26.19 in. Hg)
Peripheral Pressure:	1020 Mb	(30.12 in. Hg)
Radius to Maximum Winds:	21 nm	(24 miles)
Forward Speed:	20 knots	(23 mph)
Maximum Sustained Wind:	160 knots	(184 mph)
Shortest Distance from site:	31.3 nm	(36 miles)

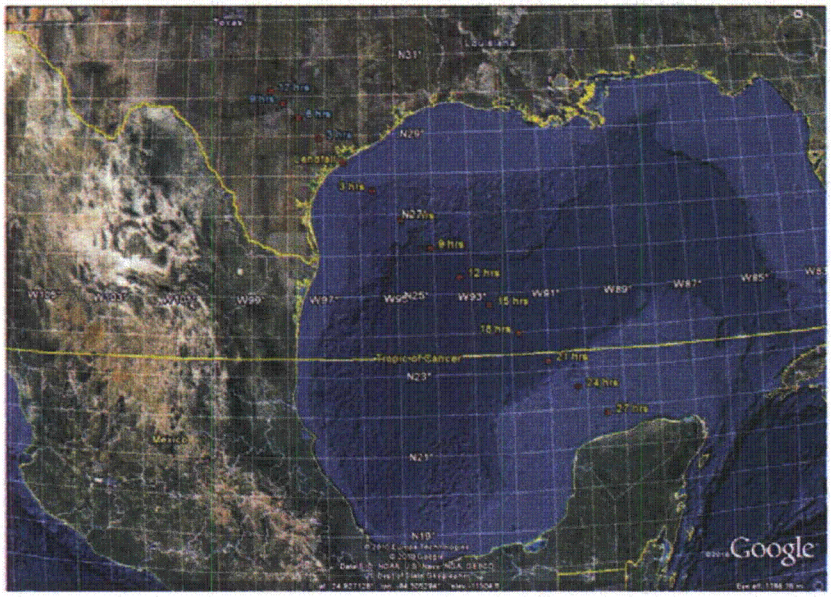

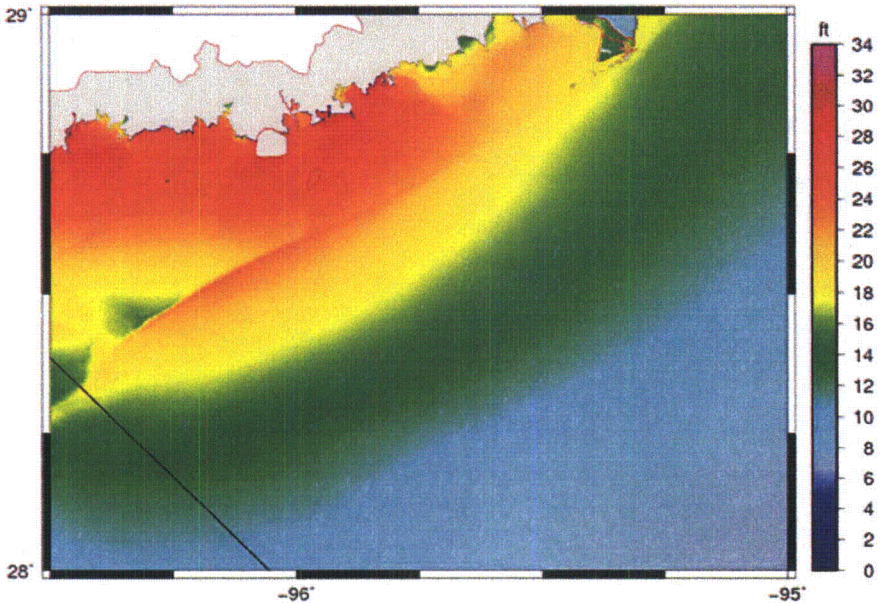

SCENARIO 4 (24 North)

Center of Cyc	Time to Landfall (hrs)	Coordinates Latitude (°N)	Coordinates Longitude (°W)	Storm Features Category (SS)	Storm Features Central Pressure (Mb)	Storm Features Radius to Max. Winds (miles)	Distance Between Points (nm)	Distance Between Points (miles)	Forward Speed (mph)	Forward Speed (knots)
5	-12	30.29	96.51	1	990	60	70	80	10	8.7
6	-9	30.66	96.51	2	979	53	69	79	19	16.5
7	-6	29.89	96.51	3	968	38	60	69	17	14.7
8	-3	29.15	96.51	4	948	32	52	60	20	17.2
Landfall	0	28.29	96.51	5	887	24	60	69	23	20
1	3	27.29	96.51	5	887	24	60	69	23	20
2	6	26.29	96.51	5	887	24	60	69	23	20
3	9	25.29	96.51	5	887	24	60	69	23	20
4	12	24.29	96.42	5	887	24	60	69	23	20
5	15	23.30	96.29	5	887	24	60	69	23	20
6	18	22.32	96.06	5	887	24	60	69	23	20
7	21	21.34	95.85	4	948	20	60	69	23	20
8	24	20.35	95.61	3	964	18	60	69	23	20
9	27	19.37	95.36	2	979	13				

NORTH

PMH Storm Features		
Central Pressure:	887 Mb	(26.19 in. Hg)
Peripheral Pressure:	1020 Mb	(30.12 in. Hg)
Radius to Maximum Winds:	21 nm	(24 miles)
Forward Speed:	20 knots	(23 mph)
Maximum Sustained Wind:	160 knots	(184 mph)
Shortest Distance from site:	21 nm	(24 miles)

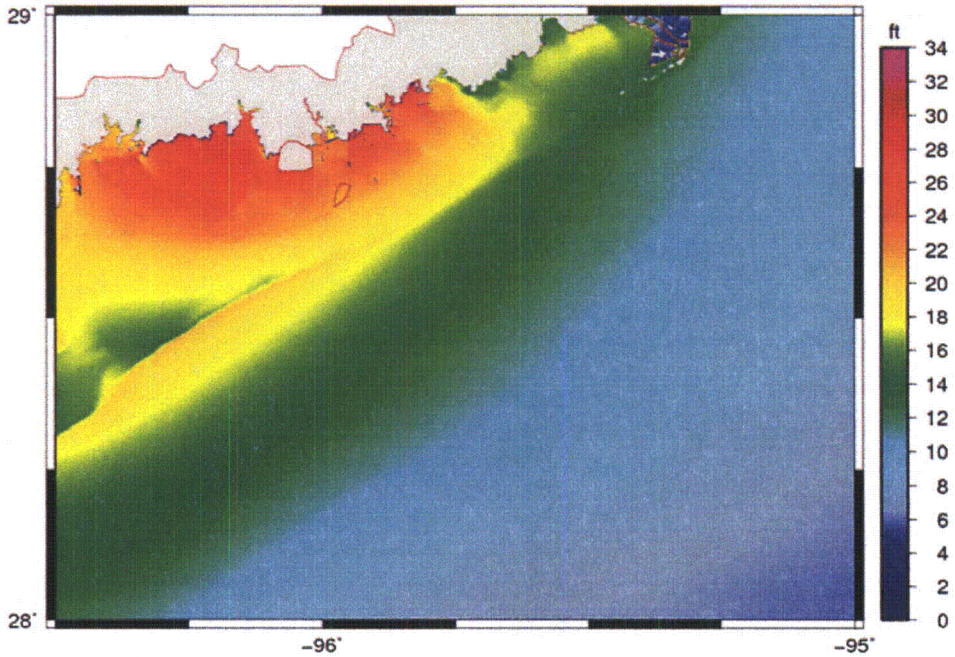

SCENARIO 5 (24 N-NW)

Center of Eye	Time to Landfall (hrs)	Coordinates Latitude (°N)	Coordinates Longitude (°W)	Storm Features Category (SSI)	Storm Features Central Pressure (Mb)	Storm Features Radius to Max. Winds (miles)	Distance Between Points (nm)	Distance Between Points (miles)	Forward Speed (mph)	Forward Speed (knots)
D	-12	30.30	90.36	1	968	30	36	30	30	26
C	-9	30.47	97.12	2	939	15	84	39	33	28.7
B	-6	23.93	96.32	3	894	16	44	51	37	32.2
A	-3	25.23	96.18	3	943	25	52	60	29	25.2
Landfall	0	28.20	96.36	5	887	24	60	69	23	20
1	3	27.45	96.03	5	887	24	60	69	23	20
2	6	26.50	95.65	5	887	24	60	69	23	20
3	9	25.55	95.30	5	887	24	60	69	23	20
4	12	24.60	94.95	5	887	24	60	69	23	20
5	15	23.65	94.60	5	882	24	60	69	23	20
6	18	22.70	94.25	5	887	24	60	69	23	20
7	21	21.75	93.90	4	944	20	60	69	23	20
8	24	20.80	93.55	3	964	16	60	69	23	20
9	27	19.85	93.20	2	979	13				

NORTH-NORTHWEST

PMH Storm Features		
Central Pressure:	887 Mb	(26.19 in. Hg)
Peripheral Pressure:	1020 Mb	(30.12 in. Hg)
Radius to Maximum Winds:	21 nm	(24 miles)
Forward Speed:	20 knots	(23 mph)
Maximum Sustained Wind:	160 knots	(184 mph)
Shortest Distance from site:	21 nm	(24 miles)

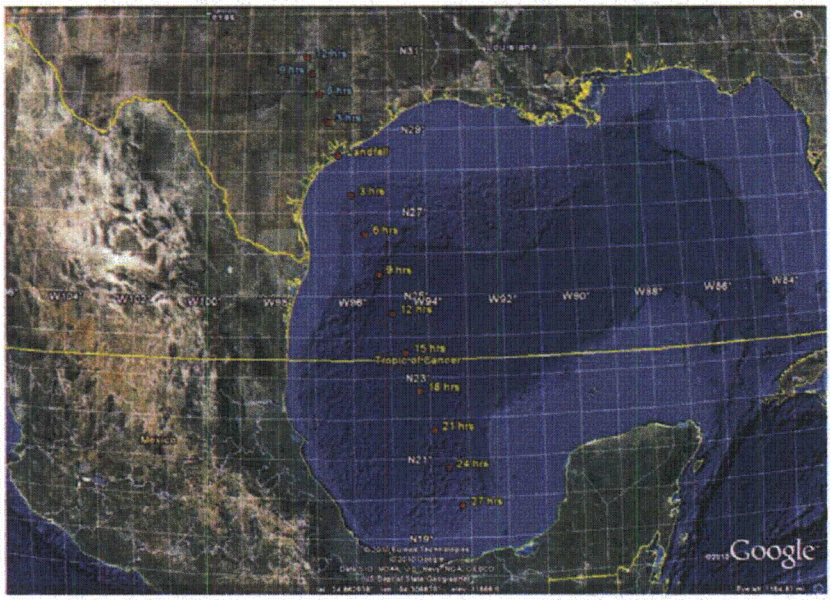

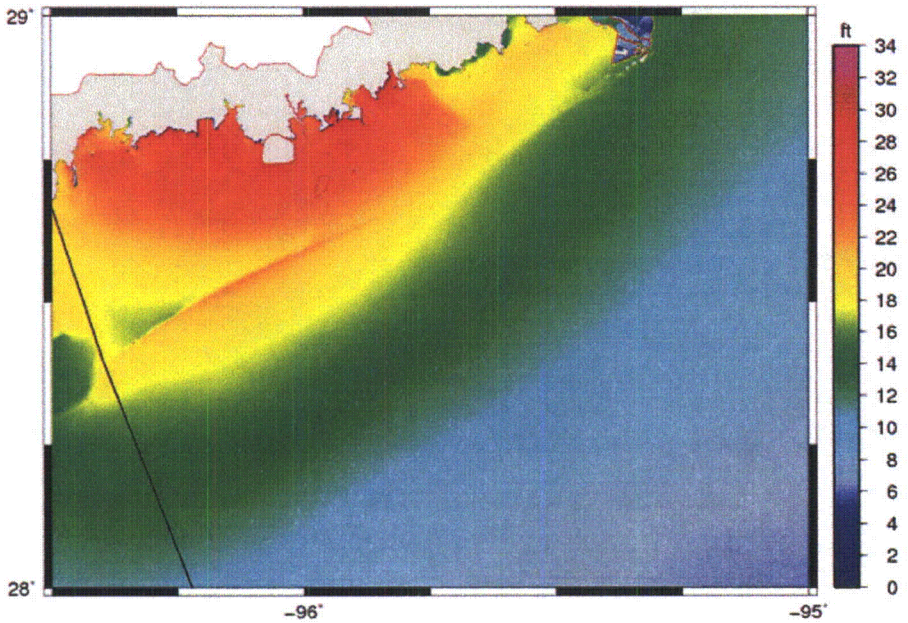

SCENARIO 6 (24 W-NW)

Center of Eye	Time to Landfall (hrs)	Coordinates Latitude (°N)	Coordinates Longitude (°W)	Storm Features Category (SSI)	Storm Features Central Pressure (Mb)	Storm Features Radius to Max. Winds (miles)	Distance Between Points (nm)	Distance Between Points (miles)	Forward Speed (mph)	Forward Speed (knots)
0	32	21.41	99.04	1	958	65	24	28	10	8.7
1	30	20.27	98.56	2	979	33	34	39	13	11.3
2	28	19.05	97.93	3	964	16	41	47	17	14.7
3	24	18.21	97.24	4	944	20	32	36	20	17.4
Landfall	0	28.44	96.30	5	887	24	60	69	23	20
1	3	28.05	95.25	5	887	24	60	69	23	20
2	6	27.67	94.21	5	887	24	60	69	23	20
3	9	27.30	93.17	5	887	24	60	69	23	20
4	12	26.92	92.13	5	887	24	60	69	23	20
5	15	26.55	91.09	5	887	24	60	69	23	20
6	18	26.17	90.05	5	887	24	60	69	23	20
7	21	25.79	89.02	4	944	20	60	69	23	20
8	24	25.42	87.98	3	964	16	60	69	23	20
9	27	25.04	86.95	2	979	33				

WEST-NORTHWEST

PMH Storm Features		
Central Pressure:	887 Mb	(26.19 in. Hg)
Peripheral Pressure:	1020 Mb	(30.12 in. Hg)
Radius to Maximum Winds:	21 nm	(24 miles)
Forward Speed:	20 knots	(23 mph)
Maximum Sustained Wind:	160 knots	(184 mph)
Shortest Distance from site:	21 nm	(24 miles)

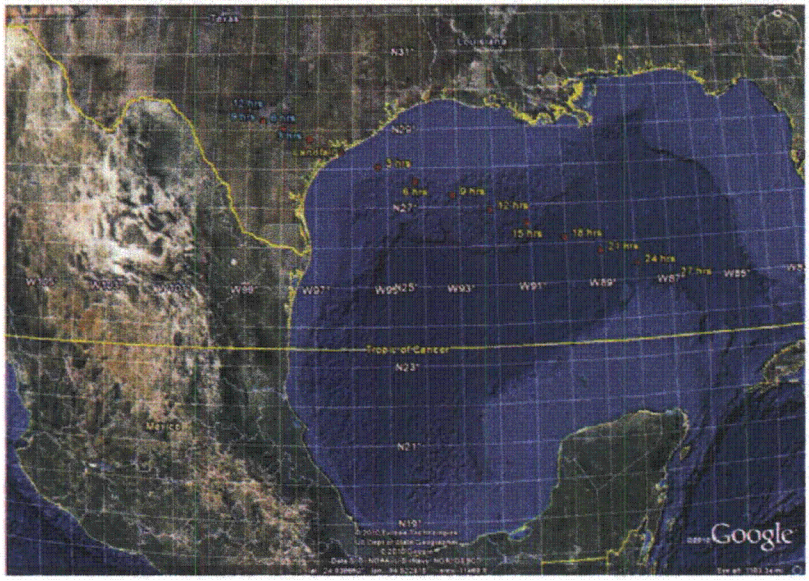

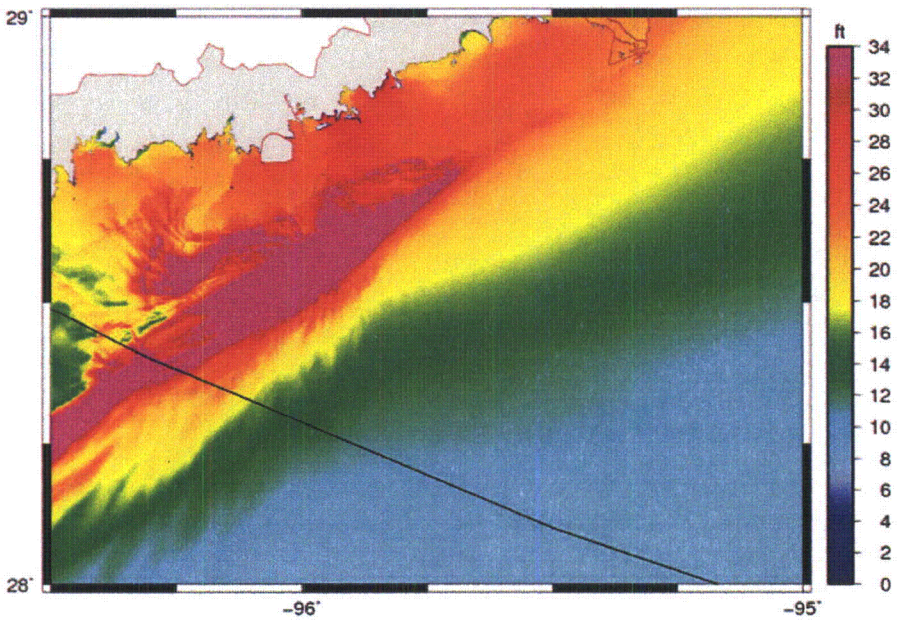

SCENARIO 7 (24-W)

Center of Eye	Time to Landfall (hrs)	Coordinates Latitude (°N)	Coordinates Longitude (°W)	Storm Features Category (SSI)	Storm Features Central Pressure (Mb)	Storm Features Radius to Max. Winds (miles)	Distance Between Points (nm)	Distance Between Points (miles)	Forward Speed (mph)	Forward Speed (knots)
D	-12	28.40	99.32	1	994	10	26	30	10	8.7
C	-9	28.40	98.82	2	979	13	34	39	13	11.3
B	-6	28.40	98.18	3	964	16	44	51	17	14.7
A	-3	28.40	97.35	4	944	20	52	60	20	17.3
Landfall	0	28.40	96.37	5	887	24	60	69	23	20
1	3	28.40	95.24	5	887	24	60	69	23	20
2	6	28.40	94.11	5	887	24	60	69	23	20
3	9	28.40	92.98	5	887	24	60	69	23	20
4	12	28.40	91.85	5	887	24	60	69	23	20
5	15	28.40	90.72	5	887	24	60	69	23	20
6	18	28.40	89.59	5	887	24	60	69	23	20
7	21	28.40	88.46	4	944	20	60	69	23	20
8	24	28.40	87.33	3	964	16	60	69	23	20
9	27	28.40	86.20	2	979	13				

WEST

PMH Storm Features		
Central Pressure:	887 Mb	(26.19 in. Hg)
Peripheral Pressure:	1020 Mb	(30.12 in. Hg)
Radius to Maximum Winds:	21 nm	(24 miles)
Forward Speed:	20 knots	(23 mph)
Maximum Sustained Wind:	160 knots	(184 mph)
Shortest Distance from site:	21 nm	(24 miles)

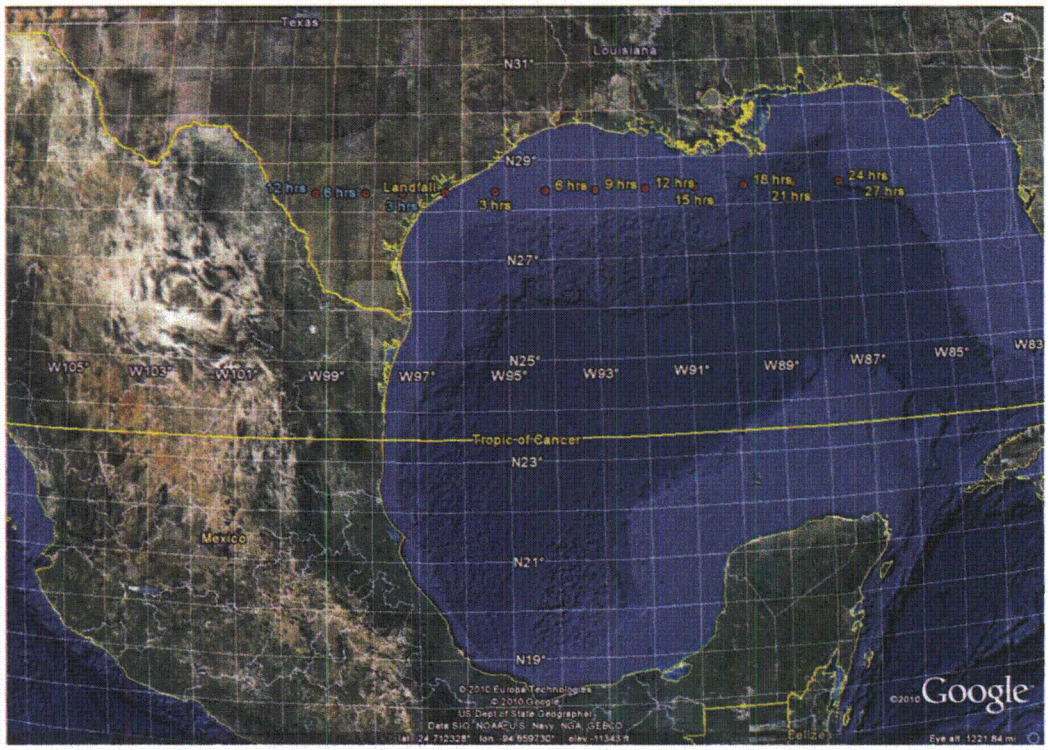

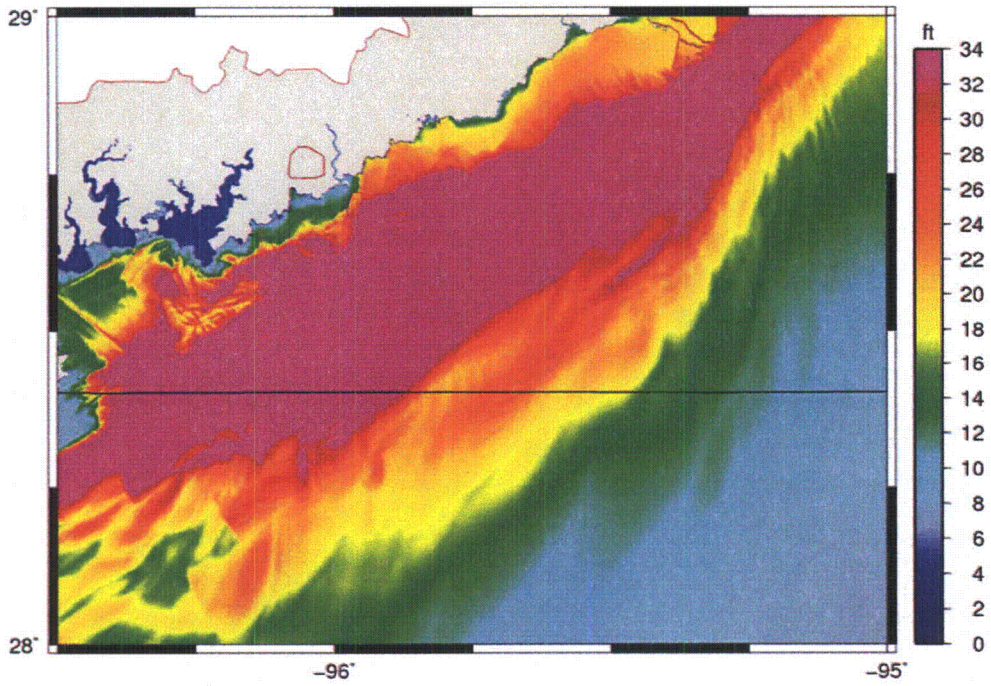

Scenario 7 – 24 W: Stopped at Landfall with MWS = 160 knots

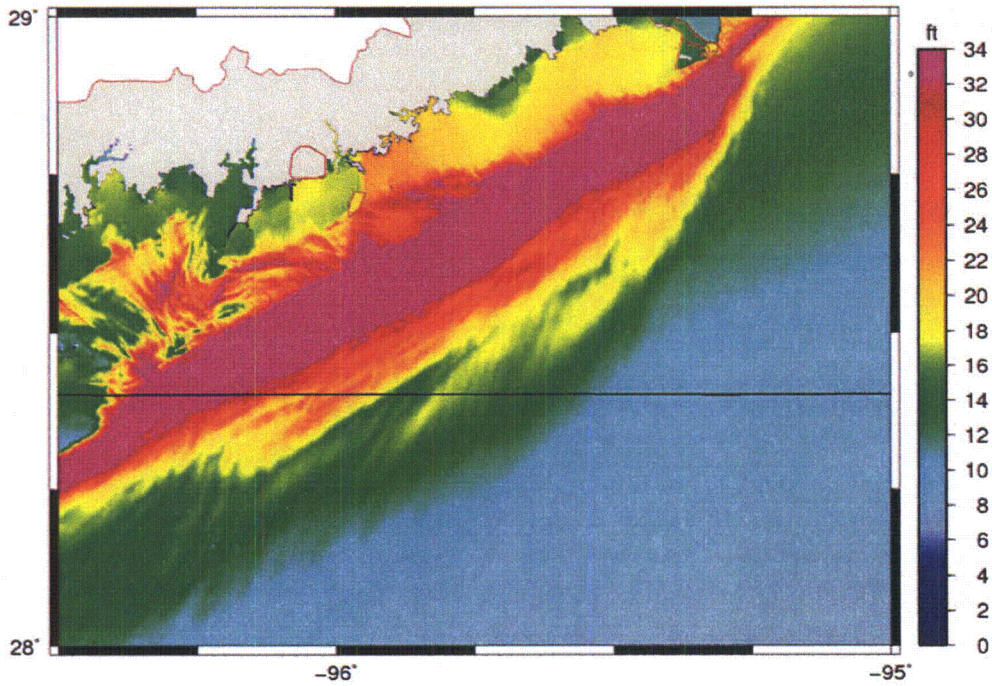

Scenario 7 – 24 W: Continue with MWS = 140 knots

Item 4: A Description and Justification of Why Other Plausible PMH Scenarios Were Not Selected as Conservative

The basis for selecting the storm scenarios as described in response to Item 3 reflect ranges of PMH parameters for the STP site as set forth by NWS 23. The storm features as summarized in Table 1 and as illustrated in scenarios provided at the end of this section represent the most conservative combination of storm scenarios in terms of features that contribute most to amplification of storm surge height. Specifically, the storms scenarios use:

- the greatest pressure differential which will create a stronger storm,
- the greatest radius to maximum winds which will create a larger storm,
- the greatest forward speed which will increase surge heights,
- a maximum sustained wind speed that remains constant up to landfall,
- tracks which direct storm surge in paths that are least resistant to wave build-up, and
- a wind profile that is considered conservative when compared to other wind profiles.

A credible storm scenario could not be identified within the parameters set forth in NWS 23 that would be viewed as more conservative than the seven scenarios as defined in Item 3.

Item 5: A Description of the Sensitivity of the ADCIRC-simulated PMSS to PMH Parameters, Including Radius to Maximum Winds, Forward Speed, Track Direction, and Location of Landfall

ADCIRC was run for the seven scenarios as discussed in response to Item 3. The results are summarized in Table 2 below. The storm track and graphic output files showing the predicted surge height are shown in Figures labeled Scenario 1 through Scenario 7.

TABLE 2. Results of ADCIRC Runs

Scenario	1	2	3	4	5	6	7
Shortest Distance from site	12 miles (10.4 nm)	24 miles (20.9 nm)	36 miles (31.3 nm)	24 miles (21 nm)	24 miles (21 nm)	24 miles (21 nm)	24 miles (21 nm)
Track Direction	NW	NW	NW	N	N-NW	W-NW	W
Maximum Surge Height (ft)	26.5 (8.08 m)	29.3 (8.93 m)	28.5 (8.67 m)	25.0 (7.62 m)	29.0 (8.84 m)	26.0 (7.92 m)	20.0 (6.10 m)

Figure 4 shows the maximum storm surge at the site as a function of the shortest distance of the storm track from the site. For these three scenarios, the track direction remained constant (northwest path). As indicated in Figure 4, the greatest storm surge occurs when the shortest distance of the storm track from the site is equal to the radius to maximum winds.

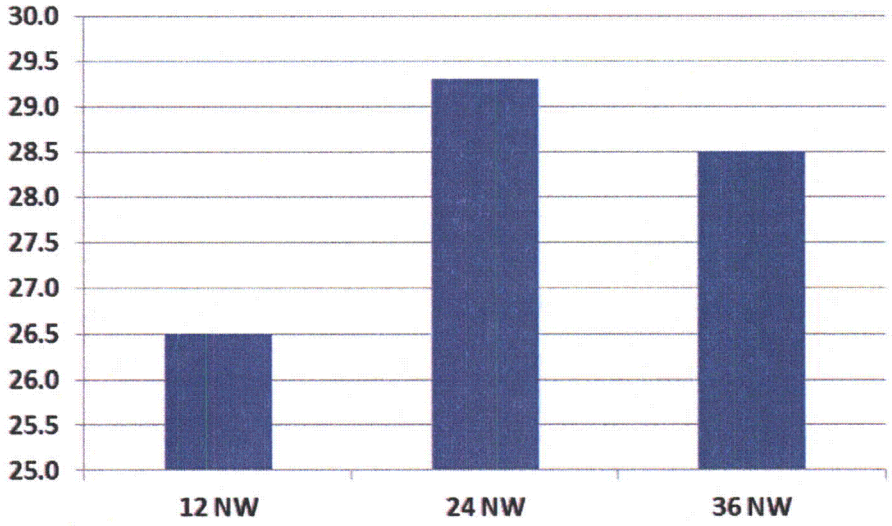

Figure 4. Storm Surge Height (ft above MSL) vs. Distance from Site

Figure 5 shows the maximum storm surge at the site as a function of the track direction relative to the site. For these five scenarios, the shortest distance of the storm track from the site remained constant (24 miles). As indicated in Figure 5, the greatest storm surge occurs when the track is generally heading in a northwesterly direction.

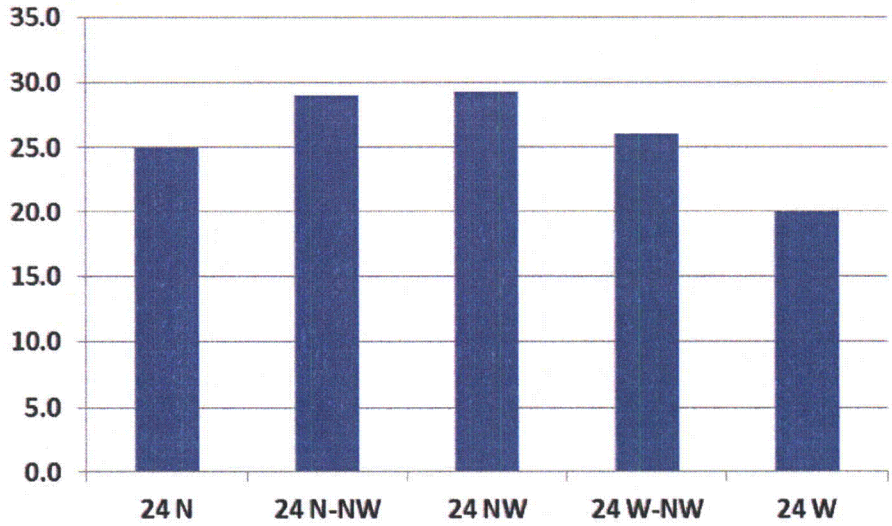

Figure 5. Storm Surge Height (ft above MSL) vs. Direction

A series of figures are provided to illustrate the impact of the PMSS on the MCR as estimated by ADCIRC. Figure 6 shows a surface elevation map created from the actual ADCIRC input file, with two cross sections that cut through the MCR, labeled Section AA' and Section BB'. Figure 7 shows boundary node features and barrier heights for Section AA' and Section BB', which are part of the ADCIRC, input file. Figure 8 and Figure 9 show vertical elevations of Section AA' and Section BB', respectively, using the topographic data files selected for the ADCIRC model runs (blue line), along with the PMSS level produced by ADCIRC (purple line). Also shown on Figure 8 and Figure 9 are vertical elevations based on topographic data currently incorporated into the SLOSH model (red line). As discussed in response to Item 2, the TX2008 grid model used in ADCIRC accounts for pronounced vertical features with small horizontal scales relative to the grid scale, specifically features like the levee surrounding the City of Matagorda and inter-coastal canals.

Overflow errors were encountered within ADCIRC during execution of Scenario 7 with the storm heading in a westerly direction. Such errors occur when the grid cells become overwhelmed in both number and magnitude of surge height, thus resulting in termination of the program (see Scenario 7). When the program terminated, the storm had made landfall along the Texas coastline, with the STP site shown as dry. To determine if the STP site would have been inundated had the storm continued to progress inland following landfall, the scenario was re-run at a lower maximum wind speed of 140 knots versus 160 knots. Execution was subsequently successful, with the site showing a surge level of 18 feet above MSL. Earlier sensitivity runs using ADCIRC showed that a 20-knot difference in the maximum wind speed for a northwesterly track would produce a difference in surge height of approximately 1.5 feet. The estimated surge height for Scenario 7 as shown in Table 2 and Figure 5 was therefore estimated to be approximately 20 feet above MSL.

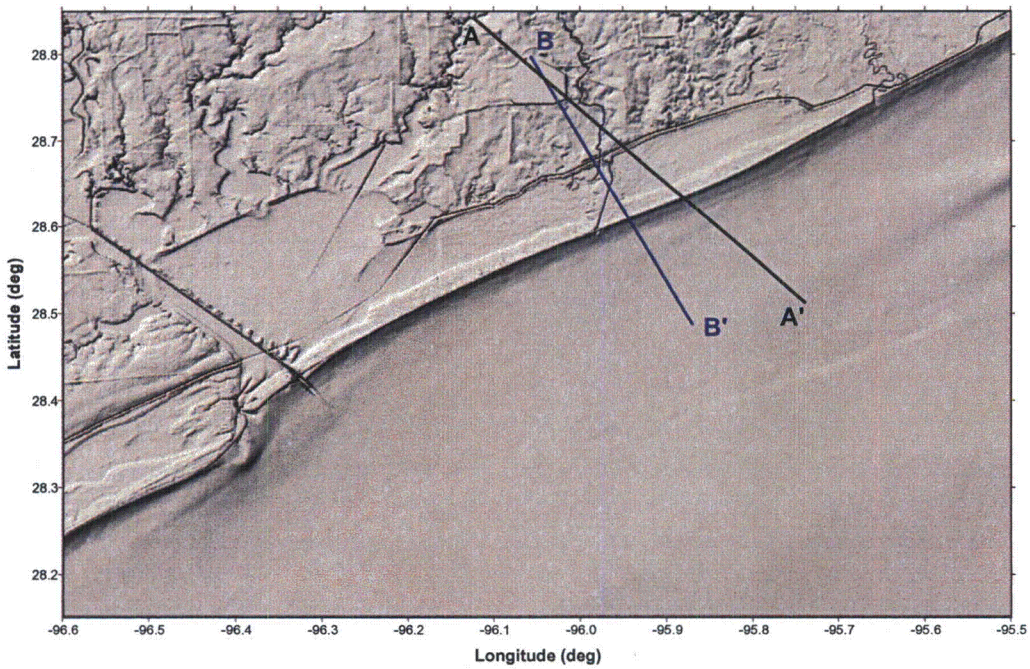

Figure 6. ADCIRC Surface Elevation Map

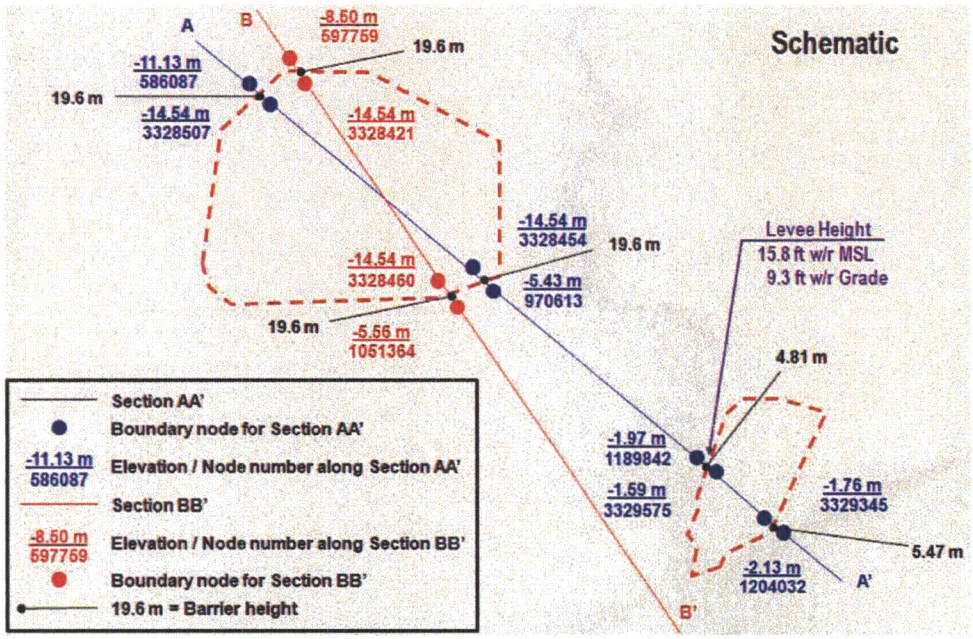

Figure 7. Boundary Node Features and Barrier Heights for Section AA' and Section BB'

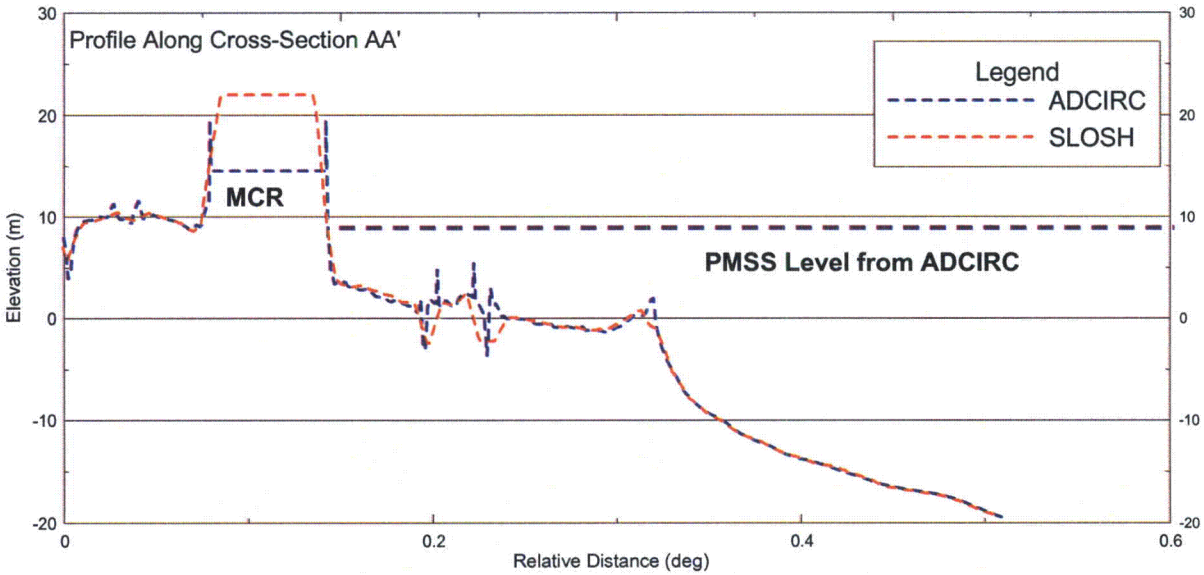

Figure 8. Vertical Elevations of Section AA'

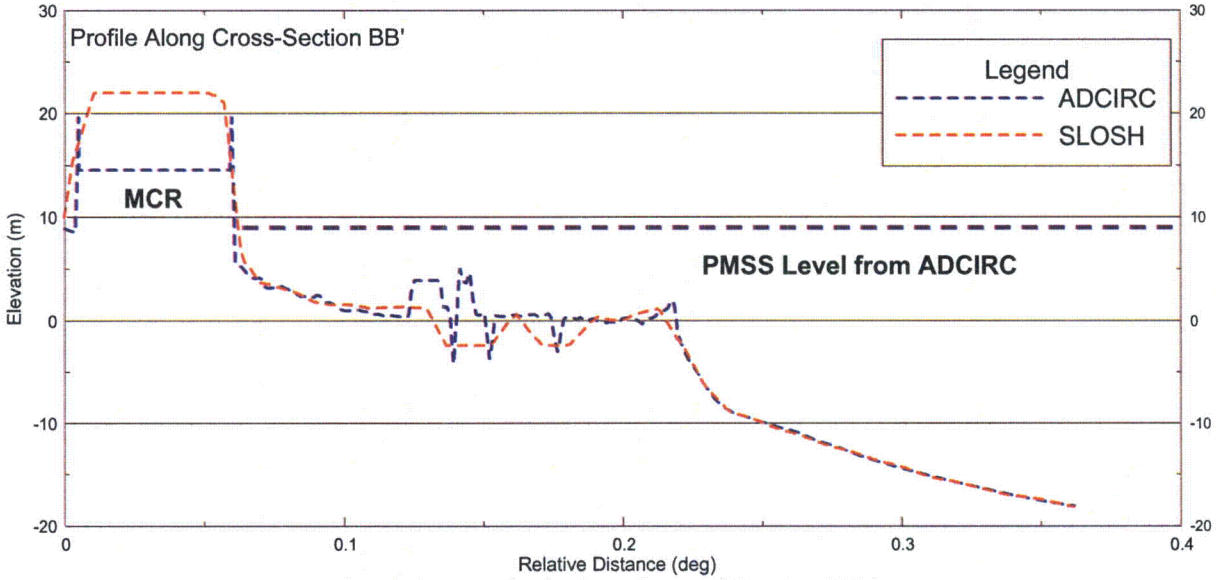

Figure 9. Vertical Elevations of Section BB'

Item 6: A Description of Nonlinearity in Estimated PMSS Corresponding to Various Combinations of PMH Parameters

The results as shown in response to Item 5 indicate, to a limiting degree, that the surge height does not vary linearly with respect to either track direction or distance from the site. It is difficult to describe the exact nature of this non-linearity, as it could be attributable to many factors. However, the outcomes are consistent with the observed behavior of hurricanes with respect to storm surge impacts along the western portion of the Gulf of Mexico.

Item 7: The Selected PMSS Near the STP Site Including Wind/Wave Run-up

Based on the outcome as presented in response to Item 5, the PMSS as generated by ADCIRC, using NWS 48 wind profile, is estimated to be 29.3 ft above MSL. This PMSS will occur as the result of a hurricane traveling in a northwesterly direction (i.e., an approach direction of 135° clockwise from the north) passing within 24 miles of the STP site. During its life up to the point of landfall, the storm will have a constant forward speed of 23 mph, a central barometric pressure of 887 Mb, and a maximum sustained wind speed of 160 knots (184 mph). Upon landfall, the storm will continue in a northwesterly direction and begin to decay gradually as it moves inland.

The resulting storm surge value of 29.3 feet is 2.8 feet greater (approximately 10 percent) than the value of 26.5 feet above MSL as presented to the NRC Audit Team on August 31, 2010. The 26.5 ft value was estimated running ADCIRC with a Holland wind profile and a smaller pressure differential (126 Mb vs. 133 Mb).

Part 2: Additional Information about Main Cooling Reservoir Embankment Breach

RAI 02.04.05-10 and this RAI both requested that STP postulate that the PMSS from a PMH induces a failure of the north face main cooling reservoir (MCR) embankment because of the sloshing and erosive action of floodwaters surrounding the main cooling reservoir during a PMH surge.

As stated in the response to RAI 02.04.05-10, the PMH, the starting point for all of the PMSS prediction models, is described in NOAA Technical Report NWS 23 as the most severe hurricane possible in a particular geographic area. A PMH, an unlikely event, is even less likely to occur with the specific combination of parameters (i.e., storm track direction; landfall location; forward speed; and radius of maximum wind) that results in the highest possible storm surge at one particular location. Adding the assumptions that this specific PMH would not decay as it approached the coast and that the PMH landfall would occur concurrently with a 10% exceedance high tide, an initial rise or sea level anomaly, and with a long term sea level rise predicted for the end of plant life, makes a specific PMH (i.e., the PMH that could cause the PMSS at STP) a highly improbable event.

This response, the response to RAI 02.04.05-10 and presentations by STPNOC during a site audit conducted by the NRC staff on August 31-September 1, 2010, provided details of the four different computer models used to predict the PMSS based on the PMH and the assumptions described above. Three of the four models, including the ADCIRC model described in this response, predict that the storm surge will be less than the nominal plant grade of 34 feet MSL, the elevation on the north side of the MCR embankment. For reasons already stated in this response and the response to RAI 02.04.05-10, and discussions during the August 31-September 1, 2010, site audit, STPNOC has concluded that ADCIRC provides the most credible and an acceptably conservative prediction of the PMSS. ADCIRC predicts that the PMSS for the STP site, including wave runup, is 29.3 feet MSL. This prediction of the PMSS is significantly lower than the 34-foot MSL nominal plant grade at the northern face of the MCR embankment. Therefore, a PMH induced failure of the north face of the MCR embankment due to sloshing and erosive action of floodwaters surrounding the main cooling reservoir is not a credible event.

Although STPNOC evaluations concluded the PMSS predictions based on the April 2010 Version of the SLOSH model are not credible, RAI 02.04.05-10 acknowledges that PMSS predictions using this model do exceed the nominal plant grade of 34 foot MSL. Specifically, the April 2010 version of SLOSH predicts a PMSS of 38.46 feet MSL, assuming a PMH with an intensity that does not decay as it approaches landfall. If wave action is included, this surge could approach 41.76 feet MSL. RAI 02.04.05-10 also presented the surge level time history predicted by this model stating that "surge levels during the PMH, excluding wave action, will be as follows: i) at or above 34 feet MSL (i.e., site grade) for approximately 80 minutes; ii) at or above 36 feet MSL for approximately 50 minutes; and, iii) at or above 38 feet MSL for approximately 25 minutes." Any damage to the MCR embankment due to the direct action of the storm surge would have to occur during this very short window.

Wave action during this short interval is not considered a threat to the MCR embankment because, as described in the response to RAI 02.04.05-10, the wind direction necessary to create the PMSS would create waves in the direction away from the face of the MCR embankment. However, the north face of the MCR embankment could experience strong currents along the outside of the levee, as a large quantity of water is moved past the site in a short period. The response to RAI 02.04.05-10 identified this scenario as Model 4 and stated that:

> ...current velocities associated with the PMSS could damage the MCR embankment. However, the MCR levee is designed to contain water above ground level and the external side of the levee is a grass and maintained slope that is similar to levees designed specifically for protection from both hurricane surge and flooding rivers. A grass surface works well for short-term exposure because plant roots act to keep particles of soil together, creating a flexible system that can deform without tearing. Waves and currents of short duration (i.e., less than several hours) on a well-vegetated cohesive material embankment would not be expected to lead to erosion related concerns. Model 4, the worst case, predicts the surge level is at or above 36 feet MSL for approximately 50 minutes.

Items 8 through 11 of this RAI request technical justification as to why current velocities described above allow STP to conclude, "Any erosion at the base of the levee that might occur with less than an hour of exposure to the current would not threaten the levee."

Before responding to items 8 through 11, it is helpful to describe the MCR embankment and provide a general assessment of the potential for an embankment failure. FSAR 2.4S.8.2 states that the MCR embankment is constructed of compacted clay fill. The embankment has an exterior slope of 3:1 H:V and an interior slope of 2.5:1 H:V on the reservoir side. The top of embankment varies from elevation 65.8 feet MSL to 67.1 feet MSL. The reservoir side of the peripheral embankment is lined with a 30-inch-thick layer of soil-cement to protect against erosion and it has a characteristic stepped surface that provides additional roughness. The outside of the peripheral embankment is sodded for erosion protection.

A typical cross section is shown in Figure 10. Also shown on the figure is a typical section of flood protection levee for Texas City. The Texas City levee has provided protection from hurricane surge over its life, and although that levee sustained damage during Hurricane Ike, the levee did fulfill its intended purpose of withstanding a substantial surge and wave attack over a period of many hours without a breach occurring anywhere along the 17 miles of the protective works (Reference 5). The MCR embankment is similar to, but much larger than, the hurricane surge protection levees that have, for the most part, successfully withstood major hurricane events along the US Gulf coast.

For perspective, Figure 10 also shows the typical hurricane surge level experienced by the Texas City levee and the peak surge level predicted by the 2010 version of SLOSH. There is no possibility that the STP PMSS could breach the MCR embankment. In contrast, the infamous levee failure in New Orleans during hurricane Katrina occurred due to the breach of a piling wall. This wall was constructed in dredged materials and sustained an impact force from a surge wave of significant height generated over a very short time period. The situation of New Orleans is vastly different from the MCR embankment because of the substantial size of the MCR embankment relative to that of a piling wall; the MCR foundation consists of competent clay materials relative to the failed levee location in New Orleans being founded on dredged material; and the landward side of the New Orleans levees are well below sea level.

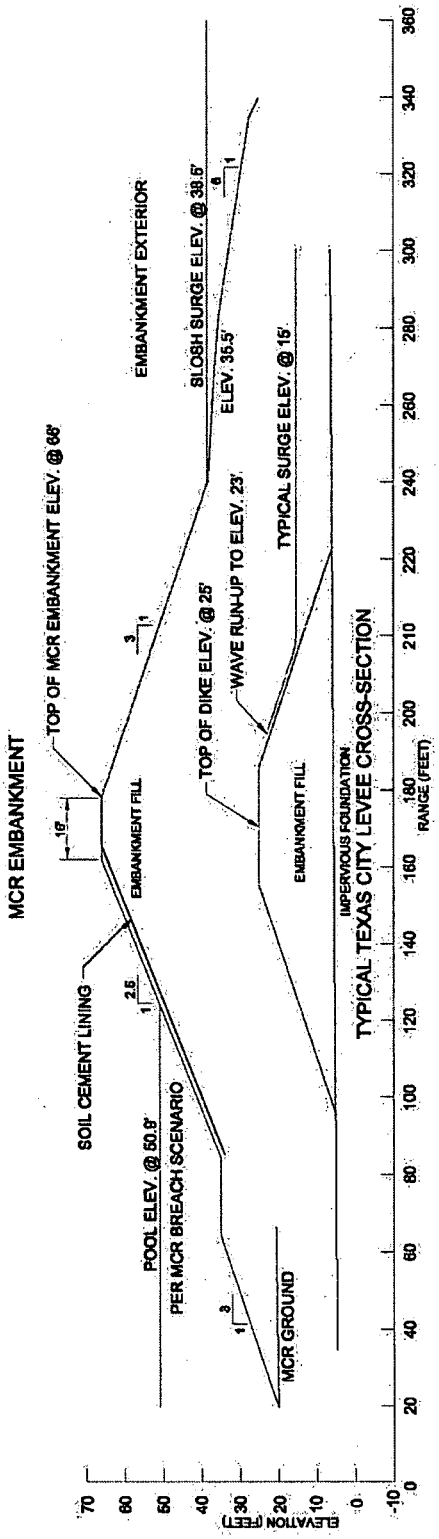

Figure 10 Cross Sections of the STP MCR Embankment and a Typical Texas City Levee

The following are presented in response to the specific requests in the RAI:

Item 8: Detailed description of various methods used to estimate current velocities during a PMSS event.

Water will flow past the MCR levee under the PMSS scenario generated by the 2010 version of SLOSH. If currents were very fast and sufficiently prolonged, erosion would be produced. The SLOSH output does not include currents, but currents can be estimated estimating the area around Units 3 & 4 that experiences surge and calculating the velocities required to fill the area in the time predicted by SLOSH. Currents can also be estimated using Manning's n and a friction slope estimated by change in water surface elevations. Finally, current speeds can also be estimated by tracking the surge wave front past the site. All three methods were employed on the data from the Version 2010 SLOSH surge scenario. The results are presented in response to Item 10.

Item 9: Detailed description and justification of simplifying assumptions made

For reasons already stated in this response and the response to RAI 02.04.05-10, and discussions during the August 31-September 1, 2010, site audit, a storm surge that exceeds the nominal plant grade of 34 feet MSL is not considered a credible event. STPNOC has concluded that ADCIRC provides the most credible and an acceptably conservative prediction of the PMSS. ADCIRC predicts that the PMSS for the STP site, including wave runup, is 29.3 feet MSL. This prediction of the PMSS is significantly lower than the 34-foot MSL nominal plant grade at the northern face of the MCR embankment. Therefore, a PMH induced failure of the north face of the MCR embankment due to sloshing and erosive action of floodwaters surrounding the main cooling reservoir is not a credible event.

Even the worst-case PMSS predicted by the 2010 Version of SLOSH were to occur, the predicted surge poses no threat to the MCR embankment because the surge elevation only rises to the lowest portion of the levee and then only for a very short period. Even in the worst-case prediction for the PMSS, the surge level and associated wave action never approach the levee crest where a breach might be initiated. Any erosion at the base of the levee that might occur with less than an hour of exposure to the current would not threaten the levee.

Item 10: Current velocities and durations for which these currents will affect the MCR embankment

The results for the current velocity calculated from each of the methods described in Item 8 are as follows:

- Maximum velocity to fill the area is 11.6 ft/sec
- Maximum velocity with Manning's n is 3.1 ft/sec
- Maximum velocity with Wave front estimate 6.2 to 13.2 ft/sec

RAI 02.04.05-10 presented the surge level time history predicted by this model stating that "surge levels during the PMH, excluding wave action, will be as follows: i) at or above 34 feet MSL (i.e., site grade) for approximately 80 minutes; ii) at or above 36 feet MSL for approximately 50 minutes; and, iii) at or above 38 feet MSL for approximately 25 minutes."

Based on these flood durations, flow past the base of the levee will have a maximum duration of less than 80 minutes.

Item 11: Ability of the grass-lined outer face of the northern MCR embankment to withstand the current velocities without erosion severe enough to cause an embankment breach

The US Army Corps of Engineers' manual for hydraulic design of flood control channels (Reference 2) recommends a design velocity of 5 to 8 feet/second for stable grass-lined flood channels. The grassed surface of the MCR embankment can be expected to sustain a short exposure to currents slightly larger than the currents assumed in the design of flood channels, which typically have a project life of many decades and would be expected to experience flood currents for considerably longer than 80 minutes. There is no mechanism, wave attack or current flow, which could cause significant erosion to the base of the MCR embankment below the level of 38.5 feet MSL during the very limited time available for the surge predicted by 2010 Version of SLOSH.

References:

1. "Design and Implementation of a Real-Time Storm Surge and Flood Forecasting Capability for the State of North Carolina," Mattocks et al, Carolina Environmental Program, University of North Carolina, November 30, 2006; "A Basin- to Channel-Scale Unstructured Grid Hurricane Storm Surge Model Applied to Southern Louisiana," Westerlink et al, American Meteorological Society, March 2008; "A High-Resolution Coupled Riverine Flow, Tide, Wind, Wind Wave, and Storm Surge Model for Southern Louisiana and Mississippi. Part I: Model Development and Validation," Bunya et al, American Meteorological Society, February 2010; "A High-Resolution Coupled Riverine Flow, Tide, Wind, Wind Wave, and Storm Surge Model for Southern Louisiana and Mississippi. Part II: Synoptic Description and Analysis of Hurricanes Katrina and Rita," Dietrich et al, American Meteorological Society, February 2010.

2. "Modeling Hurricane Waves and Storm Surge using Integrally-Coupled, Scalable Computations," J.C. Dietrich et al., Coastal Engineering, July 9, 2010.

3. "Flood Insurance Study: Coastal Counties, Texas, Intermediate Submission 1: Scoping and Data Review," 7 January 2010, USACE New Orleans District and FEMA Region 6.

4. Light Detection and Ranging (LIDAR) is a remote sensing system used to collect topographic data.

5. "Final Environmental Assessment, Emergency Repairs to Texas City and Vicinity, Texas Hurricane Protection Project, Galveston County, Texas", U.S. Army Corps of Engineers, Galveston District, April, 2009.

6. "Hydraulic Design of Flood Control Channels", EM 1110-2-1601, U.S. Army Corps of Engineers, 1 June, 1994.

STPNOC will revise the Part 2, Tier 2, Section 2.4S.5.2 of the COLA to include a description of the ADCIRC model and the PMSS prediction based on the ADCIRC model:

2.4S.5.2.2 Storm Surge Analysis

~~Two~~Three different approaches were used to estimate the storm surge at STP 3 & 4. The first approach was based on use of the computer program "Quasi Two-Dimensional Open Coast Storm Surge," known as SURGE (Reference 2.4S.5-3). This approach included two steps to estimate the PMSS water surface elevation near STP 3 & 4. First, SURGE was used to estimate the PMSS water surface elevation at the coast near Matagorda, Texas (Figures 2.4S.5-1 and 2.4S.5-5). Second, the PMSS water surface elevation was used as a boundary condition for a backwater calculation using a calibrated and modified model developed by Halff Associates, Inc., for the Colorado River (References 2.4S.5-9 and 2.4S.5-10).

The second approach was based on the use of the numerical model "Sea, Lake, and Overland Surges from Hurricanes" (SLOSH) (Reference 2.4S.5-2). SLOSH was used to obtain estimates of water surface elevation near STP 3 & 4 due to a hypothetical Category 5 'maximum of maximum' (MOM) hurricane impacting the Matagorda Bay region. The MOM is the maximum of the composite of the maximum envelope of water (MEOW), which incorporates all of the peak values for a hurricane of a particular category, speed, and landfall direction. Therefore, it should be noted that a graphical presentation or hydrograph of the SLOSH output is not available since the MEOW scenarios are composites of numerous runs and are therefore not time dependent for individual cells. Rather, the SLOSH MOM only yields the peak water surface elevations for each cell by hurricane category (i.e., Category 1, Category 2, Category 3, Category 4, and if available, Category 5). It is also noted that SLOSH does not incorporate the ten percent exceedance of the astronomical high tide or a user-specified initial sea-level rise like SURGE (Reference 2.4S.5-2). SLOSH just assumes a constant initial tide elevation of 2 feet above MSL.

The third approach used to predict the PMSS used the numerical Advanced Circulation (ADCIRC) Model, a hydrodynamic circulation model that simulates water level and current over an unstructured gridded domain. The ADCIRC model was selected to validate the results obtained with first two approaches in recognition that that "current best practices" for predicting storm surge are evolving rapidly due to the very high level of interest and active involvement of the Federal Emergency Management Agency (FEMA), the National Oceanic and Atmospheric Administration (NOAA), and the US Army Corps of Engineers (USACE). Associated supporting research has been ongoing at several major universities. These ongoing efforts have resulted in major improvements to the more complex multidimensional computer models used to predict storm surge. Additionally, digital elevation maps based on Light Detection and Ranging (LIDAR) for use with ADCIRC were recently made available for a wider area, including the STP site. The LIDAR based maps improve the accuracy and resolution of the topographic grid, an important input to the computer models, such as ADCIRC, that predict storm surge. Assumptions and initial conditions used with the ADCIRC model were, to the maximum extent possible, consistent with the assumptions and initial conditions used with the SLOSH model.

2.4S.5.2.4 Storm Surge Analysis with SLOSH and ADCIRC

2.4S.5.2.4.1 Storm Surge Analysis with SLOSH

The second approach for the estimation of the maximum storm surge at STP 3 & 4 used output from the computer model "Sea, Lake, and Overland Surges (SLOSH)" (Reference 2.4S.5-2). SLOSH was developed by the National Oceanic and Atmospheric Administration (NOAA) and evolved from a simpler model known as the "Special Program to List Amplitudes of Surges from Hurricanes (SPLASH)." SLOSH is a two-dimensional finite difference code that uses an adaptive curvilinear grid for regions along the Gulf and Atlantic coasts. SLOSH assumes uniform friction to solve the equations of motion for reference basins along the Gulf of Mexico and Atlantic Ocean coast. Unlike SURGE, SLOSH can estimate water surface elevations due to the storm surge for both the open coast and on land.

The validity of the SLOSH model has been demonstrated and documented extensively (Reference 2.4S.5-14). While the model validity varies by station, the mean error of the SLOSH predictions for 523 observations within the Gulf of Mexico was reported as 0.09 m (0.29 ft) with a standard deviation of 0.61 m (2.0 ft) (Reference 2.4S.5-14, p. 1410). The maximum difference between the predicted storm surge elevations and the measured storm surge elevations was 2.69 m (8.83 ft) (Reference 2.4S.5-14, p. 1410). For Freeport, Texas, the model predictions replicate the observed surge elevations of approximately 11 ft MLW (10.32 ft MSL) within the mean error during Hurricane Carla (1961) (Reference 2.4S.5-2, p. 61).

The SLOSH MOM scenario predicts that STP 3 & 4 is dry for Category 1 through Category 5 hurricanes (Figure 2.4S.5-7). However, an estimate of the PMH PMSS using SLOSH can be made by using cells near STP 3 & 4 in the Lower Colorado River (Figure 2.4S.5-7). With respect to the windfield conditions, the SLOSH MOM estimate is based on a hurricane with a forward speed of 15 mph (13.03 knots) and a northwest wind. Since the Category 5 hurricane is a less severe scenario than the PMH, the SLOSH estimate needs to be adjusted to be comparable to the SURGE results. By assuming an extrapolation based on the maximum water surface elevation of a MOM Category 2 hurricane through a MOM Category 5 hurricane, the SLOSH PMH PMSS was estimated to be 27.2 ft MSL. Additionally, since the SLOSH model assumes an initial condition of 2 feet MSL for Matagorda Bay, its storm surge estimate needs to be adjusted to be comparable to the SURGE results. First, to account for the long-term sea level rises due to global climate change, it is assumed that the historical mean sea level trend at Freeport, Texas of 5.87 mm per year or 1.93 feet per century, with a standard error of 0.74 mm/yr, from 1954 to 1999 (Reference 2.4S.5-13) will continue. Second, the 2 ft MSL tide assumed by SLOSH needs to be differenced with the 10% exceedance of the astronomical high tide of 2.2 feet MLW (1.52 feet MSL) and the initial water rise of 2.4 feet. Therefore, the PMSS at STP 3 & 4 predicted by SLOSH, with the sea level adjustments, is 31.1 feet MSL. This value is more conservative than the SURGE estimate of 24.29 feet MSL at STP 3 & 4. ~~Since, as shown in Subsection 2.4S.4, the flood elevation caused by a Main Cooling Reservoir (MCR) embankment breach is significantly higher than the storm surge, it can be concluded that the PMH is not a design basis event for a maximum flood water surface elevation at the safety-related STP 3 & 4 plant structures or for hydraulic forces acting against those structures.~~

2.4S.5.2.4.2 Storm Surge Analysis with ADCIRC

The third approach used for the estimation of the maximum storm surge at STP 3 & 4 used output from the computer model Advanced Circulation (ADCIRC). Specifically, version 49 of ADCIRC-2DDI, the two-dimensional, depth-integrated implementation of the ADCIRC coastal ocean model, was used to perform the hydrodynamic computations used to estimate storm surge levels at the site. This model uses depth-integrated equations of mass and momentum conservation subject to incompressibility, Boussinesq, and hydrostatic pressure approximations (References 2.4S.5-15 through 2.4S.5-18). ADCIRC is linked to a computer program called SWAN that calculates the wave-induced setup in addition to the wind-induced setup calculated by ADCIRC. SWAN is a third-generation wave model developed by Delft University of Technology. SWAN computes random, short-crested wind-generated waves in coastal regions and inland waters (Reference 2.4S.5-19). The unstructured-mesh SWAN spectral wave model and the ADCIRC shallow-water circulation model have been integrated into a tightly coupled SWAN + ADCIRC model. Hurricane waves and storm surge as estimated by the coupled SWAN + ADCIRC model have been validated for Hurricane Katrina and Hurricane Rita, demonstrating the importance of inclusion of the wave-circulation interactions.

The Federal Emergency Management Agency (FEMA) certified ADCIRC for use in performing storm surge analyses as part of their program for developing Flood Insurance Rate Maps (FIRMs) along coastal areas of the United States. This model is the standard coastal model used by the Unites States Army Corps of Engineers (USACE). In addition to USACE projects, it is used the National Oceanic and Atmospheric Administration (NOAA) and the Naval Research Laboratory (NRL).

The ADCIRC model as applied to the STP analysis underwent an extensive flood level evaluation process to validate it over a range of conditions to ensure that the flow physics of the system were accurately characterized. The set of validation storms specific to the Texas coastal areas included Hurricanes Carla (1961), Celia (1970), Allen (1980), Alicia (1983), Bret (1999), Rita (2005), and Ike (2008). Hurricanes Rita and Ike were particularly useful storms for validation because of the large degree of surge they produced, and the accurate measurements of wind, atmospheric pressure, waves, and surge levels that exist for these two storms.

Topography for Texas was obtained predominantly using 10-meter LIDAR data supplied by FEMA. Light Detection and Ranging (LIDAR) is a remote sensing system used to collect topographic data. All topographic and bathymetric data were spatially averaged to the local mesh scale. The topographic data were applied to the grid by searching for all LIDAR points within a rectangle defined by the average distance from the node for which we are assigning a topographic value to the connected nodes. The topographic grid used for the ADCIRC analysis at STP accounts for pronounced vertical features with small horizontal scales relative to the grid scale. While features such as barrier islands and riverbanks are generally well resolved in grids with resolutions down to about 100 feet, features like levees, floodwalls, railroads, and raised highways will not be sufficiently well resolved with 100-foot grid resolution. Frequently, these small-scale features can be significant horizontal obstructions to flow causing water to rise or be diverted elsewhere, which proved to be the case at STP. These obstructions must

therefore be carefully incorporated into the model. All raised feature heights are defined using the most recent surveys available from the various sources, including LIDAR sources, USACE SWG surveys, and surveys from local jurisdictions. In this case, vertical positions were typically defined from the Texas 10-meter-by-10-meter LIDAR data set. However, the elevations were also confirmed or adjusted with 1-meter-by-1-meter LIDAR where available.

A series of hurricane scenarios were simulated using ADCIRC to determine the maximum water surface elevation near STP Units 3 and 4 resulting from storm surge. The PMH parameters selected for the ADCIRC runs were based on the storm scenario that that produced the maximum surge at the site during the prior analysis with SLOSH. Specifically, the PMH parameters selected for the ADCIRC runs based on NWS 23 are a radius to maximum winds of 24 miles (21 nm), an approach direction of 135° clockwise from the north (i.e. a northwesterly direction), a forward speed of 23 mph (20 knots), a central pressure of 26.19 in Hg, and a peripheral pressure of 30.12 in Hg. The only variables were the distance of the storm track from the site and the track direction.

The PMSS generated by ADCIRC, using NWS 48 wind profile, is estimated to be 29.3 ft above MSL. This PMSS will occur as the result of a hurricane traveling in a northwesterly direction (i.e., an approach direction of 135° clockwise from the north) passing within 24 miles of the STP site. During its life up to the point of landfall, the storm will have a constant forward speed of 23 mph, a central barometric pressure of 887 Mb, and a maximum sustained wind speed of 160 knots (184 mph). Upon landfall, the storm will continue in a northwesterly direction and began to decay gradually as it moves inland. The limiting storm and corresponding ADCIRC prediction are shown in Figures 2.4S.5-9 and 2.4S.5-10.

2.4S.5.2.4.3 Storm Surge Analysis Conclusions

Subsection 2.4S.4 provides the flood elevation caused by a Main Cooling Reservoir (MCR) embankment breach. The flood level caused by the MCR breach is significantly higher than the probable maximum storm surge as calculated by SURGE, SLOSH, or ADCIRC. Therefore, the probable maximum storm surge caused by the PMH is not a design basis event for the maximum floodwater surface elevation at the safety-related STP 3 & 4 plant structures or for hydraulic forces acting against those structures.

2.4S.5.6 References

2.4S.5-15 "Design and Implementation of a Real-Time Storm Surge and Flood Forecasting Capability for the State of North Carolina," Mattocks et al, Carolina Environmental Program, University of North Carolina, November 30, 2006

2.4S.5-16 "A Basin- to Channel-Scale Unstructured Grid Hurricane Storm Surge Model Applied to Southern Louisiana," Westerlink et al, American Meteorological Society, March 2008.

2.4S.5-17 "A High-Resolution Coupled Riverine Flow, Tide, Wind, Wind Wave, and Storm Surge Model for Southern Louisiana and Mississippi. Part I: Model Development and Validation," Bunya et al, American Meteorological Society, February 2010.

2.4S.5-18 "A High-Resolution Coupled Riverine Flow, Tide, Wind, Wind Wave, and Storm Surge Model for Southern Louisiana and Mississippi. Part II: Synoptic Description and Analysis of Hurricanes Katrina and Rita," Dietrich et al, American Meteorological Society, February 2010.

2.4S.5-19 "Modeling Hurricane Waves and Storm Surge using Integrally-Coupled, Scalable Computations," J.C. Dietrich et al., Coastal Engineering, July 9, 2010.

Center of Eye	Time to Landfall (hrs)	Coordinates Latitude (°N)	Coordinates Longitude (°W)	Storm Features Category (SSI)	Storm Features Central Pressure (Mb)	Storm Features Radius to Max. Winds (miles)	Distance Between Points (nm)	Distance Between Points (miles)	Forward Speed (mph)	Forward Speed (knots)
D	-12	30.26	98.43	1	994	10	26	30	10	8.7
C	-9	29.55	98.06	2	979	13	34	39	13	11.3
B	-6	29.56	97.60	3	964	16	44	51	17	14.7
A	-3	29.04	97.01	4	944	20	52	60	20	17.3
Landfall	0	28.42	96.32	5	887	24	60	69	23	20
1	3	27.72	95.52	5	887	24	60	69	23	20
2	6	26.99	94.73	5	887	24	60	69	23	20
3	9	26.27	93.96	5	887	24	60	69	23	20
4	12	25.54	93.19	5	887	24	60	69	23	20
5	15	24.81	92.43	5	887	24	60	69	23	20
6	18	24.09	91.67	5	887	24	60	69	23	20
7	21	23.37	90.91	4	944	20	60	69	23	20
8	24	22.68	90.12	3	964	16	60	69	23	20
9	27	21.98	89.34	2	979	13				

NORTHWEST

PMH Storm Features		
Central Pressure:	887 Mb	(26.19 in. Hg)
Peripheral Pressure:	1020 Mb	(30.12 in. Hg)
Radius to Maximum Winds:	21 nm	(24 miles)
Forward Speed:	20 knots	(23 mph)
Maximum Sustained Wind:	160 knots	(184 mph)
Shortest Distance from site:	20.9 nm	(24 miles)

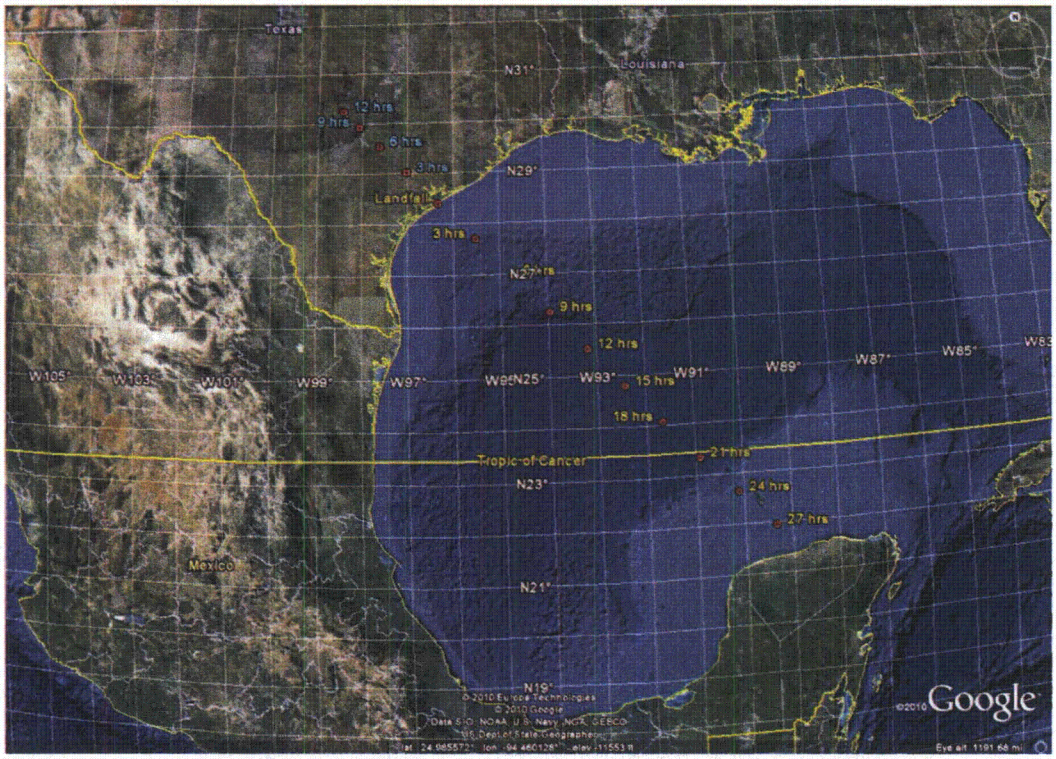

Figure 2.4S.5-9 PMH used in conjunction with ADCIRC model

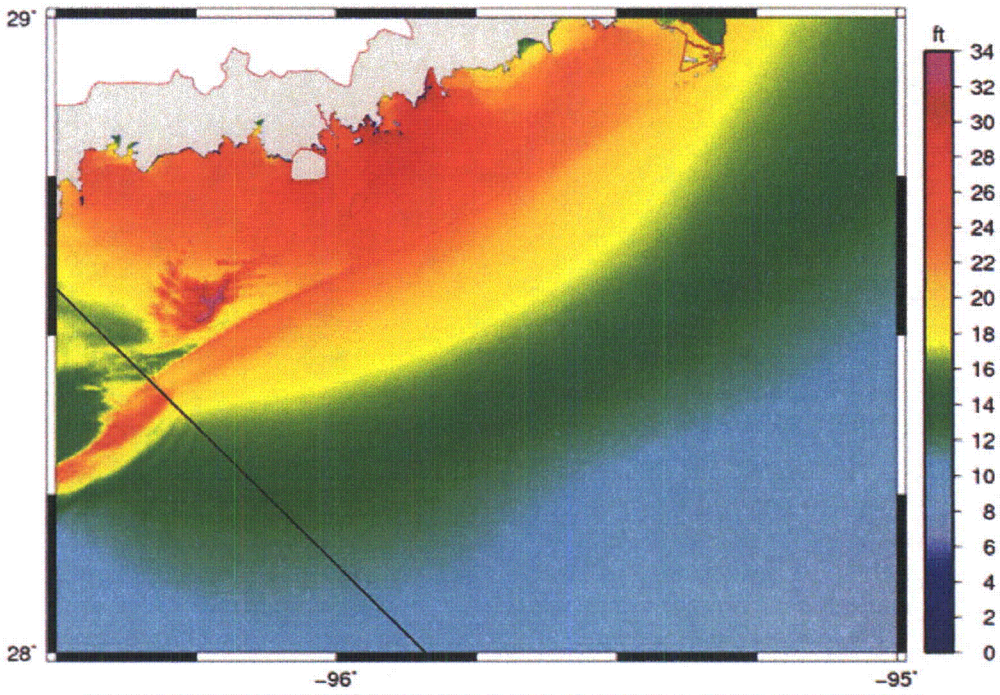

Figure 2.4S.5-10 PMSS Prediction based on the ADCIRC model

02.04.12-51

QUESTION:

Provide a conservative analysis and supporting data on the potential for infiltration and groundwater table rise during the design-basis flood event which results from a breach of the MCR embankment. Supporting data for the analysis must include (a) a diagram showing the ground surface cover conditions in the region, (b) hydraulic properties of surface and underlying materials sufficient to estimate infiltration rates and times, (c) an assessment of the survivability of the surface during the flood event (e.g., scour) especially near safety-related structures, and (d) an assessment of the aging of the surface with regard to seasonal climate extremes and the potential development of preferential infiltration pathways through the surface especially near safety-related structures. Using a conservative plausible alternative conceptual model of infiltration, the applicant shall provide an analysis of the potential groundwater table rise during the Design Basis Flood, and an analysis of the potential for saturation of the uppermost 2 feet (i.e., materials between plant grade and 2 ft below plant grade). If the impacts are thought to be potentially local and not throughout the powerblock, then the analysis should address whether local impacts would occur near or adjacent to safety-related structures.

Alternatively, if the design of the power block surface protects against infiltration during the design-basis flood, and scour and degradation of the designed power block surface are not plausible, provide the technical justification. If maintenance of the designed power block surface plays a role in the survivability of the surface, describe the maintenance effort.

The applicant shall provide FSAR updates to include a summary of either (1) the analysis (i.e., method and results) of potential infiltration during the flood event and its influence on both the water table elevation and saturation of the uppermost 2 ft of surface materials, or (2) the technical justification that the power block surface protects against infiltration during a design-basis flood event over the life of the plant. If the former (i.e., #1 above) is the approach selected, then the FSAR markup shall include a brief discussion of the alternative conceptualizations considered, and the justification for selection of the most conservative one.

RESPONSE:

The existing site has a clay layer extending 20 feet below the existing grade elevation of approximately 30 feet (FSAR Figures 2.4S.12-20 and 2.4S.12-29). This clay layer will be removed during the excavation for the power block structures.

The power block island will be built up to a plant grade elevation of 34 feet. Once the power block structures are constructed the area adjacent to the structures will be backfilled with granular structural fill. After placement of the structural backfill a minimum of 2-foot thick clay layer will be provided as a cap as part of the backfill in the power block island around the buildings to prevent flood water infiltration into the groundwater table. Conservatively, assuming the permeability of the clay layer as $5x10^{-6}$ cm/sec (see response to RAI 02.04.12-48, Letter U7-C-STP-NRC-100195, dated August 30, 2010), the water would penetrate approximately 0.108

cm per hour with approximately 6 feet of depth of water during the design basis flood. During the design basis flood the period of inundation of the power block is approximately 20.5 hours and therefore the maximum infiltration will be of the order of 2.22 cm (0.9 inches). Due to this insignificant infiltration, the flood water will not affect the groundwater table.

Minor excavations into the clay cap that could occur over the life of the plant will not affect the ground water table during short term flooding events. Given the large extent of the aquifer, the amount of infiltration that could enter the aquifer through a limited extent of the excavation will not affect the ground water table.

The plant buildings and concrete and asphalt paved areas and roads will occupy approximately 40 percent of the total surface area of the power block island. The rest of the power block island will have compacted crushed stone surfacing. This surfacing will allow for the normal plant traffic and will withstand erosion. This stone surfacing will normally be maintained by the plant personnel during the plant operation.

The crushed stone surfacing will be able to withstand the flow due to the MCR dike breach flooding with low potential for scour or degradation.

FSAR will be revised as follows as a result of this response.

Subsection 2.4S.12.5.1 will be added as follows:

2.4S.12.5.1 Effect of Design Basis Flood due to MCR Breach on the Design Groundwater Level

The existing site has a clay layer extending 20 feet below the existing grade elevation of approximately 30 feet (Figures 2.4S.12-20 and 2.4S.12-29). This clay layer will be removed during the excavation for the power block structures.

The power block island will be built up to a plant grade elevation of 34 feet. Once the power block structures are constructed the area adjacent to the structures will be backfilled with granular structural fill. After placement of the structural backfill a minimum of 2-foot thick clay layer will be provided as a cap as part of the backfill in the power block island around the buildings to prevent flood water infiltration into the groundwater table. Conservatively, assuming the permeability of the clay layer as $5x10^{-6}$ cm/sec, the water would penetrate approximately 0.108 cm per hour with approximately 6 feet of depth of water during the design basis flood. During the design basis flood the period of inundation of the power block is approximately 20.5 hours and therefore the maximum infiltration will be of the order of 2.22 cm (0.9 inches). Due to this insignificant infiltration, the flood water will not affect the groundwater table.

Minor excavations into the clay cap that could occur over the life of the plant will not affect the ground water table during short term flooding events. Given the large extent of the aquifer, the amount of infiltration that could enter the aquifer through a limited extent of the excavation will not affect the ground water table.

The plant buildings and concrete and asphalt paved areas and roads will occupy approximately 40 percent of the total surface area of the power block island. The rest of the power block island will have compacted crushed stone surfacing. This surfacing will allow for the normal plant traffic and will withstand erosion. This stone surfacing will normally be maintained by the plant personnel during the plant operation.

The crushed stone surfacing will be able to withstand the flow due to the MCR dike breach flooding with low potential for scour or degradation.

Subsection 2.5S.4.5.3 will be updated as follows:

2.5S.4.5.3 Compaction Specifications

Once structural fill sources are identified, as discussed in Subsection 2.5S.4.5.1, several samples of materials are obtained and tested for index properties and for engineering properties, including grain size and plasticity characteristics, moisture-density relationships, and dynamic properties. For foundation support and for backfill against walls, structural fill is compacted to a minimum of 95% of its maximum dry density and within + or -3% of its optimum moisture content, as determined based on the modified Proctor compaction test procedure (Reference 2.5S.4-42).

A clayey soil layer will be placed above the granular structural backfill around the structures within the excavation area. The clay layer will be a minimum of 2 feet thick and comprise the layer between the granular backfill and the final surface treatment (i.e., crushed stone, paving, etc.). The clay layer will minimize any flood water infiltration into the groundwater table.